UNIVERSIDAD COMPLUTENSE DE MADRID

FACULTAD DE FARMACIA

TESIS DOCTORAL

Papel del intercambiador mitocondrial sodio/calcio (NCLX) en la respuesta a la hipoxia y en los efectos mitocondriales del litio

Role of the mitochondrial sodium/calcium exchanger (NCLX) in the response to hypoxia and in the mitocondrial effects of lithium

MEMORIA PARA OPTAR AL GRADO DE DOCTORA

PRESENTADA POR

Carmen Choya Foces

DIRECTOR

Dr. Antonio Martínez Ruiz

© Carmen Choya Foces, 2024

UNIVERSIDAD COMPLUTENSE DE MADRID

FACULTAD DE FARMACIA

PROGRAMA DE DOCTORADO EN BIOQUÍMICA, BIOLOGÍA MOLECULAR Y BIOMEDICINA

TESIS DOCTORAL

Papel del intercambiador mitocondrial sodio/calcio (NCLX) en la respuesta a la hipoxia y en los efectos mitocondriales del litio

Role of the mitochondrial sodium/calcium exchanger (NCLX) in the response to hypoxia and in the mitochondrial effects of lithium

El presente trabajo ha sido realizado en la Unidad de Investigación del Hospital Universitario Santa Cristina del Instituto de Investigación Sanitaria de la Princesa, bajo la dirección del **Dr. Antonio Martínez Ruiz**

OPTA AL GRADO DE DOCTORA

Carmen Choya Foces

Madrid, 2024

AGRADECIMIENTOS

ACKNOWLEDGEMENTS

Gracias a todes y punch.

INDEX

TABLES:

FIGURES:

RESUMEN

Las mitocondrias son el orgánulo celular encargado de realizar la respiración celular, por lo que son las principales consumidoras de oxígeno en la célula. En consecuencia, la disminución de oxígeno disponible, situación conocida como hipoxia, afecta de manera directa a esa función mitocondrial. Hemos demostrado que el intercambiador mitocondrial sodio/calcio/litio (NCLX) es esencial en la señalización redox inducida por la hipoxia aguda. Como consecuencia de inducir hipoxia, el complejo I (CI) de la cadena transportadora de electrones mitocondrial se desactiva y pierda su función de bombear protones, por lo que la matriz mitocondrial se acidifica. En consecuencia, los gránulos de fosfato cálcico mitocondriales se disuelven parcialmente, haciendo que aumente el calcio soluble mitocondrial. Este incremento activa a NCLX, produciendo la importación de sodio a la matriz mitocondrial. Los iones de sodio, al interaccionar con los fosfolípidos de la membrana mitocondrial interna (IMM), hacen que la fluidez de la misma disminuya, alterando así la difusión de la coenzima Q y produciendo un estallido de superóxido durante los primeros minutos de hipoxia.

Teniendo en cuenta el efecto de NCLX en hipoxia aguda, hemos profundizado en los efectos a largo plazo de la activación de NCLX en la vía de los factores inducibles por hipoxia (HIF), un mecanismo fundamental de señalización y adaptación a la hipoxia. En resultados previos del grupo de investigación se había observado que la inhibición de NCLX impedía la estabilización de HIF-1α en hipoxia, evitando, así, la activación de la vía de HIF. Sin embargo, hemos observado que en un modelo de deleción crónica de NCLX la estabilización de HIF-1α en hipoxia no está bloqueada, excepto si previamente a la hipoxia las células se tratan con N-acetil-L-cisteína o L-cisteína. Estos resultados resaltan la estrecha relación de la vía de HIF con los niveles redox celulares y el efecto a largo plazo de la actividad de NCLX en hipoxia.

Además, dado que NCLX es sensible a litio y que el mecanismo de acción del mismo no se conoce con exactitud, hemos analizado el efecto de la adición de litio en varios aspectos mitocondriales. Hemos observado que, durante la hipoxia aguda, los iones de litio son importados a la matriz mitocondrial por NCLX, sustituyendo a los iones de sodio, inhibiendo la reducción de la fluidez de la IMM y, consecuentemente, la producción de superóxido durante los primeros minutos de hipoxia. Además de la estimulación de las dinámicas de calcio mitocondrial debido a la activación de NCLX, la adición de litio produce efectos en las mitocondrias independientes de dicho intercambiador, pero en los que está involucrado el CI. Estos resultados evidencian que hay efectos mitocondriales del litio, tanto dependientes como independientes de NCLX, que podrían explicar algunos aspectos de sus mecanismos de acción y que, además, abren la puerta a nuevas aplicaciones farmacológicas para el litio.

ABSTRACT

Mitochondria are the cellular organelle in charge of cellular respiration; thus, they are the main cellular oxygen consumers. Accordingly, a deficiency in available oxygen, a situation known as hypoxia, directly affects this mitochondrial function. We have shown that the mitochondrial sodium/calcium/lithium exchanger (NCLX) is essential in redox signaling in acute hypoxia. Hypoxia-induced deactivation of mitochondrial complex I (CI) of the electron transport chain produces the loss of its proton pumping activity, thereby acidifying the mitochondrial matrix. Consequently, mitochondrial calcium phosphate granules partially dissolve, increasing mitochondrial soluble calcium. This activates NCLX, resulting in the import of sodium into the mitochondrial matrix. Sodium ions, by interacting with phospholipids of the inner mitochondrial membrane (IMM), decrease the fluidity of the IMM, which alters the diffusion of coenzyme Q and produces a superoxide burst during the first minutes of hypoxia.

Considering the NCLX effect in acute hypoxia, we examined the long-term effects of NCLX activation on the hypoxia inducible factors (HIF), a fundamental mechanism of signaling and adaptation to hypoxia. Previous results from the research group had observed that NCLX inhibition prevented HIF-1α stabilization in hypoxia, thus avoiding HIF pathway activation. However, we have observed that in a chronic NCLX deletion model HIF-1α stabilization in hypoxia is not blocked, except if prior to hypoxia cells are treated with N-acetyl-L-cysteine or L-cysteine. These results highlight the close relationship of the HIF pathway with cellular redox levels and the long-term effect of NCLX activity in hypoxia.

Furthermore, since NCLX is sensitive to lithium and the lithium's mechanism of action is not completely understood, we have analyzed the effect of lithium addition on various mitochondrial aspects. We have observed that, during acute hypoxia, lithium ions are imported into the mitochondrial matrix by NCLX, replacing sodium ions and, thus, inhibiting the reduction of IMM fluidity and, consequently, superoxide production during the first minutes of hypoxia. In addition to the mitochondrial calcium dynamics enhancement due to NCLX activation, lithium addition produces effects on mitochondria that are independent of NCLX, but in which CI is involved. These results show that there are both NCLX-dependent and NCLX-independent mitochondrial effects of lithium that could explain some aspects of its action mechanisms and open the door to new pharmacological applications for lithium.

ABBREVIATIONS AND SYMBOLS

AA:	antimycin A
AD:	Alzheimer's disease
BD:	bipolar disease
cAMP:	cyclic adenosine monophospate
CB:	carotid body
CGP:	CGP-37157, 7-chloro-5-(2-chlorophenyl)-1,5-dihydro-4,1-benzothiazepin-2(3H)-one
CL:	cardiolipin
CoQ:	ubiquinone
Cytc:	cytochrome *c*
DHE:	dihydroethidium
DMOG:	dimethyloxalylglycine
dnNCLX:	dominant negative NCLX form (S468T mutation)
ETC:	mitochondrial electron transport chain
FCCP:	carbonyl cyanide-p-trifluoromethoxyphenyl hydrazone
FET:	forward electron transport
GF-AAS:	graphite furnace atomic absorption spectrometry
GM:	glutamine/malate
GSH:	reduced glutathione
GSSG:	oxidized glutathione
ICP-MS:	inductively coupled plasma mass spectrometry
IMM:	inner mitochondrial membrane
IMS:	intermembrane space
$_{i}Ca^{2+}$:	cytosolic or extramitochondrial calcium
$_{i}Li^{+}$:	cytosolic or extramitochondrial lithium
$_{i}Na^{+}$:	cytosolic or extramitochondrial sodium
$_{m}Ca^{2+}$:	mitochondrial calcium
$_{m}Li^{+}$:	mitochondrial lithium
$_{m}Na^{+}$:	mitochondrial sodium
MAFs:	mouse adult fibroblasts
MEFs:	mouse embryonic fibroblasts
mitoRFP:	red fluorescent protein targeted into IMM
mtCU:	mitochondrial calcium uniporter complex
MPTP:	mitochondrial permeability transition pore
NAC:	N-acetyl-cysteine
NCLX:	mitochondrial sodium/calcium/lithium exchanger
NHE:	sodium/proton exchanger
OCR:	oxygen consumption rate
OMM:	outer mitochondrial membrane
OXPHOS:	oxidative phosphorylation
PDE2:	phosphodiesterase 2
PKA:	phosphokinase A
PHD:	HIF prolyl hydroxylase
PRDX1:	peroxiredoxin 1
PC:	phosphatidylcholine
pNCLX:	human NCLX protein
PS:	phosphatidylserine
pVHL:	Von-Hippel Lindau protein
RET:	reverse electron transport
Rhod2:	rhodamine-2 acetoxymethyl
ROS:	reactive oxygen species

SBFI:	sodium benzofuran isophthalate tetra-ammonium salt
TCA:	tricarboxylic acid
TMRM:	tetramethylrhodamine methyl ester
ΔpH_{mt}:	mitochondrial pH gradient
$\Delta \mu_{mt}$:	mitochondrial proton-motive force
$\Delta \Psi_{mt}$:	mitochondrial membrane potential

INTRODUCTION

1. Hypoxia

Life of eukaryotic cells and organisms depends on oxygen. The condition known as hypoxia describes a situation in which there is a deficiency of available oxygen for maintaining adequate homeostasis in cells within a tissue. Hypoxia can be caused by a low blood supply or by a low oxygen level in the blood, known as hypoxemia.

There are some physiological processes in which hypoxia necessarily occurs. For example, during embryonic development, hypoxia is needed for the viability and correct maturation of tissues (Dunwoodie, 2009). Also, high altitude induces metabolic changes to improve the efficiency of oxygen transport and utilization (Moore, 2017) or, during exercise, our body responds to hypoxia by increasing ventilation to ensure enough oxygen concentration in blood (Weir et al., 2005).

However, hypoxia is also present in many pathological situations. For example, in cancer, due to the uncontrollable cell proliferation and the abnormal tumor blood vessels growth, hypoxia becomes one of the main features of solid tumors and correlates with poor prognosis of cancer patients (Muz et al., 2015). Hypoxia is also a common feature of cardiovascular pathologies such as atherosclerosis, vascular remodeling or heart failure, and both the impaired circulation and hypoxic signaling can worse the cardiovascular pathology development (Abe et al., 2017). Also, stroke survivors are at risk of developing Alzheimer's Disease (AD) since hypoxia improves the amyloid-ß protein formation and accumulation (Lall et al., 2019).

Cells and organisms are able to detect hypoxia and induce different responses to adapt their metabolism and other physiological functions. Depending on hypoxia duration and/or severity, the response to hypoxia may vary through long- or short-term mechanisms. Knowing the pathways involved in these responses may be crucial to avoid the lethal effects of uncontrolled hypoxia.

1.1. Long-term response to hypoxia

The main pathway involved in long-term response to hypoxia is the alteration of gene expression programs through the activation of hypoxia-inducible factors (HIF), known as HIF pathway. HIFs are heterodimeric transcription factors formed by a constitutively expressed subunit (HIF-β, also referred as the aryl hydrocarbon receptor nuclear translocator ARNT) and an oxygen-dependent subunit (HIF-α) (Semenza, 2007a). When oxygen levels are normal or during normoxia conditions, the three homologous α subunits

(HIF-1α, HIF-2α and HIF-3α) are modified through an oxygen-dependent hydroxylation performed by specific HIF prolyl-hydroxylases (PHDs) (Semenza, 2007a). The hydroxylation is produced in two proline residues, which allow the α subunits to be recognized by the E3 ubiquitin ligase Von-Hippel Lindau protein (pVHL). Subsequently, the α subunits are ubiquitinated and directed to degradation through the 26S proteasome (Semenza, 2007a). However, in hypoxia PHDs are inactivated so, the α subunits are not degraded and, consequently, are stabilized (Semenza, 2007a). HIF-α subunits heterodimerize with HIF-β and the complexes are translocated to the nucleus, where they bind to the hypoxia response elements (HREs), which are specific sequences in the promoter region of target genes (Semenza, 2007a). The main HIF-dependent genetic expression or repression effect drives metabolic adaptation to reduced oxygen availability and to increase oxygen delivery (Semenza, 2007b), such as angiogenesis-inductor (e.g., vascular endothelial growth factor) or glycolysis-enhancer (e.g., glucose transporter 1) genes (Semenza & Wang, 1992). One of the classic HIF-induced genes is the erythropoietin (EPO) gene; indeed, the hypoxic induction of EPO allowed the discovery of the first described HIF, HIF-1 (Semenza & Wang, 1992).

Altogether, crucial discoveries of this pathway led William Kaelin, Jr., Sir Peter Ratcliffe and Gregg Semenza to be awarded the Nobel Prize in Physiology or Medicine in 2019 “for their discoveries of how cells sense and adapt to oxygen availability”. However, there are different alternative or non-canonical HIF pathways described, in addition to the canonical activation pathway in response to hypoxia (Iommarini et al., 2017). It has been shown that some metabolites can inhibit or boost PHDs or pVHL activity, as well as HIF-α subunits can be degraded by other pathways that do not exclusively depend on oxygen availability (Iommarini et al., 2017). Indeed, before the role of PHDs in HIF pathway was described, mitochondrial reactive oxygen species (ROS) production was demonstrated to be involved in HIF-1α stabilization (Chandel et al., 1998). Nowadays it is widely demonstrated that mitochondrial damage and/or increased ROS production directly affect HIF pathway (Brunelle et al., 2005; Guzy et al., 2005; Mansfield et al., 2005).

1.2. Short-term response to hypoxia

Since mitochondria has been demonstrated to be involved in long-term hypoxic signaling, some research groups have focused on these organelles to look for the oxygen sensor within them. Moreover, knowing that each organ has a different metabolic rate, and, thus, a different oxygen demand/consumption, the acute response to hypoxia is cell-type specific.

One of the most studied short-term responses to hypoxia is during acute hyperventilation, in which the carotid body (CB) is the key organ that senses hypoxemia and sends a neural signal to induce an increase of the ventilation rate (López-Barneo & Ortega-Sáenz, 2022). The CB is a small organ located at the bifurcation of each carotid artery and contains specialized cells that are sensitive to partial pressure of arterial oxygen and carbon dioxide, as well as to blood pH changes. The signal produced by CB reaches the central nervous system through the afferent fibers of the glossopharyngeal nerve. Although the molecular mechanism underlying oxygen-sensing by CB is not fully understood, several features have been described. It is well stablished that hypoxia induces depolarization of chemoreceptors within CB due to the inhibition of voltage potassium channels, which, in turn, induces the voltage-dependent calcium channels opening. Therefore, the cytosolic calcium levels are increased which produces the exocytosis of vesicles with neurotransmitters to the afferent fibers (Gao et al., 2022). It has been recently discovered that HIF-2α levels are basally increased in the CB and, consequently, CB's mitochondria present atypical subunits within the mitochondrial complex IV (CIV) (Jiménez-Gómez et al., 2023), that increase their oxygen sensitivity. Additionally, during hypoxic signaling, mitochondrial complex I (CI) has been described as the main ROS source and their production inhibits the plasmatic potassium channels (Fernández-Agüera et al., 2015). In line with this, by expressing an alternative NADH dehydrogenase from yeast, oxygen sensing is restored in CI knock out conditional mice (Jiménez-Gómez et al., 2023). However, some data indicates that mitochondrial complex II (CII) may also be involved in oxygen sensing in the CB (Piruat et al., 2004). So, some details need to be further explorer to complete the puzzle.

Furthermore, we have proposed an operating mechanism in unspecialized cells, which are also able to detect and respond to acute hypoxia (Hernansanz-Agustín et al., 2014, 2017, 2020). In previous results, our research group demonstrated that cells produce a superoxide burst during the first minutes to hypoxia (Hernansanz-Agustín et al., 2014) in which CI is involved (Hernansanz-Agustín et al., 2017). We have recently dilucidated how this superoxide burst is produced (Hernansanz-Agustín et al., 2020), as summarized in **Figure 1**. We observed that the superoxide burst caused by acute hypoxia is inhibited by blocking the mitochondrial sodium/calcium exchanger (NCLX), localized in the inner mitochondrial membrane (IMM). Firstly, acute hypoxia somehow impairs CI activity, inducing the CI conformational transition from its active to its deactive form and leading to a loss of its proton pumping activity. As a consequence, mitochondrial matrix is acidified (Hernansanz-Agustín et al., 2017). Surprisingly, we have shown that mitochondrial matrix acidification leads to a partially dissolution of mitochondrial calcium phosphate precipitates.

These precipitates, identified years ago (Greenawalt et al., 1964), were also described as sensitive to pH changes due to their mainly composition of hydroxyapatite. The partial dissolution of precipitates increases free mitochondrial calcium which activates NCLX. As a sodium/calcium exchanger, NCLX imports three sodium ions into the mitochondrial matrix while one mitochondrial calcium ion is released to the cytosol. Remarkably, these sodium ions interact with the phospholipids of the inner leaflet of IMM which, in turn, decreases the IMM fluidity. As a consequence, the ubiquinone cycle between mitochondrial complexes II and III (CII and CIII, respectively) slows down, which eventually induces the superoxide burst (Hernansanz-Agustín et al., 2020).

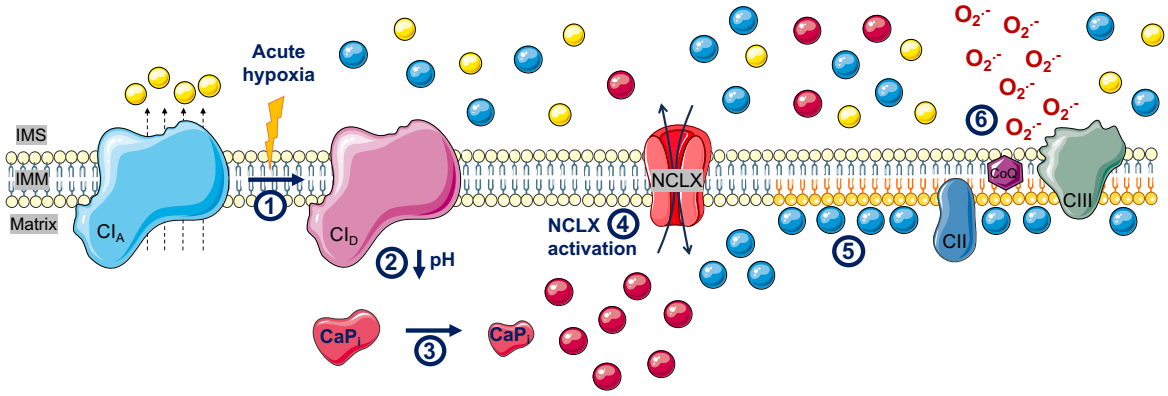

Figure 1. Scheme of the molecular pathway inducing ROS production in acute hypoxia. Acute hypoxia induces complex I conformational transition from active (CI_A) to deactive (CI_D) form **(1)**, leading CI to lose its proton pumping activity. Consequently, mitochondrial matrix is acidified **(2)**. This acidification induces that the partial dissolution of calcium phosphate precipitates, increasing free mitochondrial calcium **(3)**, which is extruded through NCLX **(4)**, importing sodium into mitochondrial matrix. Sodium ions interact with the phospholipids of the inner leaflet of IMM **(5)**, decreasing the IMM fluidity. This reduction of IMM fluidity slows down the Q cycle between CII and CIII, which eventually induces the superoxide burst **(6)**. Scheme made using illustrations available on Elsevier Medical Art.

Taken together, mitochondria are clearly involved in hypoxia signaling, as well as the CI seems to be one of the major players underlying hypoxic mechanism. In order to find out a plausible link between long and short-term response to hypoxia, and since we have demonstrated that NCLX is involved in hypoxic signaling, our research group decided to analyze whether NCLX activity may affect HIF-1α stabilization in hypoxia. Thus, in previous work, we have showed that HIF-1α stabilization after 4 hours of hypoxia was prevented by acute inhibition of NCLX in several cell types (including bovine aortic endothelial cells (BAECs), human umbilical vein endothelial cells and HT-22 cells (mouse hippocampal neuronal cell line)) and in mouse hippocampal slices (Hernansanz-Agustín, 2017). However, in a mouse model of colorectal cancer, the chronic ablation of NCLX has been observed to induce HIF-1α stabilization without hypoxic stimulus and, as a consequence, the primary tumor growth is reduced, but also metastasis is enhanced (Pathak et al., 2020). So, further experiments are required to elucidate the underlying mechanism.

2. Mitochondrial metabolism

Mitochondria are eukaryotic intracellular organelles, thought to have evolved, through endosymbiosis, from bacteria living within larger cells million years ago. They have their own genome, multiple circular DNA molecules per organelle, which encodes small number of proteins and transfer RNAs (tRNAs) mainly involved in oxidative phosphorylation (OXPHOS) and their own translation machinery. However, the mitochondrial DNA replication machinery and most of the mitochondrial proteins (around 95%) are encoded in the nuclear genome; consequently, they are translated in the cytosol and imported into mitochondria (Cooper, 2019).

2.1. Mitochondrial structure

Mitochondria consist of two distinct membranes, the outer mitochondrial membrane (OMM) and the inner mitochondrial membrane (IMM). The space between them is known as the intermembrane space (IMS), while the area enclosed by the IMM is refered to as the mitochondrial matrix. This precise compartmentalization is essential for a correct mitochondrial functioning.

2.1.1. Outer mitochondrial membrane

The OMM delimits mitochondria and mediates contact with the endoplasmic reticulum (ER), known as mitochondria-associated ER membranes (MAMs), through which bi-directional lipid trafficking (Achleitner et al., 1995; Gaigg et al., 1995; Vance, 1990) or calcium exchange (Rizzuto et al., 1998) occur. Remarkably, the protein mitofusin 2 (Mfn2) has a crucial role in the mitochondrial-ER tethering (de Brito & Scorrano, 2008).

The lipid:protein ratio is higher in the OMM in comparison with the IMM (Daum & Vance, 1997), but in both membranes the lipid composition is asymmetric. This means that the lipid composition of each leaflet of each bilayer is different (Daum & Vance, 1997) and there are proteins (scramblases, flippases and floppases) that keep this asymmetry (Pomorski & Menon, 2016). The most abundant lipid components of the OMM are phosphatidylcholine (PC), followed by phosphatidylethanolamine (PE) and phosphatidylinositol (PI) (Daum & Vance, 1997). Other lipids such as cardiolipin (CL) or phosphatidylserine (PS) are less abundant (Daum & Vance, 1997). PC presents a cylindrical shape, characterized by a headgroup size similar to its hydrophobic region. This structural feature allows the planar bilayers formation and is essential for eukaryotic membranes structure (Cooper, 2019). However, PE presents a conical structure, which means that its head group is smaller than

the rest of the molecule (Cooper, 2019). Conical phospholipids do not form planar bilayers as PC does, but they favor hexagonal phase formations. These phospholipids induce tension within membranes, contributing to protein incorporation and the generation of negative curvature of membranes, both are necessary features for proper mitochondrial function (Mejia & Hatch, 2016).

Additionally, the most abundant protein in the OMM is the voltage-dependent anion channel (VDAC), a non-selective channel which allows the exchange of substrates, metabolites and ions between the cytosol and the IMS (Hodge & Colombini, 1997). VDAC is also known to participate in apoptotic signaling, either by mediating the cytochrome *c* (cytc) release (Garrido et al., 2006) or interacting with pro-apoptotic proteins such as Bcl-2 family (Tsujimoto & Shimizu, 2000).

2.1.2. Inner mitochondrial membrane

The IMM is approximately three times larger than the OMM. This increase in size is due to the IMM forms variably shaped invaginations within the matrix, known as cristae, where the mitochondrial electron transport chain (ETC) and the ATP synthase are located (Mannella et al., 2013). Cristae are closed by proteins called Opa1 (optic atrophy 1) (Frezza et al., 2006) and MICOS (mitochondrial contact site and cristae organizing system) (van der Laan et al., 2016), creating two different IMS: the intracristae and the peripheral, which differ in structure and function (Wolf et al., 2019). Both, Opa1 and MICOS stabilize the cristae and prevents their detachment (Rabl et al., 2009). MICOS is a hetero-oligomeric complex formed by two subcomplexes: Mic10, which forms the structural crista junctions, and Mic60, which connects IMM and OMM (van der Laan et al., 2016). Lipids (Aaltonen et al., 2016) and proteins (Horvath et al., 2015) trafficking occur through MICOS. Additionally, specific proteins are responsible for transporting each type of phospholipid between the two membranes (Connerth et al., 2012; Horibata et al., 2016; Miliara et al., 2015) and possibly there may be other structures that serve as bridges between them (Epand et al., 2007). Furthermore, the loss of the mitochondrial ATP synthase dimers results in aberrant cristae morphology (Paumard et al., 2002; Strauss et al., 2008) and the absence of Opa1 (Quintana-Cabrera et al., 2018) or MICOS (Rampelt et al., 2017) results in the loss of ATPase dimers, suggesting the close connection between mitochondrial structure and function.

The cristae formation is allowed by the negative curvature of IMM, in part due to conical phospholipids presence, reason why PE is the most abundant phospholipid in IMM, closely followed by PC (Daum & Vance, 1997). Indeed, PE is formed in the external leaflet of IMM, by PS decarboxylation (Zborowski et al., 1983). However, regarding IMM composition, the

most important feature is the abundance of CL in IMM, around 15-20% of the total phospholipids and located mainly in the inner leaflet (Daum & Vance, 1997). CL is also a conical phospholipid synthetized within mitochondria, in the IMM (Schlame & Haldar, 1993). It is composed by three glycerol groups, two phosphate moieties and four acyl chains (Schlame et al., 1993). For optimal function, CL requires symmetric and moderately unsaturated acyl chains, a modification mediated by three acyl-transferases. These enzymes remodel CL's acyl chains by transferring them from other phospholipids within the IMM (Cao et al., 2004; Taylor & Hatch, 2009; Xu et al., 2006). Mutations in tafazzin, one of these acyl-transferases (Xu et al., 2006), lead to develop Barth syndrome (Barth et al., 1983). These generic alterations are linked to the X chromosome and induce cardiomyopathy, skeletal myopathy and neutropenia, as well as reduction of life expectancy (Barth et al., 1983). Besides its tight structure, flipping CL from IMM to OMM is one of the first steps in apoptosis and mitophagy (X.-X. Li et al., 2015). Therefore, maintaining CL structure and location is essential to keep the intact IMM integrity and, in turn, maintain the complex stabilization and supercomplex oligomerization (Dudek et al., 2013; M. Zhang et al., 2002), crista formation and maintenance (Pfeiffer et al., 2003) or fission and fusion events (Ban et al., 2017, 2018).

The IMM is more impermeable than the OMM to solutes and presents selective and highly controlled channels for almost each metabolite. This selectivity is essential for maintaining the mitochondrial proton-motive force ($\Delta\mu_{mt}$), which is crucial for mitochondrial metabolism (Nicholls, 2008).

2.1.3. Mitochondrial ultrastructure

Mitochondria are not statical organelles, their shape and ultrastructure are dynamics and correlate with the mitochondrial function (Quintana-Cabrera & Scorrano, 2023). Certainly, mitochondrial morphology is highly controlled by mitochondrial-shaping proteins and alterations in these proteins result in genetic diseases (W. Chen et al., 2023). There are two main events that define the mitochondrial ultrastructure: fission and fusion.

Mitochondrial fission is the process of constricting and severing one mitochondrion to produce smaller mitochondria. Mitochondrial fission plays a crucial role in maintaining mitochondrial homeostasis by sorting out young/healthy mitochondrial from old/damaged ones, which may be degraded by mitophagy (W. Chen et al., 2023). Mitochondrial fission is a complex process which requires cytoskeleton and ER participation, involving several proteins. Within them, the protein in charge of mitochondrial fission control is the GTPase dynamin-related protein (Drp1) (Kamerkar et al., 2018). Briefly, the ER membrane spreads and wraps around mitochondria where actin polymerizes to form filaments. Together, actin

and myosin drive the initial mitochondrial constriction and then, Drp1 oligomerization induces the OMM excision. This process is tightly regulated by the release of calcium from ER, coordinating mitochondrial fission between IMM and OMM (Chakrabarti et al., 2018).

Conversely, mitochondrial fusion is the process of merging two or more mitochondria to produce a larger organelle. Mitochondrial fusion is characterized by the sequential fusion of the OMM and IMM, and both steps are carried out by GTPases (Song et al., 2009). For OMM fusion, heterodimers or homodimers of mitofusin 1 (Mfn1) and Mfn2 tether and dock both OMMs. Once the OMM is fused, Opa1 helically oligomerizes and, by docking with CL in both IMMs, the IMM fusion is performed. However, some details about IMM fusion remain unknown (Quintana-Cabrera & Scorrano, 2023).

In addition to the effect of cytosolic or ER signals in mitochondrial fission and fusion (Giacomello et al., 2020), both events are subjected to multiple levels of regulation, including post-transcriptional and post-translational modifications of the involved proteins (Liesa & Shirihai, 2013). Furthermore, these dynamic processes are interconnected, consequently there is a balance between mitochondrial fission and fusion as a response to metabolic and bioenergetic demands (Mishra & Chan, 2016). Usually, elongated mitochondria are linked to increased respiration and ATP production, while mitochondrial fragmentation occurs as a response to heterogenous mitochondrial potential ($\Delta\Psi_{mt}$), defects in the ETC or cationic dysregulations.

2.2. Mitochondrial oxidative phosphorylation

The main mitochondrial function is the oxidative phosphorylation (OXPHOS), process by which energy is produced through the reduction of oxygen into water, summarized in **Figure 2**. The OXPHOS system is enclosed in the crista and is composed by five complexes, complexes I to IV form the mitochondrial electron transport chain (ETC) and the complex V (CV), namely, the mitochondrial ATP synthase. The ETC performs serial redox reactions, using the reduced equivalents NADH and $FADH_2$ formed mainly in the tricarboxylic acid (TCA) cycle, channeling electrons until the final electron acceptor, molecular oxygen. During these reactions, complexes I, III, and IV of ETC pump proton ions across the IMM, producing an electrical difference (mitochondrial membrane potential, $\Delta\Psi_{mt}$) and a pH difference (mitochondrial proton gradient, ΔpH_{mt}) between the mitochondrial matrix and the IMS. The combination of $\Delta\Psi_{mt}$ and ΔpH_{mt} results in the proton motive force ($\Delta\mu_{mt}$), energy used by the CV to phosphorylate ADP and produce ATP.

The CI or NADH-ubiquinone oxidoreductase complex oxidizes NADH while reduces ubiquinone (CoQ) to ubiquinol and, during this process, four proton ions are pumped across the IMM. Others $FADH_2$-dependent enzymes located at both sides of IMM are able to reduce CoQ, but only CI pumps protons across IMM. This is the case of mitochondrial complex II (CII) or succinate dehydrogenase complex which catalyzes the conversion of succinate to fumarate in the TCA cycle. During this reaction, electrons are transferred to form $FADH_2$ and, then, used to form ubiquinol, which eventually transfers the electrons to the CIII or ubiquinol-cytochrome *c* oxidoreductase complex. The electron transfer within CIII is done by the so-called Q cycle: one ubiquinol molecule binds to the outer CoQ site of CIII (Q_o) and donates one electron to the Rieske iron-sulphur protein (RISP) and the other electron is transferred, through hemes b_L and b_H intermediates, to another CoQ molecule placed in the inner ubiquinone site of CIII (Q_i), producing the semiquinone radical. RISP transfers the electron to the cytochrome c1 which, in turn, transfers it to the cytc. Through another Q cycle round, the semiquinone in Q_i is reduced to ubiquinol and another cytc is reduced. Besides, CIII pumps two proton ions in each Q cycle round, so oxidizing one molecule of NADH or $FADH_2$ implies pumping four proton ions by CIII. Finally, cytc is oxidized by the CIV or cytochrome *c* oxidase which, in turn, reduces oxygen into water and pumps four proton ions.

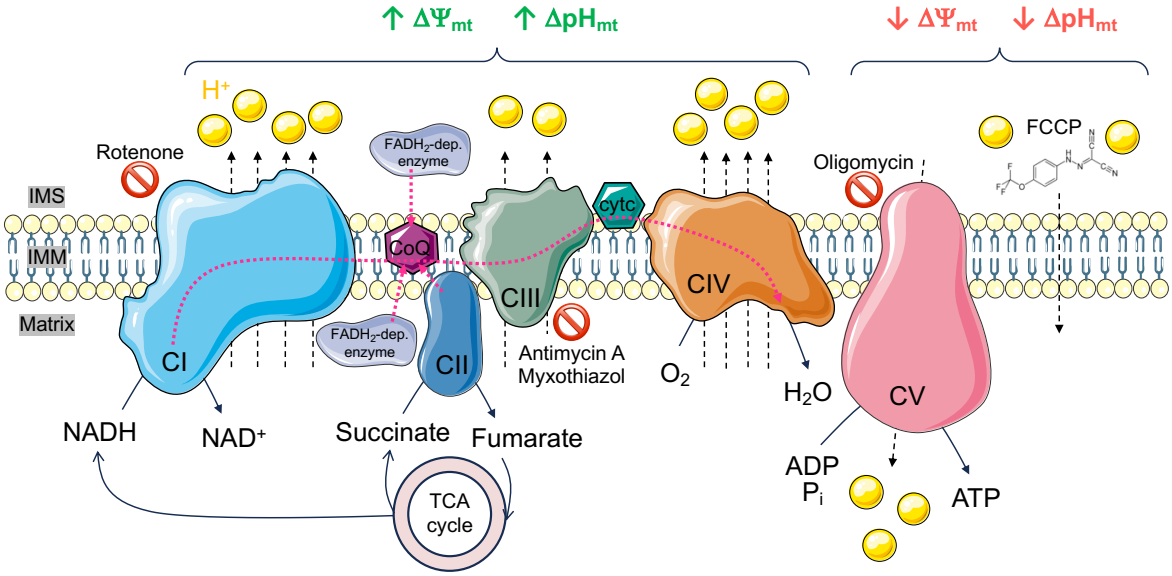

Figure 2. Scheme of OXPHOS system and forward electron transfer (FET). Electrons coming from CI, CII or other $FADH_2$-dependent enzymes at both side of IMM arrive to CoQ which transports them to CIII. Electrons are transported from CIII to CIV by cytc and CIV reduces oxygen to water using those electrons. During this electron transfer, CI, CIII and CIV pump protons from the matrix side to IMS and, thus, an increase in electrical gradient ($\Delta\Psi_{mt}$) and proton concentration gradient (ΔpH_{mt}) is induced between both sides of IMM. CV, by pumping protons back to matrix and, in turn, decreasing these gradients, phosphorylates ADP to produce ATP. FCCP (carbonyl cyanide-p-trifluoromethoxyphenylhydrazone) is an ionophore which transports protons to match their concentration at both sides of IMM; thus, FCCP is an uncoupler of OXPHOS system. Black dotted line means proton pumping, pink dotted line means electron transfer, line arrow means TCA cycle origin, triangle arrow means chemical reaction and prohibition sing means complex inhibitor (rotenone for CI, antimycin A for Q_i of CIII, myxothiazol for Q_o of CIII, and oligomycin for CV). Scheme made by using illustrations available on Elsevier Medical Art.

Then, the CV couples the translocation of three proton ions from the IMS to the mitochondrial matrix with ATP generation, approximately three protons per molecule of ATP formed. CV consists of two subcomplexes, the F_0, which is the rotor by which the proton ions are translocated, and the F_1, which phosphorylates the ADP. The movement of F_0 is also contributing to the negative curvature of IMM (Almendro-Vedia et al., 2021). Furthermore, CV is able to rotate in the other direction, hydrolyzing ATP and releasing proton ions to IMS from the mitochondrial matrix in healthy mitochondria (Acin-Perez et al., 2023).

2.2.1. Respiratory complexes superassembly

Except for CII, mitochondrial complexes assemble into supercomplexes, co-existing with individual complexes (Lapuente-Brun et al., 2013a). CIII is always in a dimeric form ($CIII_2$), which may be associated with CI ($CI+CIII_2$) or with CIV monomer/dimer ($CIII_2+CIV_{1-2}$, known as Q-respirasome) or with both CI and CIV ($CI+CIII_2+CIV_{1-2}$, known as N-respirasome). Besides, CIV and CV are found as monomers, dimers or multimers (Cogliati et al., 2016) and CI is usually forming supercomplexes due to its weak stability (Acín-Pérez et al., 2004). This wide range of possibilities provides plasticity and dynamism to the OXPHOS system. Indeed, changes on supercomplex abundancy and their composition depending on substrates (Zheng et al., 2023) or under stress (García-Poyatos et al., 2020) have been described.

Notably, supercomplexes increase the electron transport efficiency and, as a consequence, there is a decrease of ROS production (Calvo et al., 2020; Lapuente-Brun et al., 2013a; Maranzana et al., 2013). Thus, supercomplexes present their own CoQ and cytc pools (Calvo et al., 2020; Letts et al., 2019), allowing mitochondria to respond specifically to cellular requirements (Hernansanz-Agustín & Enríquez, 2021a). Accordingly, we have demonstrated that the superoxide burst in acute hypoxia is produced by an ineffective electron transfer between CII and CIII, due to a reduction in the IMM fluidity caused by the interaction of sodium ions with phospholipids, which slows down CoQ diffusion (Hernansanz-Agustín et al., 2020). As CI and CIII are forming supercomplexes, the electron transfer through CoQ between them is not affected by sodium ions (Hernansanz-Agustín et al., 2020). In addition, it has been recently demonstrated that CIII forms a complex with the Q reductase electron-transfer flavoprotein dehydrogenase and the Q-biosynthesis regulator COQ2 and, thus, electrons derived from lipid substrates reach CIII in a more effective way and, indeed, this complex is essential for muscle physiology (Herrero Martín et al., 2024). Therefore, OXPHOS system is not only involved in energy production energy, but it also participates in mitochondrial signaling.

2.3. Mitochondrial cation gradients

Apart from the OXPHOS system, the IMM presents a large number of transporters for substrates (Arnold & Finley, 2023), proteins (Priesnitz & Becker, 2018) and ions whose function is coupled to the mitochondrial potential ($\Delta\Psi_{mt}$) and, thus, to OXPHOS activity (Nicholls, 2008).

Regarding the mitochondrial cationic balance, potassium is known to maintain the mitochondrial volume, controlling the water content and, in turn, mitochondrial swelling (Garlid & Paucek, 2001). Potassium ions are imported into mitochondria through mitochondrial ATP-sensitive K^+ channel (mitoK$_{ATP}$) (Paggio et al., 2019) and are released to the cytosol by a low activity exchanger, the potassium/proton antiporter (KHE) (Jung et al., 1977). There are also voltage-dependent potassium channels, as well as calcium-activated or magnesium-inhibited channels (Laskowski et al., 2016), indicating the fine balance in potassium levels to maintain the $\Delta\Psi_{mt}$ and *vice versa*.

Due to its function as a cofactor in ATP-involved reactions (Ko et al., 1999) and as the main intracellular antagonist of calcium (Blomeyer et al., 2016), magnesium is another essential ion in mitochondrial metabolism (Pilchova et al., 2017). Indeed, dehydrogenases related to OXPHOS system and TCA cycle are known to be magnesium-dependent (Panov & Scarpa, 1996; Rodríguez-Zavala & Moreno-Sánchez, 1998; Yamanaka et al., 2016). Through the magnesium transporter Mrs2, magnesium ions are imported into mitochondria (Yamanaka et al., 2016) and its extrusion is performed by the sodium/magnesium exchanger SCL41A3, (Mastrototaro et al., 2016). Similar to calcium, magnesium is accumulated into mitochondria in a $\Delta\Psi_{mt}$ dependent manner (Shindo et al., 2011) and its release induces cytosolic effects (Shindo et al., 2010). Furthermore, magnesium dysregulations are known to be involved in several diseases (de Baaij et al., 2015). However, the understanding of magnesium dynamics is poorly understood, primarily because of the intertwined and overlapping pathways shared by magnesium and calcium, which make both signals difficult to distinguish, and the dominant calcium-centrism in cellular and mitochondrial biology.

2.3.1. Mitochondrial calcium signaling

Given its involvement and relevance in most cell signaling pathways, calcium may be considered “The Signaling King” and, in turn, its concentration and movement between cellular compartments are highly controlled. Thus, after an increase in cytosolic calcium ($_{i}Ca^{2+}$) concentration, calcium is quickly taken up by the intracellular stores, ER and mitochondria, to keep the resting $_{i}Ca^{2+}$ concentration around 100 nM (Rizzuto et al., 2009).

However, the increase in $_{i}Ca^{2+}$ can also trigger the calcium-induced calcium release mechanism by which calcium is released from ER, amplifying the $_{i}Ca^{2+}$ signal (Rizzuto et al., 2009). To avoid this $_{i}Ca^{2+}$ expansion and as mentioned earlier, MAMs are an essential part of calcium signaling between ER and mitochondria, allowing key calcium microdomains for cellular calcium signaling (Rizzuto et al., 1998).

Therefore, an increase in $_{i}Ca^{2+}$, imported from extracellular media or released from ER or both, is quickly translated to an increase in mitochondrial calcium ($_{m}Ca^{2+}$). This increase can vary among mitochondria, depending on their localization within cell, as elegantly demonstrated (Stoler et al., 2022). Calcium ions are mainly imported into mitochondrial matrix through the mitochondrial calcium uniporter complex (mtCU), a huge multiprotein channel located in the IMM and formed by: four subunits of mitochondrial calcium uniporter (3 MCU and 1 MCUB), their correspondent four subunits of essential mitochondrial response element (EMRE), the mitochondrial calcium uniporter regulator 1 (MCUR1) and one dimer of regulatory proteins of mitochondrial calcium uptake (MICU), formed by MICU1 with MICU2 or MICU3; summarized in **Figure 3** (Garbincius & Elrod, 2022). Driven by the $\Delta\Psi_{mt}$, mtCU mediates a rapid $_{m}Ca^{2+}$ uptake and, although MCU knock out (KO) models are viable and this ablation is protective in some scenarios, such as myocardial ischemia/reperfusion injury (Luongo et al., 2015) or Alzheimer's disease (AD) progression (Jadiya, Kolmetzky, et al., 2023), MCU is essential for maintaining skeletal muscle metabolism (Pan et al., 2013). However, MICU1 deletion in different species results lethal (Antony et al., 2016; Tufi et al., 2019), indicating MICU proteins have more functions apart from forming mtCU as showed (Tomar et al., 2023).

In addition to mtCU, other proteins have been demonstrated to allow $_{m}Ca^{2+}$ uptake (Garbincius & Elrod, 2022), such as the mitochondrial calcium/proton exchanger, LETM1 (leucine zipper and EF-hand containing transmembrane protein 1). Its sensitivity to calcium ions is higher than mtCU, mediating $_{m}Ca^{2+}$ uptake at lower $_{i}Ca^{2+}$ concentration, but it is also known to allow $_{m}Ca^{2+}$ efflux (Jiang et al., 2009).

Once inside mitochondrial matrix, $_{m}Ca^{2+}$ activates some TCA and OXPHOS proteins (Denton, 2009). It also accumulates with phosphate and other metals to form electrodense granules sensitives to matrix pH (Greenawalt et al., 1964), producing two interconvertible $_{m}Ca^{2+}$ pools. Indeed, we have demonstrated that these calcium phosphate precipitates take part in the response to acute hypoxia. After CI-dependent mitochondrial matrix acidification (Hernansanz-Agustín et al., 2017), the calcium-phosphate granules are partially dissolved into free calcium ions which activate NCLX (Hernansanz-Agustín et al., 2020). NCLX is the mitochondrial sodium/calcium exchanger that drives the main $_{m}Ca^{2+}$ efflux, as well as, the main mitochondrial sodium ($_{m}Na^{+}$) import, by exchanging one calcium ion per three sodium ions (**Figure 3**). In fact, NCLX is the rate-limiting step regarding $_{m}Ca^{2+}$ transients due to its

activity is much slower than $_{m}Ca^{2+}$ uptake mediated by mtCU (Palty et al., 2010). Thus, when the $_{m}Ca^{2+}$ efflux is insufficient or is unbalanced regarding $_{m}Ca^{2+}$ uptake and, consequently, an exacerbated amount of calcium is accumulated into mitochondria, situation known as $_{m}Ca^{2+}$ overload, the mitochondrial permeability transition pore (mPTP) is opened. This non-selective channel opening leads to cell death, due to mitochondrial swelling and its subsequent disruption (Garbincius & Elrod, 2022).

Therefore, NCLX has been thought as a powerful therapeutic target for human diseases driven by $_{m}Ca^{2+}$ overload. NCLX bibliography highlights its relevance in neuronal plasticity (Katoshevski et al., 2022) and learning (Stavsky et al., 2021), not only by enhancing neuronal survival (Rozenfeld et al., 2022) but also by regulating glycolysis in astrocytes (Cabral-Costa et al., 2023). Thus, the observed loss of NCLX expression in cortex samples from postmortem sporadic AD patients (Jadiya et al., 2019) aligns with results in neuronal NCLX KO mice that show an increased age-associated cognitive decline (Jadiya, Cohen, et al., 2023) which can be rescued by recovering NCLX-dependent $_{m}Ca^{2+}$ efflux (Jadiya et al., 2019). Furthermore, loss of NCLX expression has been observed in Friedreich ataxia models (Purroy et al., 2018) and the improvement of NCLX activity attenuates the pathological scenario in a mouse model of Parkinson's disease (Kostic et al., 2015). Apart from NCLX implication in neurological diseases, NCLX is known to be essential for heart viability (Luongo et al., 2017) and enhancement of NCLX activity diminishes heart remodeling after heart failure (Garbincius et al., 2022; Luongo et al., 2017). Furthermore, NCLX is involved upon thermogenesis in brown adipose tissue (Assali et al., 2020) and, regarding cancer, NCLX presents dual role in tumor growth and metastasis in a mouse model of colorectal cancer (Pathak et al., 2020).

Considering everything, due to its function as the main $_{m}Ca^{2+}$ exporter, NCLX has been demonstrated as the main character in some pathological situations and the enhancement of its activity has been verified as a beneficial treatment in some diseases.

2.3.2. Mitochondrial sodium signaling

Contrary to calcium, the role of sodium in cellular biology has been confined as a plasma membrane potential driver and, consequently, as bargaining chip for exchanging many molecules and ions. The potential role of sodium in signaling leads to considered it as "The Great Unknown", due to the limited number of studies in which it is considered.

Thanks to the sodium/potassium ATPase, responsible for maintaining the plasma membrane potential by importing two extracellular potassium ions while exporting three intracellular sodium ions (Kaplan, 2002), the cytosolic sodium concentration is kept around 8-10 mM (Murphy & Eisner, 2009; Nita et al., 2015). However, mitochondrial sodium ($_{m}Na^{+}$)

concentration is low due to the high activity of sodium/proton exchanger (NHE), which exports one sodium ion from mitochondrial matrix while imports one proton into it (Douglas & Cockrell, 1974; Murphy & Eisner, 2009). Although NHE's molecular identity still remains unknown, a recent study is pointing out that, independently to the other modules, the proton-pumping module (P-module) of CI presents NHE activity and, through it, a sodium gradient across the IMM is formed and is contributing to the $\Delta\Psi_{mt}$ (Hernansanz-Agustín et al., 2023). In line with this, the NHE activity of CI and its independence from its redox activity were also observed in isolated CI some years ago (Roberts & Hirst, 2012).

As mentioned above, $_{m}Na^{+}$ import is mainly mediated by NCLX, but, because of the technical difficulties for measuring sodium, it is usually ignored and, in turn, all NCLX-dependent effects are assumed to be just $_{m}Ca^{2+}$ efflux-dependent effects. However, we demonstrated that $_{m}Na^{+}$ import is the main character in the acute response to hypoxia. After NCLX activation, $_{m}Na^{+}$ ions interact with the phospholipids of the inner leaflet of IMM, decreasing the IMM fluidity and, eventually, inducing the hypoxic superoxide burst (Hernansanz-Agustín et al., 2020). Different research group found similar results and demonstrated that this sodium effect on OXPHOS system perturb T cells and induce a pro-inflammatory metabolism (Côrte-Real et al., 2023). Additionally, we have seen that sodium-dependent $_{m}Ca^{2+}$ efflux not only requires NCLX presence but requires the modulation of other mitochondrial proteins (Garbincius et al., 2023).

Therefore, NCLX activity appears to be essential for mitochondrial metabolism not only by preventing $_{m}Ca^{2+}$ overload, but also by controlling $_{m}Na^{+}$ movements (Assali & Sekler, 2021).

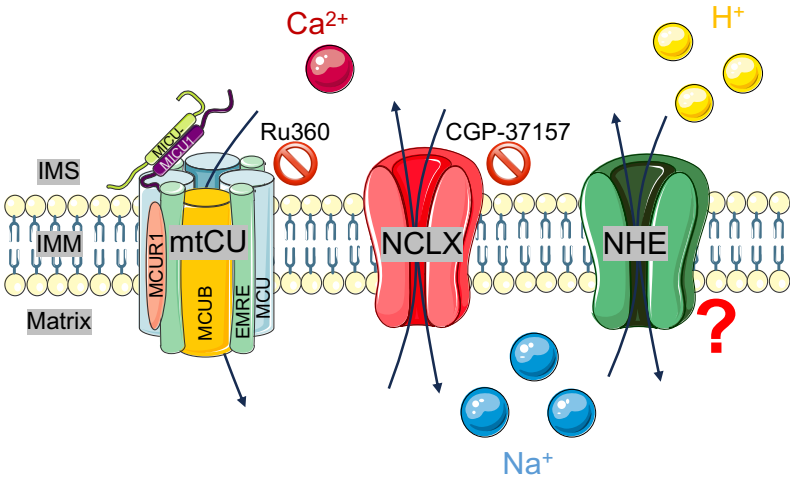

Figure 3. Scheme of NCLX activity and its related mitochondrial transporters. NCLX exports 1 mitochondrial calcium ion per 3 sodium ions imported into mitochondrial matrix. Then, sodium ions are exchanged with proton ions by NHE and calcium ions are again imported into mitochondrial matrix by mtCU. Question mark means that the molecular identity of NHE is unknown and prohibition sing means complex inhibitor (Ru360 for mtCU and CGP-37157 for NCLX). Scheme made using illustrations available on Elsevier Medical Art.

2.4. Mitochondria as a source of ROS

Due to respiration, mitochondria are the largest ROS producers in cells (Brand, 2016; Hernansanz-Agustín & Enríquez, 2021b). Flavin and quinone sites in ETC and other mitochondrial proteins handle unpaired electrons that may react with oxygen molecules, producing superoxide anions (Brand, 2016). Superoxide is quickly dismutated, being reduced into hydrogen peroxide (H_2O_2) and oxidized to oxygen, either spontaneously or by superoxide dismutases (Alvarez et al., 2022). H_2O_2 is the most studied ROS as a signaling molecule due to its relative instability, the fact that it can cross biological membranes and that it oxidizes thiols within cysteines (Alvarez et al., 2022). This last feature has been used to develop H_2O_2 detection tools and to understand the role of ROS production in cell signaling (Alvarez et al., 2022).

The major sources of ROS in mitochondria are CI and CIII (Brand, 2016; Hernansanz-Agustín & Enríquez, 2021b). During the forward electron transfer (FET, explained above), ROS production is low, and it is known to be produced by CI, the Q_o of CIII and 2-oxoglutarate dehydrogenase (Brand, 2016; Quinlan et al., 2013). However, during the reverse electron transport (RET) (**Figure 4**), larger amounts of ROS are produced (Robb et al., 2018) and it is an essential underlying mechanism for ROS production in physiological (Mills et al., 2016) and pathophysiological (Chouchani et al., 2014) conditions. RET occurs when CoQ ratio is over reduced by CII or other $FADH_2$-dependent enzymes together with mitochondrial hyperpolarization, so, in that situation, electrons are able to flow back through CI which, in turn, reduces NAD^+ to NADH and produces higher amounts of ROS (**Figure 4**). Thus, RET is the main source of ROS upon reperfusion due to the succinate accumulation during ischemia (Chouchani et al., 2014). In addition, and as explained above, we showed that $_mNa^+$ ions are able to modulate ROS production (**Figure 1**) by interfering electron transfer between CII or other $FADH_2$-dependent enzymes and CIII through IMM fluidity modification which alters CoQ diffusion (Hernansanz-Agustín et al., 2020). Thus, we hypothesize that $_mNa^+$ ions may be able to decrease ROS production by RET through the IMM fluidity impairment, contributing to the beneficial effect of NCLX-overexpression in some scenarios.

Altogether, mitochondrial ROS production is an indicative of the electron transfer efficiency and knowing the exact site of ROS source is essential for downstream consequences (Scialò et al., 2016).

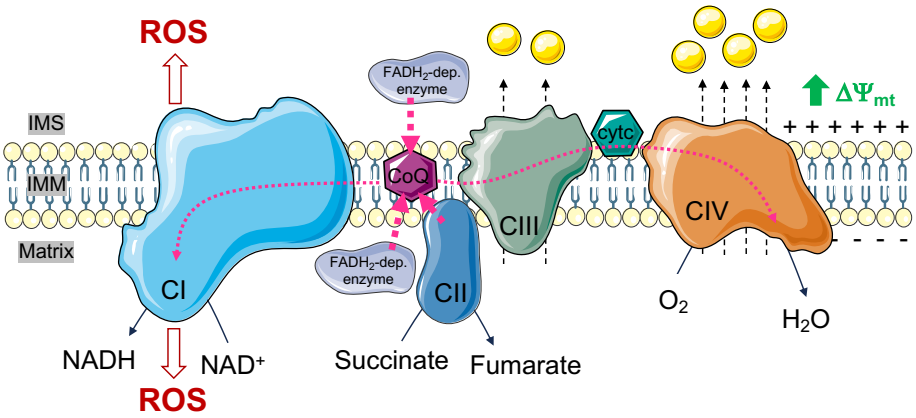

Figure 4. Scheme of ROS production by reverse electron transfer (RET). Accumulation of reduced CoQ due to CII and/or $FADH_2$-dependent enzymes together with mitochondrial hyperpolarization induce that electron flow within CI works in reverse mode, producing NADH from NAD^+ and ROS. Scheme made using illustrations available on Elsevier Medical Art.

Apart from mitochondria, other sources of ROS are present in cells. Some cytosolic enzymes, such as NADPH oxidases or monooxygenases, among others, have been shown to produce ROS and are essential for proper cellular signaling (Bae et al., 2011). Overall, ROS production is a normal and required event occurring in cells. Therefore, coupled to ROS production, cells present a whole system to buffer them (Alvarez et al., 2022). Superoxide dismutases reduce superoxide to H_2O_2, which is reduced to oxygen plus water by catalase or is incorporated into specific cysteine residues, within proteins or small peptides such as glutathione. The thioredoxin-thioredoxin reductase (Trx-TR) system and the glutaredoxin-glutathione reductase (Grx-GR) system reduce hydroperoxides from proteins and/or lipids (Alvarez et al., 2022) to maintain the correct cellular function. ROS levels and antioxidant systems are kept in a strict balance: ROS levels induce the antioxidant proteins expression and exogenous antioxidants can increase ROS production (Poljsak et al., 2013). Therefore, transient and controlled ROS bursts are necessary for cell signaling, but unbalanced or exacerbate ROS production may lead to cell damage and death.

3. Lithium in cellular biology

Lithium is the smallest alkali metal and is a good conductor of electricity and heat in its metallic form as well as a highly reactive element. However, after losing the outer electron, the two remaining electrons are in the 1s orbital, making lithium cation the least reactive of the alkali cations. This electron configuration also allows lithium to have the highest melting and boiling points. Although it was synthetized in The Big Bang, lithium is notably less abundant in the universe due to its relative nuclear instability which allows lithium to have important uses in nuclear physics, and industrial applications such as batteries.

In living organisms, lithium is bioaccumulated in plants, with the maximum amount that can be absorbed and the concentration of lithium that can be tolerated in the environment varying across different species (Bach & Gallicchio, 1990). Since lithium ions are soluble in water, it is found in the ocean water and, in turn, marine organisms tend to accumulate more lithium than terrestrial ones. The concentration of lithium in drinking water determines the blood lithium levels in healthy humans, which is consistently fall within the nanomolar (nM) range (Bach & Gallicchio, 1990). Additionally, the intracellular lithium concentration in erythrocytes from patients undergoing lithium treatment is known to be half of their blood concentration (Mendels & Frazer, 1973), but it is unknown in non-treated people. Thus, due to the detrimental effects on fertility showed in deliberately lithium-deprived animals (Pickett & O'Dell, 1992), lithium is considered an essential trace element, however, no human illness is known to be caused by lithium deficiency.

3.1. Historical perspective of lithium as a drug

Lithium was initially used to treat gout conditions associated with excessive uric acid, due to lithium carbonate's capacity to dissolve uric acid *in vitro*. This effect on uric acid, combined with the prevalent theories of the 1870s that connected uric acid levels in the brain to certain mental disorders, led some psychiatrists to recommend lithium bromide or carbonate for treating mental illness. However, by the early 1900s this hypothesis was abandoned (Shorter, 2009). Nonetheless, lithium salts became popular and were even included in a carbonated beverage marketed as a hangover remedy, which later became known as 7Up. After some reports about lithium toxicity, the United States' Food and Drugs Administration (FDA) restricted their uses but kept lithium salts as a supplement for low-sodium diets, resulting in some lethal cases. At that time, the psychiatrist John Cade analyzed the safety dose for lithium salts in guinea pigs and used it to demonstrate their beneficial effects in patients with mania (nowadays known as bipolar disorder (BD)) (Cade, 1949). John Cade's work was corroborated by other psychiatrists (Noack & Trautner, 1951;

Schou et al., 1954) leading to the establishment of the therapeutic range of lithium in plasma. Thus, lithium salts were widely approved as a treatment for BD and, currently, they are also used as a treatment for depression, schizophrenic disorders, and to prevent suicide, sometimes in combination with others drugs. Due to its toxicity and side effects, lithium blood concentration must be regularly controlled to keep it within 0.6 and 1.2 mM (Nolen et al., 2019) and always below 2 mM. Besides, lithium treatment is contraindicated during pregnancy (Harari et al., 2015) and in combination with some other drugs due to their interactions (Mahli et al., 2020).

3.2. Lithium's mechanism of action in cells

Lithium's mechanism of action is poorly understood. Like other metal cations, lithium interacts with membranes (Hauser & Shipley, 1981). However, the effect of lithium on these membranes is intermediate between that of other monovalent cations and the divalent cations calcium and magnesium (Hauser & Shipley, 1984). All these cations increase the membranes order (Hauser & Shipley, 1983), but lithium ions exhibit a unique affinity, penetrating more deeply into the membranes and altering their structure to a greater extend (Roux & Bloom, 1990). Nevertheless, by analyzing the effect of lithium in healthy erythrocytes at therapeutic concentration, it was shown that lithium ions alter the electrostatic interactions of molecules close to the membrane surface, improving their motion and slightly reducing the membrane surface anisotropy (Pettegrew et al., 1987). Also, it has been observed that the chronic therapeutic lithium treatment of rodent brain membranes modifies the lipid composition (López-Corcuera et al., 1988; Zanni et al., 2017), but the underlying mechanism remains obscure.

Regarding the cellular import, lithium ions generally use some sodium exchangers to get in and out of cells because both ions present the same charge (Jakobsson et al., 2017), but there is not any specific mechanism to control lithium transportation into cells. Indeed, lithium ions are reabsorbed in the kidney by the sodium-phosphate cotransporter (Uwai et al., 2014), keeping lithium inside the body, so the the kidney becomes one of the most sensitive organs to lithium toxicity (McKnight et al., 2012). Relating to the mitochondrial lithium transport, when the mitochondrial sodium/calcium/lithium exchanger (NCLX) was discovered, it was demonstrated to be sensitive to lithium ions (Palty et al., 2010), and the residues conferring its sensitivity have been described (Roy et al., 2017). However, lithium concentrations used in several studies are higher than lithium concentration in patients' blood and sometimes all sodium ions are replaced with lithium ions (Blaustein & Wiesmann, 1970; Palty et al., 2010; Roy et al., 2017; Rysted et al., 2021; Shalbuyeva et al., 2007; Stepanova et al., 2015); thus, it is unclear if NCLX is able to transport lithium at therapeutical

concentrations. For mitochondrial lithium ($_mLi^+$) efflux, even though it is not demonstrated yet, it is believed that sodium/proton exchanger (NHE) is able to mediate this function, despite it has been observed that lithium ions replace protons in the plasmatic NHE (Busch et al., 1995).

Table 1. **Comparison of ionic radius and blood concentration of lithium, sodium, magnesium and calcium.** *Lithium blood concentration measured in patients on lithium treatment.

Li^+	0.90 Å 0.6 – 1.2 mM*	Ionic radius Blood concentration	0.86 Å 0.75 – 1 mM	Mg^{2+}
Na^+	1.16 Å 140 mM	Ionic radius Blood concentration	1.14 Å 2.5 mM	Ca^{2+}

Once inside cells, lithium ions can replace magnesium ions as a cofactor in some enzymes, lowering their activities, because both present quite similar ionic radius (Jakobsson et al., 2017). Indeed, the best-known lithium function is to block glycogen synthase kinase 3 β (GSK3β), a magnesium-dependent enzyme, which is a central protein in cellular biology that controls several transcription factors (Grimes & Jope, 2001) through the phosphorylation of more than 100 substrates related to apoptosis, stress, inflammation or glutamate exicitotoxicity, among others (Beurel et al., 2015). Besides, GSK3β enzyme also presents different phosphorylation sites for its own regulation, so, the exact effect of lithium by blocking GSK3β and its consequence in different pathologies is hard to determine (Snitow et al., 2021).

3.3. Role of lithium in pathological scenarios

The beneficial effect of lithium in some mental disorders has been clearly demonstrated for years. Indeed, lithium is a well-known antidepressant and mood stabilizer drug as well as it is used to prevent suicides (Bschor, 2014). Therefore, several studies have tried to correlate lithium concentration in drinking water with the suicide rate, without reaching a solid conclusion (Ishii & Terao, 2018). Although lithium's mechanism of action in BD and its link with GSK3β are not robustly exhibited, lithium is known to be neuroprotective by increasing grey matter (Hajek & W. Weiner, 2016) and by inducing one of the most important neurotrophins, brain-derived neurotrophic factor (BDNF), even at a subtherapeutic concentration (De-Paula et al., 2016). Also, there are some additional mechanisms related to serotonin release (Treiser et al., 1981) or inositol metabolism (Kofman & Belmaker, 1993) that could be behind of some lithium-induced effects. Furthermore, it has been shown that the free intracellular calcium concentration of the BD patients is increased in platelets and lymphocytes compared to healthy individuals (Harrison et al., 2021). In addition, chronic

lithium treatment modulates intracellular calcium dynamics in B lymphocytes derived from both BD patients and healthy individuals (Wasserman et al., 2004). In line with this, due to the downregulation of some ETC proteins (Scaini et al., 2021), mitochondrial OXPHOS is known to be reduced in BD patients and lithium is able to enhance mitochondrial activity measured *ex vivo* in leukocytes from BD patients (de Sousa et al., 2015), but also, *in vitro* in human brain tissue (Maurer et al., 2009), specially related to mitochondrial complex I activity (Scola et al., 2014) and expression (X. Sun et al., 2006). These data suggest that mitochondrial dysfunction may be the cause and/or consequence underlying the severity and outcome in BD (Scaini et al., 2021).

Due to the neuroprotective properties of lithium, it has been also tested in stroke. Despite the small number of studies, it has been showed that stroke is less frequent in lithium chronic-treated patients (Almeida et al., 2022; Harrison & Luciano, 2021). Additionally, among stroke survivors, lithium treatment has been associated with potential imporvements in motor recovery (Mohammadianinejad et al., 2014) and verbal memory (Y. R. Sun et al., 2019). Accordingly, different timelines, methodological procedures, lithium concentrations and treatments in different animal models have been analyzed (Almeida et al., 2022). All these studies demonstrated that lithium treatment improves the pathological outcome, by decreasing stroke volume and apoptosis, increasing neurogenesis processes or improving the neurological score. However, results regarding lithium-induced GSK3β inhibition and its impact on stroke differ between studies (B. Chen et al., 2022; Doeppner et al., 2017), which could be explained by differences on the lithium treatments that were used. Also, although it is known that $_{m}Ca^{2+}$ overload is a powerful apoptosis inducer, none of these articles have analyzed whether calcium dynamics may be affected by lithium in stroke. Moreover, in a mouse model of mild traumatic brain injury, which associated with localized hypoxia, it has been observed that NCLX is upregulated in the hippocampus, suggesting a compensatory effect induced by increased $_{m}Ca^{2+}$ levels caused by the lesion (Mira et al., 2023). Therefore, it is plausible that the beneficial effects derived from GSK3β inhibition may be masking or enhancing additional effects of lithium directly on calcium dynamics and, in turn, mitochondrial metabolism.

Regarding neurodegenerative diseases, such as Alzheimer's disease (AD) or dementias, a reduction rate of cognitive decline has been observed with continued lithium treatment (Kessing et al., 2008; Nunes et al., 2007). Indeed, higher lithium levels in drinking water have been significantly correlated with lower levels of dementia (Kessing et al., 2017). In addition, AD patients treated with lithium have higher BDNF serum concentration which, in turn, was associated with a cognitive improvement (Leyhe et al., 2009). However, considering that magnesium levels in some regions of AD patients' brains are reduced (Andrási et al., 2005) and increased magnesium blood concentration has been

demonstrated to be protective in different mouse models of AD (W. Li et al., 2014; Xiong et al., 2022), it is paradoxical to state that the beneficial effect of lithium is due to GSK3β inhibition by replacing magnesium ions. Nevertheless, since one of the features of AD is $_{m}Ca^{2+}$ overload and NCLX sensitivity to lithium has been observed, lithium ions may be able to attenuate AD progression by improving $_{m}Ca^{2+}$ efflux through NCLX. The beneficial effect of NCLX-dependent $_{m}Ca^{2+}$ efflux enhancement has been demonstrated in other pathological conditions (Garbincius et al., 2022; Kostic et al., 2015) and, recently, it has been shown that AD progression is accelerated by impairing $_{m}Ca^{2+}$ efflux (Jadiya et al., 2019) and delayed by blocking $_{m}Ca^{2+}$ uptake (Jadiya, Kolmetzky, et al., 2023).

Apart from neurological diseases, it is known that lithium plays a role in the immune system too. The antiviral activity of lithium has been demonstrated for years (Bach & Gallicchio, 1990), including its beneficial effect during SARS-CoV-2 infection in patients (Spuch et al., 2022). It is considered to act by directly inhibiting viral replication, but also by inducing leukocytosis (Rybakowski, 2022). In addition, it is known that GSK3β inhibition reduces the production of pro-inflammatory cytokines and increases the production of anti-inflammatory cytokines (Martin et al., 2005). The same effect has been observed in many studies as a consequence of lithium treatment through *in vitro*, *in vitro* and *ex vivo* experiments reviewed in (Rybakowski, 2022). Moreover, as mentioned above, calcium dynamics and mitochondrial function are altered in leukocytes from BD patients and lithium has been demonstrated to modulate them.

Altogether it seems clear that subtherapeutic and/or therapeutic lithium treatment is beneficial in some pathological scenarios, yet it is evident that lithium's mechanism of action is a compendium of effects on different pathways. Moreover, while mitochondria are directly affected by lithium, no specific mechanism of action relating lithium to mitochondrial metabolism has yet been proposed.

HYPOTHESIS AND OBJECTIVES

The mitochondrial sodium/calcium/lithium exchanger (NCLX) has a fundamental role in mitochondrial functions regulation as it is the main mitochondrial calcium exporter as well as the mitochondrial sodium importer.

We have recently demonstrated that acute hypoxia signaling is mediated by NCLX activation, through its fundamental function as mitochondrial sodium importer. Recent studies of our group have also shown that acute inhibition of NCLX hampers the activation of mid-term responses to hypoxia mediated by activation of the HIF pathway through HIFα subunits stabilization. Therefore, we hypothesize that activation of the HIF pathway in response to hypoxia would be impaired in a cellular model of NCLX chronic deletion due to the hampering of mitochondrial ROS production.

In addition to importing sodium and exporting calcium from mitochondria, NCLX is known to be sensitive to lithium. Thus, we hypothesize that mitochondrial lithium import could have important effects on mitochondrial functions, especially in the acute response to hypoxia, either by direct mitochondrial effects of lithium import or by altering mitochondrial sodium import and/or mitochondrial calcium cycling.

According to these hypotheses, the main objectives of this Thesis are:

1. To elucidate the role of chronic deletion of NCLX in the activation of the HIF pathway in response to hypoxia, by:
    1.1. Evaluating HIF-1α stabilization in a cellular model of NCLX chronic deletion.
    1.2. Investigating the effect of hypoxia-induced ROS production on HIF-1α stabilization.

2. To investigate whether lithium ions affect mitochondrial functions, and if those effects depend on NCLX function, through:
    2.1. Studying mitochondrial redox signaling in response to acute hypoxia in presence of lithium.
    2.2. Analyzing the effect of lithium on different aspects of mitochondrial functions (calcium dynamics, respiration, ultrastructure, ROS production and membrane potential).

MATERIALS AND METHODS

1. Pharmacological inhibitors

Table 2. List of pharmacological inhibitors and their targets.

Inhibitor	Target
Antimycin A (AA)	Q_i of mitochondrial complex III (CIII)
BAY 60-7550 (Bay)	Phosphodiesterase 2 (PDE2)
CGP-37157 (CGP)	Mitochondrial sodium/calcium/lithium exchanger (NCLX)
DMOG	Prolyl hydroxylases (PHD)
Myxothiazol	Q_o of mitochondrial complex III (CIII)
Oligomycin	Mitochondrial complex V (CV)
Rotenone	Mitochondrial complex I
Ru360	Mitochondrial calcium uniporter complex (mtCU)

2. Cell culture and transfection

Mouse embryonic fibroblasts (MEFs, C57BL/6J *Slc8b1*$^{fl/fl}$) were provided by Dr. John W. Elrod (Temple University, Philadelphia, PA, USA) and were cultured at 37 ºC and 5% CO_2 in Dulbecco's Modified Eagle Medium (DMEM; which contains 4 mM L-glutamine and 4.5 g/L glucose) supplemented with 10% FBS, 100 U/mL penicillin and 100 µg/mL streptomycin. NCLX chronic ablation in *Slc8b1*$^{fl/fl}$ MEFs was obtained by infection with adenoviruses expressing Cre recombinase in cytomegalovirus vector (ad-CRE, Vector Biolabs), according to the manufacturer's instructions. Immortalization of MEFs was performed by retrovirus infection. 293T cells were transfected with 12 µg pCL-Ampho and 12 µg pBABE-SV40-puro using Lipofectamine RNA iMAX (Invitrogen). After two days, ½ dilution of 293T cell media with 8 µg/mL polybrene were added on MEF cultures for 4 h. Then, the infection was repeated, but adding 4 µg/mL polybrene overnight. The next day, the first infection was repeated and, after 4 h, MEFs media was replaced with fresh media. When MEFs grown enough to fulfill the plate, cell culture was expanded. One non-infected plate of MEFs was used as a comparative control though visual inspection.

Mouse adult fibroblasts (MAFs, C57BL/6J) were provided by Dr. José Antonio Enríquez (Centro Nacional de Investigaciones Cardiovasculares (CNIC), Madrid, Spain) and were cultured at 37 ºC and 5% CO_2 in DMEM (which contains 4 mM L-glutamine and 4.5 g/L glucose) supplemented with 10% heat-inactivated FBS, 100 U/mL penicillin and 100 µg/mL streptomycin.

FBalb cells were provided by Dr. José Antonio Enríquez (CNIC, Madrid, Spain) and were cultured at 37 ºC and 5% CO_2 in DMEM (which contains 4 mM L-glutamine and 4.5

g/L glucose) supplemented with 10% heat-inactivated FBS, 100 U/mL penicillin and 100 µg/mL streptomycin.

Primary culture of hippocampal neurons was done from 0-3 days old mouse pups (C57BL/6J Wild Type) as previously described (Gitler et al., 2004) and cells were cultured at 37 ºC and 5% CO_2 for 10-15 days before experimentation in Neurobasal-A medium supplemented with 5% heat-inactivated FBS, 2 mM glutamax, 100 U/mL penicillin and 100 µg/mL streptomycin. This culture was done by Dr. Maya Rozenfeld during my stay at Ben-Gurion University of The Negev (Beer Sheva, Israel).

AC16 human cardiomyocyte cell line was cultured at 37 ºC and 5% CO_2 in DMEM F12 supplemented with 12% heat-inactivated FBS and 100 U/mL penicillin and 100 µg/mL streptomycin. This culture was done during my stay at Temple University.

Transfection of 1 µg S468T NCLX (dominant negative NCLX form (dnNCLX), provided by Dr. Israel Sekler), human NCLX (pNCLX, Addgene) or pDsRed2-Mito, which encodes a red fluorescent protein targeted into IMM (mitoRFP, Clontech) vector DNA per 60 mm plates was carried out using Lipofectamine 2000 (Invitrogen) and opti-MEM (ThermoFisher), according to the manufacturer's specifications.

All cultures were routinely checked for mycoplasma contamination by DAPI (4',6'-diamidino-2-phenylindole) fluorescence test.

3. Detection of superoxide by fluorescence microscopy in fixed cells

These experiments were performed as we have described (Hernansanz-Agustín et al., 2021). Cells were seeded on glass coverslips and all the solutions for hypoxic treatments were pre-equilibrated to hypoxic condition by incubating them in the hypoxia chamber one day before experimentation. In some experiments, cells were treated with 1 mM LiCl, 10 µM antymicin A (AA), 1 µM myxothiazol, 1 or 10 µM rotenone or 10 µM 7-chloro-5-(2-chlorophenyl)-1,5-dihydro-4,1-benzothiazepin-2(3H)-one (CGP-37157, CGP from now on), and the treatment was maintained during the experiment.

Cells were introduced in an Invivo2 200 workstation (Baker Ruskinn) set at 1% oxygen, 5% CO_2, 37 ºC, and incubated for different times (0, 15, 30, 45 and 60 min) using the pre-equilibrated hypoxic medium. Then, cells were washed three times with Hank's balanced salt solution with Ca^{2+}/Mg^{2+} (HBSS+Ca/Mg) and incubated with 5 µM dihydroethidium (DHE) for 10 min in HBSS+Ca/Mg in darkness. Upon this incubation, cells were washed three times with HBSS+Ca/Mg and fixed inside the chamber by adding 4% paraformaldehyde (PFA) and incubating for 15 min at 4 ºC in darkness. After fixation, cells were again washed three times with HBSS+Ca/Mg and coverslips were placed on slides,

maintained at 4 ºC until analysis. The same protocol was used for normoxic conditions, but the incubations was performed in a standard cell incubator.

Three images per coverslip were taken in Leica SP-5 confocal microscope with 63x objective. The excitation was performed by using an argon/kripton laser for 515 nm and the fluorescence emission was recorded at 575-615 nm range. The images were quantified using ImageJ software. The quantification for MEFs experiments was done bysetting the same threshold for all images and obtaining the mean value from the histogram of each image. The mean value of each image from the same coverslip was averaged and the obtained number was treated as one replicate. On the other hand, the quantification for FBalb cells was done by measuring fluorescence of selected regions of interest (ROIs) in each image and the average of the value of ROIs for each condition was calculated; this obtained number was treated as one replicate.

4. Detection of inner mitochondrial membrane potential by live imaging fluorescence microscopy

These experiments were carried out in the Hospital de La Princesa, using a Leica SP-5 confocal microscope, with an automated stage for live imaging and temperature and gas control; and were performed as we have described (Hernansanz-Agustín et al., 2020).

To detect inner mitochondrial membrane (IMM) potential, cells were seeded in 8-well plates (#155411, ThermoFisher) and the next day the experiment was performed. Before the experiment, cells were washed three times with HBSS+Ca/Mg and then DMEM FluoroBrite was added with 20 nM tetramethylrhodamine methyl ester (TMRM). After 30 minutes of dark incubation at 37 ºC, cells were washed three times with HBSS+Ca/Mg, DMEM FluoroBrite with 20 nM TMRM was added and cells were placed into the microscope. Planes were focused and images were taken with a 63x objective every 5 minutes. The experiments started at 20% O_2 and 5% CO_2, and after some normoxic images were taken, then O_2 concentration was switched to 1%, allowing the quantification of the same cells during normoxia and hypoxia. The excitation was performed by using an argon/krypton laser for 488 nm and the fluorescence emission was recorded at 505-535 nm range. Calibration was achieved in situ using 1 µM oligomycin A and, then, 1 µM carbonyl cyanide 4-(trifluoromethoxy) phenylhydrazone (FCCP).

Images were quantified with ImageJ software, selecting the same ROI for each time point. At least 3 different ROIs were selected for each condition, averaging them for a replicate, and a minimum of 4 independent experiments were performed.

5. Detection of cytosolic basal ROS levels

These experiments were done by Dr. Pablo Hernansanz-Agustín at CNIC. MAFs and MEFs were transfected with the cytosolic version of Hyper7 (Pak et al., 2020). Cells were washed with phosphate-buffered saline (PBS) and maintained with HBSS + Ca/Mg. The plate was placed into a Leica SP-5 confocal microscope with an automated stage for live imaging and with temperature and gas control, which were maintained at 37 ºC and 5% CO_2. Cells were allowed to stabilize for 20 min with the new medium in the microscope stage. The objective used was ×63 and excitation was performed with a 405 diode laser for the 405 nm line and an argon/krypton laser for the 488 nm line. Fluorescence emission was recorded at 515–535 nm range and images were quantified with Image J software.

6. Detection of mitochondrial calcium dynamics in permeabilized cells by high-resolution spectrofluorometer

During my stay at Dr. John W. Elrod laboratory at Temple University (Philadelphia, USA), we performed these experiments as described in (Garbincius et al., 2023; Luongo et al., 2017) with the kind support of Dr. Joanne F. Garbincius and Henry M. Cohen.

Four million of AC16 cells were used for each measurement. Cells were centrifuged, washed with fresh medium and centrifuged again. Then, cells were resuspended in 0.5 mL of ice-cold extracellular-like Na^+- and Ca^{2+}-free buffer, which contains (in mM): 120 sucrose, 5 KCl, 1 KH_2PO_4, 0.1 2,2',2'',2'''-(ethane-1,2-diyldinitrilo)tetraacetic acid (EDTA), 20 2-[4-(2-hydroxyethyl)piperazin-1-yl]ethanesulfonic acid (HEPES), with pH adjusted to 7.4 with KOH. After 5 min on ice, cells were centrifugated and resuspended in 0.5 mL permeabilization buffer at 37 ºC, which contains: 120 mM KCl, 10 mM NaCl, 1 mM KH_2PO_4, 20 mM HEPES, 6 µM thapsigargin, 80 µg/mL digitonin, 1x EDTA-free protease inhibitor cocktail with pH adjusted to 7.2 with KOH and cleared with Chelex 100 to remove trace calcium.

While preparing cells, the assay cuvette was prepared adding one micro magnetic stir bar, 0.5 mL of 37 ºC permeabilization buffer, 1 µM Fura-FF, 4.8 µM JC-1, 5 mM succinate and, in some experiments, 10 µM CGP, 1 µM rotenone or 1 mM LiCl. The cuvette was placed into the spectrofluorometer chamber to maintain it al 37 ºC.

Next, the 0.5 mL containing the cells were added to the assay cuvette in the spectrofluorometer chamber, bringing the total volume in the cuvette to 1 mL, and immediately the recording was started.

After 350 s, using a Hamilton syringe, a bolus of 10 µM $CaCl_2$ was injected through the spectrofluorometer injection port into the cuvette, without stopping the assay recording. After 250 s, at time = 600 s, using a Hamilton syringe, 10 µM Ru360, the mitochondrial calcium uniporter complex (mtCU) inhibitor, was injected through the spectrofluorometer injection port into the cuvette, without stopping the assay recording. Finally, after 250 s, at time = 850 s, the recording was paused, the spectrofluorometer lid was opened and 10 µM FCCP was added directly into the cell suspension in the assay cuvette. Quickly the spectrofluorometer lid was closed and the recording was continued.

Fura-FF fluorescence was excited at 340 nm and 380 nm and recorded at 535 nm. The ratio was calculated as emission from 340 nm excitation / emission from 380 nm excitation. Then, the mean from the 5 seconds before time = 300 s were used to calculate the initial fluorescence ratio (R_0) and all the data were divided by it. The area under the curve (AUC) was calculated with Prism8 software, using 1 as baseline and from 350 s to 600 s for $CaCl_2$ bolus injection and from 600 s to 850 s for Ru360 injection. The slope after Ru360 injection was calculated with Prims8 software, taking the 50 seconds after Ru360 injection.

7. Detection of mitochondrial calcium in primary neurons culture by live imaging fluorescence microscopy

These experiments were carried out during my stay at Dr. Israel Sekler laboratory at Ben-Gurion University of The Negev (Beer Sheva, Israel) and were performed as described (Rozenfeld et al., 2022) with the kind support of Dr. Maya Rozenfeld and Nadezca Dadic.

Each mouse hippocampus was used to generate culture on 6 coverslips with 50,000-70,000 cells. Cells were preloaded with rhodamine-2 acetoxymethyl (Rhod2, Biotium) at 1 µM concentration for 30 min at room temperature using Ringer's solution which contains (in mM): 126 NaCl, 5.4 KCl, 0.8 $MgCl_2$, 20 HEPES, 1.8 $CaCl_2$, 15 glucose, with pH adjusted to 7.4 with NaOH. After loading, cells were thoroughly washed in fresh dye-free Ringer's solution for 30 min.

At the beginning of each experiment, cells were perfused with Ringer's solution. To trigger ionic response, cells were perfused with high K^+ Ringer's solution (high K^+, which contains in mM: 70 NaCl, 50 KCl, 0.8 $MgCl_2$, 20 HEPES, 1.8 $CaCl_2$, 15 glucose, with pH adjusted to 7.4 with NaOH) during 47 s. Then, the initial Ringer's solution was perfused until the end of the experiment.

In some experiments, after 10 minutes cells were perfused with Ringer's solution containing 1 mM LiCl and, after 10 min, lithium-free high K^+ solution was administered as described. Then, Ringer's solution with lithium was perfused again. In some experiments,

cells were pretreated with BAY 60-7550 (Bay, #sc-396772A, Santa Cruz) at 1 μM concentration for 30 min at room temperature along with rhodamine-2 acetoxymethyl (Rhod2) preloading and Bay was added to Ringer's solution during the experiment, except the high K^+ solution.

Mitochondrial calcium imaging was performed on an imaging system consisting in an Olympus IX73 inverted microscope and Cellsense division 1 Olympus software (Wendenstrasse, Hamburg, Germany), CooLed 4000 LED monochromator, Q imaging cooled Retiga 6000 camera (Surrey British Columbia, Canada) and 20x objective. Rhod2 was excited at 552 nm wavelength light and imaged with a 570 nm-long pass filter as previously described (Kostic et al., 2015). Somas and dendrites were selected as ROIs and fluorescence traces were analyzed using MATLAB software for selecting the slopes by blind analysis, as described (Rozenfeld et al., 2022).

8. Fluorescence recovery after photobleaching experiments

These experiments were carried out in the Hospital de La Princesa, using a Leica SP-5 confocal microscope, with an automated stage for live imaging and temperature and gas control, and were performed as described (Hernansanz-Agustín et al., 2020).

MEFs were transfected with pDsRed2-Mito vector which encodes a red fluorescent protein targeted into IMM (mitoRFP) two days before the experimentation and, the next day, cells were seeded in 8-well plates. Before the experiment, cells were washed three times with HBSS+Ca/Mg and DMEM FluoroBrite was added. The plate was placed into the microscope, the planes were focused and images were taken with a 63x objective with 13x zoom.

An argon/krypton laser was used for excitation at 514 nm and the fluorescence emission was detected in the 565-595 nm range. Images were recorded using TSC software (Leica). MitoRFP was scanned five times and then bleached using 15 scans at 40% laser power. 60 scans every one second were recorded to image the recovery of fluorescence intensity after photobleaching. Fluorescence recovery after photobleaching (FRAP) experiments were performed in normoxic condition (20% O_2 and 5% CO_2) and then, O_2 was switched to 1% for hypoxic condition. 15 minutes after hypoxia was started, the experiments were done. 1 mM LiCl was added in some wells in both conditions. At least five FRAPs were done per condition per experiment and five independent experiments were performed.

9. Mitochondrial network analysis

These experiments were carried out in the Hospital de La Princesa, using a Leica SP-5 confocal microscope, with an automated stage for live imaging and temperature and gas control.

As explained in the previous section, MEFs were transfected with pDsRed2-Mito vector two days before the experimentation and, the next day, cells were seeded in 8-well plates. Before the experiment, cells were washed three times with HBSS+Ca/Mg and then DMEM FluoroBrite was added. The plate was placed into the microscope and images were taken in normoxic condition (20% O_2 and 5% CO_2) and then, O_2 was switched to 1% for hypoxic condition. 15 minutes after hypoxia was started, images were taken. 1 mM LiCl was added in some wells in both conditions.

The planes were focused and images were taken with a 63x objective with 6x zoom. An argon/krypton laser was used for excitation at 514 nm and the fluorescence emission was detected in the 565-595 nm range. Images were taken and were analyzed using ImageJ software as described in the scheme of Figure 1 in (Valente et al., 2017). Then, the number of branches of the largest network and the number of branches of the second largest network were selected from the result of analysis from each image. At least four images were taken per condition per experiment and five independent experiments were performed.

10. Measurement of oxygen consumption

10.1. Measurement of oxygen consumption in whole cells

These experiments were performed as described (Hernansanz-Agustín, 2017; Hernansanz-Agustín et al., 2020). The oxygen consumption rate (OCR) was measured using an XF24 Extracellular Flux Analyzer (Seahorse Bioscience). First, we performed experiments for analyzing the confluence and cell growth, selecting the conditions herein described. One day before the experiment, MEFs, 6 x 10^4 per well, were seeded in the special 24-wells plate, half plate was used for NCLX WT MEFs and the other half for NCLX KO MEFs. Before the experiment, cells were preincubated with unbuffered DMEM supplemented with 25 mM glucose, 1 mM pyruvate and 2 mM glutamine for 1 hour at 37 ºC in an incubator without CO_2 regulation. OCR measurements were programmed with successive injections of unbuffered DMEM with or without 1 mM LiCl, 1 µM oligomycin A, 300 nM FCCP and, the last one, 1 µM rotenone and 1 µM antimycin A. After the experiment

were finished, as proliferation and cell growth may vary after plating, the plate was transferred to ice, washed twice with precooled PBS and cells were disaggregated using 25 µL RIPA Buffer (50 mM Tris-HCl at pH 8.0, 150 mM NaCl, 1 mM EDTA, 0.1% Triton X-100, 0.1% sodium deoxycholate) per well. Then, protein concentration was quantified by the bicinchoninic acid (BCA) assay to normalize the OCR.

After measuring basal respiration for three cycles, unbuffered DMEM with or without 1 mM LiCl was added, to check if lithium treatment was able to affect basal respiration. After completing four cycles, oligomycin was injected to inhibit mitochondrial respiration by blocking the mitochondrial ATP synthase. Consequently, the quantity of oxygen utilized in ATP production through oxidative phosphorylation (OXPHOS) is estimated from the difference with basal oxygen consumption, known as coupling efficiency. By moving H^+ ions from the intermembrane space to the matrix, FCCP disrupts OXPHOS, leading to an increased flow of electrons through the electron transport chain (ETC) and achieving the maximum respiration rate. This experimental approach provides insights into the stored energy within mitochondria that cells can utilize during times of high energy demand or stress, known as reserve capacity. Antimycin A and rotenone block CIII and CI, respectively, and, thus, inhibit the flow of electrons through the ETC and prevent proton ion translocation. Consequently, any remaining oxygen consumption is attributed to non-mitochondrial respiration, which represents the oxygen consumed by other enzymes within the cell.

10.2. Measurement of oxygen consumption in permeabilized cells

These experiments were carried out during my stay at Dr. John W. Elrod laboratory at Temple University (Philadelphia, USA) and were performed as described (Salabei et al., 2014) with the kind support of Dr. Andrew A. Gibb.

OCR was measured using an XF96 Extracellular Flux Analyzer (Seahorse Bioscience). After some experiments for analyzing the confluence and cell growth, two days before the experiment cardiomyocytes AC16 cells were seeded in the special 96-wells plate (8,000 cells per well which proliferated until getting a monolayer in each well). Before the experiment, cells were incubated for 1 hour at 37 ºC in an incubator without CO_2 regulation. Then, medium was replaced by mannitol and sucrose (MAS) buffer (containing 70 mM sucrose, 220 mM mannitol, 10 mM KH_2PO_4, 5 mM $MgCl_2$, 2 mM HEPES and 1 mM EGTA, adjusted to pH 7.2 with KOH) supplemented with fatty acid-free bovine serum albumin (BSA) 4 mg/mL, 25 µg/ml digitonin and 0.5, 0.75 or 1 mM LiCl in some wells, depending on each experiment. OCR measurements were programmed with successive injections of substrates dissolved in MAS-BSA buffer (final concentrations in wells were 1 mM ADP, 5 mM pyruvate and 2.5 mM malate for CI or 1 mM ADP and 10 mM succinate with or without

1 μM rotenone for CII), 1 μM oligomycin A, and, the last one, 1 μM rotenone and 10 μM antimycin A. Due to the BSA presence during the experiments and the small size of wells, we could not normalize the OCR data with the protein quantification assay.

Regarding OCR protocol, one measurement of oxygen consumption was done before injections and, then, two measurements were done after each injection. The first injection corresponded to respiration substrates; then, oligomycin and, finally, antimycin A plus rotenone. Thus, after substrates' injection, the oxygen consumption increases and, after oligomycin, oxygen consumption decreases again, due to ATP synthase inhibition. Therefore, we have analyzed OCR before substrates' injection, after substrates' injection (corresponding to respiration state 3) and after oligomycin injection (comparable to respiration state 4). Respiration state 3 is the ADP-induced oxygen consumption in isolated mitochondria in presence of substrate/s and respiration state 4 is the oxygen consumption after ADP has been consumed. Through dividing state 3 by state 4, the respiratory control ratio (RCR) is calculated, measurement that is proportional to mitochondrial coupling.

11. Mitochondrial isolation

Mitochondria were isolated from MEFs as described (Lapuente-Brun et al., 2013a). One day before the experiment, MEFs were seeded on 150 mm plates so the day of the experiment they were around to 80% of confluency. After treating cells according to each experiment, plates were transferred to ice and cells were washed twice with precooled PBS. From now on all the protocol was done at 4 ºC to prevent any enzymatic activity. Cells were split up using a scraper in 1 mL PBS and were centrifuged at 2,000 g for 5 min. The supernatant was discarded and cells were resuspended in 1.5 mL buffer A (320 mM sucrose, 10 mM Tris-HCl and 1 mM EDTA, and pH 7.4 only adjusted using 37% HCl). Cells were disrupted using a glass Potter Elvehjem homogenizer. The homogenate was centrifuged at 1,200 rpm for 10 min, to discard cells not broken, and the supernatant was again homogenized. The homogenate was centrifuged at 12,000 rpm for 15 min and the resulting pellet corresponds to the mitochondria-containing fraction. Depending on the experiment, the pellet was stored on -80 ºC or directly used.

12. Measurement of sodium in isolated mitochondria

These experiments were performed as described (Hernansanz-Agustín et al., 2020). Mitochondria were isolated as described above and resuspended in Mili-Q water. First, the protein amount was quantified by BCA analysis. Then, samples containing 5 ug of

mitochondrial protein from each condition were used to measure sodium, by using the ratiometric probe sodium benzofuran isophthalate tetra-ammonium salt (SBFI) at 1 µM final concentration. 96-well black microplates with transparent bottom were used to ensure fluorescence isolation for each well. Samples and SBFI were mixed into each well in darkness and the plate was quickly centrifugated to descend the liquid to the bottom. Then, the plate was transferred to a CLARIOstar Microplate Reader (BMG Labtech) and the recording the fluorescence with excitations at 340 nm and 380 nm and emission at 520 nm. Ratio 340/380 was calculated and, through a calibration curve, the grams of sodium were quantified and plotted.

13. Measurement of lithium in isolated mitochondria by inductively coupled plasma mass spectrometry

This measurement was carried out by Teresa Benito in the Unidad de Técnicas Geológicas at Universidad Complutense de Madrid.

Isolated mitochondria were resuspended in (v/v) nitric acid (HNO_3) and hydrogen peroxide (H_2O_2) and were kept at 40 ºC during three days. After mitochondria were disaggregated, lithium content was measured using the inductively coupled plasma mass spectrometry (ICP-MS, aurora Elite model from BRUKER).

14. Measurement of lithium, sodium and calcium in isolated mitochondria by graphite furnace atomic absorption spectrometry

These measurements were performed by Dr. Beatriz Gómez Nieto in the Departamento de Química Analítica y Análisis Instrumental at the Facultad de Ciencias from the Universidad Autónoma de Madrid.

Isolated mitochondria were resuspended in Mili-Q water and 10 µL were used to quantify protein. Then, 1% (v/v) HNO_3 was added into the mitochondrial homogenate. Some previous experiments were performed to select the temperatures and wavelengths for determining lithium, sodium and calcium. The determination was performed with a ContrAA 700 HR-CS AA spectrometer (Analytik Jena). This spectrometer is equipped with a transversely heated graphite furnace atomization unit and an MPE 60 liquid furnace autosampler (Analytik Jena).

15. Infrared spectroscopy experiments

These experiments were done by our collaborators Dr. Susana Carregal-Romero and Dr. Jesús Ruiz-Cabello in the CIC biomaGUNE (Donostia – San Sebastiáin, Spain).

Egg phosphatidyl choline (PC) liposomes were prepared using the thin-film hydration method followed by extrusion with filters of decreasing diameter (400, 200 and 100 nm) (H. Zhang, 2017). Lipids were hydrated with water with minimal metal impurities (Optima LC/MS Grade, Fisher Chemical). Liposomes were concentrated by filtration up to 72 mg/mL of lipid content. Lipid concentration was determined through the Rouser assay (Rouser et al., 1970). Sodium or lithium salt was mixed and incubated at 37 °C (for 2 h) with the liposomes. Fourier-transform IR spectra of liposomes and liposomes incubated with alkali metals were collected afterwards with a Nicolet 6700 Fourier-transform infrared (IR) spectrometer (Thermo Scientific) in transmission mode in liquid samples. All experiments were performed in triplicate.

16. Western blot analysis

The sample collection protocol depends on the target protein to analyze (see following sections 16.1., 16.2. and 16.3). The same amount of protein for each sample was diluted in reducing or non-reducing Laemmli buffer, which contains 50 mM Tris-HCl pH 7.6, 2 mM EDTA, 1% sodium dodecyl sulphate (SDS), 10% glycerol, 0.02% bromophenol blue; for reducing Laemmli buffer, 5% 2-mercaptoethanol was added freshly. Next, samples were boiled at 95 ºC for 10 min. Then, samples were loaded into 10% or 12% polyacrylamide gels using SDS and Tris-Gly Laemmli buffers so that proteins were separated mainly according to their molecular mass by electrophoresis. Proteins were transferred to polyvinylidene difluoride (PVDF) membranes, previously activated in pure methanol. Membranes were blocked for 1 hour with blocking buffer (5% non-fat milk powder in Tris-buffered saline (TBS) with 1% Tween20). Then, membranes were incubated overnight at 4 ºC with the primary antibodies (#10006421 Cayman Chemical for HIF-1α, #A3854 Sigma Aldrich for actin, #ab41906 Abcam for PRDX1, #ab110413 Abcam for total OXPHOS rodent antibody cocktail, #sc-32233 Santa Cruz for GAPDH and #sc-13156 Santa Cruz for cytochrome *c*), which were diluted at a concentration indicated by the manufacturer in 0.4% BSA in TBS with 1% Tween20. After primary antibody incubation, membranes were washed three times for 10 min each time with washing buffer (TBS with 1% Tween20). Then, membranes were incubated with, according to primary antibody, species-specific secondary antibodies labeled with horseradish peroxidase (HRP) (rabbit polyclonal anti mouse #P0260

Dako or donkey polyclonal anti rabbit #NA934V GE Healthcare) in washing buffer at room temperature for 1 hour. After, membranes were washed three times with washing buffer. HRP substrate and enhancer (Immobilon Crescendo Western HRP Substrate, WBLUR0500, ThermoFisher) were added and, using a digital luminescence image analyzer (Fujifilm LAS-4000), chemiluminescence was visualized. Images were quantified using ImageQuant TL7.0 software, applying a rolling ball method for subtracting the background and with supervised band detection and quantitation. Each band was relativized by its corresponding loading control (β-actin detection in each lane) and the ratio was plotted.

16.1. Sample collection for HIF-1α detection by Western blot

Cells were seeded the day before the experimentation to get for experimentation around to 80% of confluency. After treating cells according to each experiment, plates were transferred to ice inside the hypoxia chamber or from the normoxia incubator, cells were washed twice with precooled PBS and cells were disaggregated using RIPA. Then, protein concentration was quantified by BCA assay and the amount needed was diluted in reducing Laemmli buffer.

16.2. Sample collection for peroxiredoxin 1 detection by Western blot

The main aspect to consider for peroxiredoxins detection is their high reactivity to H_2O_2 through their peroxidatic and resolving cysteines (Alvarez et al., 2022), so it is essential to avoid any further oxidation during sample collection which can manipulate the results. Hence, a cysteine blocking buffer (blocking buffer from now on) was prepared as described (Cox et al., 2010), briefly:

- Sodium phosphate (NaPi) buffer, which contains (in mM): 80 Na_2PO_4, 0,1 diethylenetriaminepentaacetic acid (DTPA, a metal chelating compound to bind iron ions and, thus, prevent further oxidations during sample collection) and 20 NaH_2PO_4, with pH adjusted to 7.4.
- 10 µg/mL catalase was added in fresh to NaPi buffer to delete any H_2O_2 traces which NaPi buffer may contain.
- After 30 min of catalase addition, 100 mM N-ethylmaleimide (NEM, which reacts with thiols and, thus, with reduced cysteines, preventing further oxidations during sample collection) must be added in fresh to NaPi buffer with catalase.

Cells were seeded the day before the experimentation to get for experimentation around to 80% of confluency. After treating cells according to each experiment, plates were

transferred to ice and cells were washed twice with precooled blocking buffer. Then, cells were split up using a scraper in the last wash volume and were centrifuged at 2,000 g for 5 min at 4 ºC. The supernatant was discarded and cells were resuspended by pipetting in lysis buffer, which is blocking buffer with 1% 3-[(3-cholamidopropyl)dimethylammonio]-1-propanesulfonate (CHAPS), 1% SDS and 1X protease inhibitor. Next, samples were incubated for 30 min at room temperature, allowing NEM to block all remaining cysteines. Then, protein concentration was quantified by BCA assay and was divided for diluting in non-reducing Laemmli buffer for PRDX1 dimers detection or reducing Laemmli buffer for total PRDX1 detection.

16.3. Sample collection from permeabilization assay

These experiments were carried out during my stay at Dr. John W. Elrod laboratory at Temple University (Philadelphia, USA) and were performed as described (Salabei et al., 2014).

The purpose of these experiments was to determinate the digitonin concentration needed to permeabilize cells without disrupting mitochondria, in order to perform Seahorse experiments in permeabilized cells (see previous section 9.1). Therefore, AC16 cells were seeded two days before the experimentation until getting a monolayer. Cells were treated with different digitonin concentrations diluted in BSA-MAS buffer (in µg/ml: 0, 10, 25, 50, 75, 100 and 150) during 30 minutes at 37 ºC and 5% CO_2. After incubation, cells were transferred on ice, washed twice with pre-cooled PBS and disaggregated with RIPA.

17. Statistical analysis

Data are plotted as mean with standard error of the mean (SEM) and the number of independent experiments as well as the statistical analysis used is indicated in each figure.

Kolmogorov-Smirnov test was used to assess the distribution of the population. When data were not normally distributed non-parametric tests were used (Kruskal-Wallis and post hoc pair-wise comparisons with Dunn test). When normality was assumed, one-way or two-way analysis of variance (ANOVA) were performed, depends on each experiment. For data that were normally distributed, we used a standard parametric post hoc test (Tukey's test). For two-group comparisons, data were analyzed using Student t test when they were normally distributed, and the Mann-Whitney U test was run if data did not pass the assumptions for parametric analyses.

Statistical analysis and plotting were performed with GraphPad Prism 8 software.

RESULTS

1. NCLX activity is implied in HIF-1α stabilization depending on cellular ROS context

Although PHDs are inhibited when oxygen availability is decreased and, thus, HIF-1α stabilization is induced (Kaelin & Ratcliffe, 2008), there are other non-canonical pathways that induce HIF-1α stabilization, associated or not to changes in the oxygen concentration (Iommarini et al., 2017). Indeed, HIF-1α stabilization has been linked to mitochondrial activity and ROS production even before the role of pVHL and PHDs were stablished (Chandel et al., 1998). Besides, mitochondrial ROS have been shown to increase during the first minutes of hypoxia (Hernansanz-Agustín et al., 2014), involving the respiratory complexes I and III (Brunelle et al., 2005; Chandel et al., 2000; Guzy et al., 2005; Hernansanz-Agustín et al., 2017; Mansfield et al., 2005). We recently demonstrated that this hypoxic ROS burst production was caused by NCLX activation (Hernansanz-Agustín et al., 2020), so we decided to analyze the role of NCLX on HIF-1α subunits stabilization and activation of the HIF pathway.

1.1. NCLX inhibition does not prevent HIF-1α stabilization in mouse embryonic fibroblasts

Previous analysis from our research group pointed out that the acute NCLX inhibition, using its pharmacological inhibitor 7-chloro-5-(2-chlorophenyl)-1,5-dihydro-4,1-benzothiazepin-2(3H)-one (CGP-37157, CGP from now on) or a small interference RNA (siRNA) against NCLX, blocked the hypoxic HIF-1α stabilization in different cell types, including mouse hippocampal slices (Hernansanz-Agustín, 2017). However, the chronic ablation of NCLX has been demonstrated to induce HIF-1α stabilization in absence of hypoxic stimulus in a mouse model of colorectal cancer (Pathak et al., 2020). So, we wondered whether the chronic NCLX impairment could affect the stabilization of HIF-1α during hypoxia.

Thus, wild type (WT) and *Slc8b1* knock-out (KO) mouse embryonic fibroblasts (MEFs) were subjected to four hours of either normoxia, hypoxia or 1 mM dimethyloxalylglycine (DMOG), a PHD inhibitor and, so, a HIF-1α stabilizer. For hypoxic conditions, cells were transferred to the hypoxia chamber at 1% O_2 and 5% CO_2 and, for normoxic conditions, cells were maintained in regular cell culture incubators at room O_2 and 5% CO_2.

In both cell types, DMOG was able to stabilize HIF-1α (**Figure 5a**), but, surprisingly, the genetic abolition of NCLX did not prevent the stabilization of HIF-1α during hypoxia (**Figure 5a**). As there could be an effect due to the chronic inhibition of NCLX, we tested whether the acute NCLX inhibition affected HIF-1α stabilization in MEFs. Neither pharmacological NCLX inhibition using CGP (**Figure 5c**) nor overexpression of a dominant negative form of NCLX (dnNCLX) (**Figure 5d**) prevented the hypoxic HIF-1α stabilization in WT MEFs, but in both cases DMOG treatment induced HIF-1α stabilization, behaving as expected (**Figures 5c and d**). Besides, in NCLX KO MEFs CGP treatment did not affect HIF-1α stabilization neither after 4 hours of hypoxia nor in cells treated with DMOG, and in both conditions HIF-1α was stabilized (**Figure 5c**). Also, NCLX KO MEFs were transfected with the human NCLX protein (pNCLX), recovering, in turn, NCLX activity, and these transfected cells were able to stabilize HIF-1α in presence of DMOG and after 4 hours of hypoxia (**Figure 5d**). These experiments showed that in MEFs in these conditions HIF-1α stabilization is independent of NCLX activity, contrary to what we had seen in other cell types.

Then, we assessed if the response to hypoxia in MEFs could be different to the other cell types, in which the superoxide burst produced during the first minutes of hypoxia depends on NCLX activity (Hernansanz-Agustín et al., 2020). Using dihydroethidium (DHE), a fluorescent dye for cytosolic superoxide, we observed that MEFs produced a superoxide burst in response to acute hypoxia when NCLX is active and its pharmacological inhibition or its genetical deletion prevented this superoxide burst (**Figure 5b**). Also, the superoxide production was not affected in NCLX KO MEFs treated with CGP in comparison with untreated NCLX KO cells or CGP-treated WT MEFs (**Figure 5b**). The positive control for superoxide production, treating cells with 10 μM antimycin A (AA), a well-known ROS inductor by mitochondrial complex III inhibition, produced superoxide independently of NCLX presence or activity (**Figure 5b**). This result was in line with the role that we described before (Hernansanz-Agustín et al., 2020).

Thus, it seems that HIF-1α stabilization after 4 hours of hypoxia does not depend on NCLX activity or acute hypoxic ROS production in MEFs under these experimental conditions.

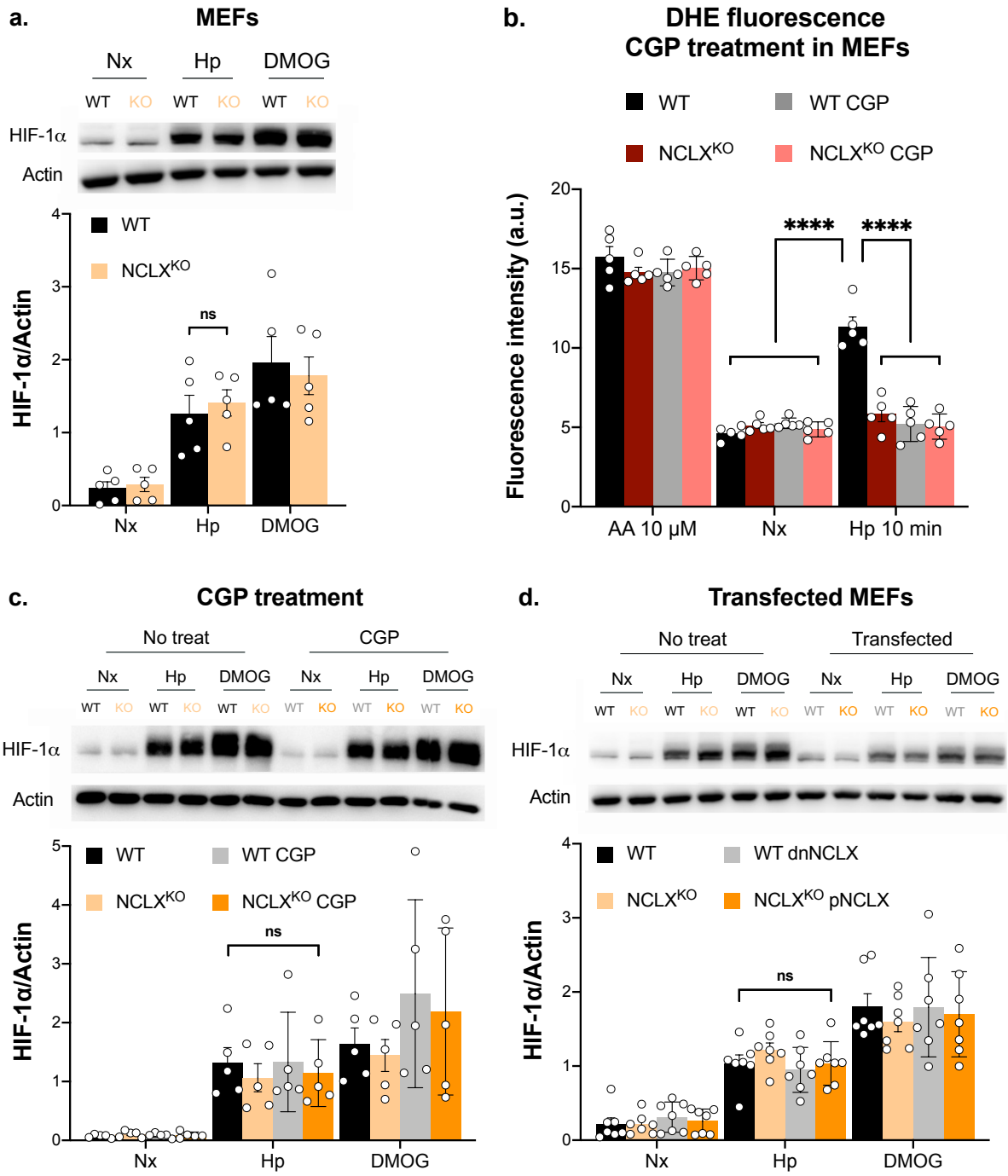

Figure 5. NCLX inhibition does not prevent HIF-1α stabilization during hypoxia in MEFs. (**a**, **c** and **d**) HIF-1α stabilization measured by western blotting in MEFs. WT and NCLX KO MEFs (**a**) or treated with 10 μM CGP (**c**) or transfected with dnNCLX or pNCLX (**d**) were exposed for 4 hours to normoxia (Nx), normoxia with 1 mM DMOG (DMOG) or hypoxia (1% oxygen, Hp). The samples were extracted, blotted against HIF-1α protein and normalized with ß-actin protein. (**b**) The detection of superoxide production was performed fluorescence microscopy in fixed cells. In normoxia, MEFs were incubated for 30 min with antimycin A (AA 10 μM) or without AA (Nx) and some cells were treated with 10 μM CGP5 μM; then, DHE was added for 10 min and cells were fixed. For hypoxic condition, some cells were treated with 10 μM CGP for 30 min in normoxia prior to hypoxia and, then, they were transferred to the hypoxia chamber (1% oxygen). Inside it, the media was replaced by the pre-hypoxic-balanced media and, quickly, 5 μM DHE was added for 10 min and cells were fixed inside the hypoxia chamber. At least five independent experiments were done. ns means not significant, ****p<0.0001, by two-way ANOVA with Tukey's post-hoc test

1.2. N-acetyl-cysteine pretreatment affects basal cellular ROS levels in MEFs, but does not scavenger mitochondrial ROS production directly

We had previously noticed that in NCLX KO MEFs the basal H_2O_2 levels were higher than in WT MEFs (Hernansanz-Agustín et al., 2020). So, we thought that possibly the basal ROS levels, and especially H_2O_2, could affect the response to hypoxia in NCLX KO MEFs. Thus, we reasoned to treat WT and NCLX KO MEFs with N-acetylcysteine (NAC) before exposing them to hypoxia.

NAC is a well-known antioxidant used as a mucolytic therapy and in the management of acetaminophen overdose (Alvarez et al., 2022). The antioxidant effect of NAC is mainly indirect, through releasing cysteine, which is directed to the biosynthesis of reduced glutathione (GSH) or to generate sulfane sulfur species. All these species can react with peroxides and then, they are reduced back by the cellular antioxidant systems (Alvarez et al., 2022). For instance, GSH is one of the most important metabolites for maintaining the cellular thiol redox homeostasis because it is essential for the proper function of glutaredoxin-glutathione reductase (Grx-GR) system (**Figure 6a**) (Alvarez et al., 2022). GR transfers electrons from NADPH to oxidized glutathione (GSSG), reducing it to GSH (**Figure 6a**). Then, Grx uses GSH to reduce some protein disulfides, glutathionylated proteins and other oxidized metabolites (**Figure 6a**) (Alvarez et al., 2022). Besides, GSH can directly reduce the glutathione peroxidases, a family of peroxidases which can reduce H_2O_2 or hydroperoxides in other substrates, such as lipids (Alvarez et al., 2022). However, it shall be noted that the release of cysteine from NAC within cells may have other metabolic effects that are not related with its antioxidant function.

Thus, we treated both NCLX WT and KO MEFs with 1 mM NAC for two hours in normoxia (NAC pretreatment) and, then, the media were replaced with fresh media without NAC for normoxic conditions or, inside the hypoxia chamber, with fresh and hypoxic-pre-stabilized media without NAC. These cells with fresh media were incubated for 4 hours in normoxia or hypoxia and after that we measured the superoxide levels using DHE. We observed that the incubation with 10 μM AA during 30 minutes induced an increase in ROS production in cells pretreated with NAC as well as in non-pretreated cells (**Figure 6b**). However, the cellular ROS levels after four hours in normoxia were affected in NAC pretreated cells compared to the non-pretreated cells respectively (**Figure 6c**). While NAC pretreatment in WT MEFs induced an increase in ROS production, in NCLX KO MEFs NAC pretreatment caused a decrease in ROS production (**Figure 6c**). Nevertheless, NAC pretreatment did not alter the behavior of cells during the first 10 min of hypoxia or after 4 hours of hypoxia: the hypoxic burst during the first minutes of hypoxia was observed in WT

cells, but it was not observed in NCLX KO cells, and both genotypes after 4 hours of hypoxia showed a low superoxide level (**Figure 6c**).

These results suggest that NAC pretreatment may change the strict redox balance in cells because it increased the superoxide level in WT MEFs (**Figure 6c**) and decreased the superoxide level in NCLX KO MEFs (**Figure 6c**), compared to the respective superoxide level in non-pretreated cells. However, NAC pretreatment did not alter the acute ROS production, as observed after AA incubation (**Figure 6b**) or during the first few minutes of hypoxia in WT MEFs (**Figure 6b**).

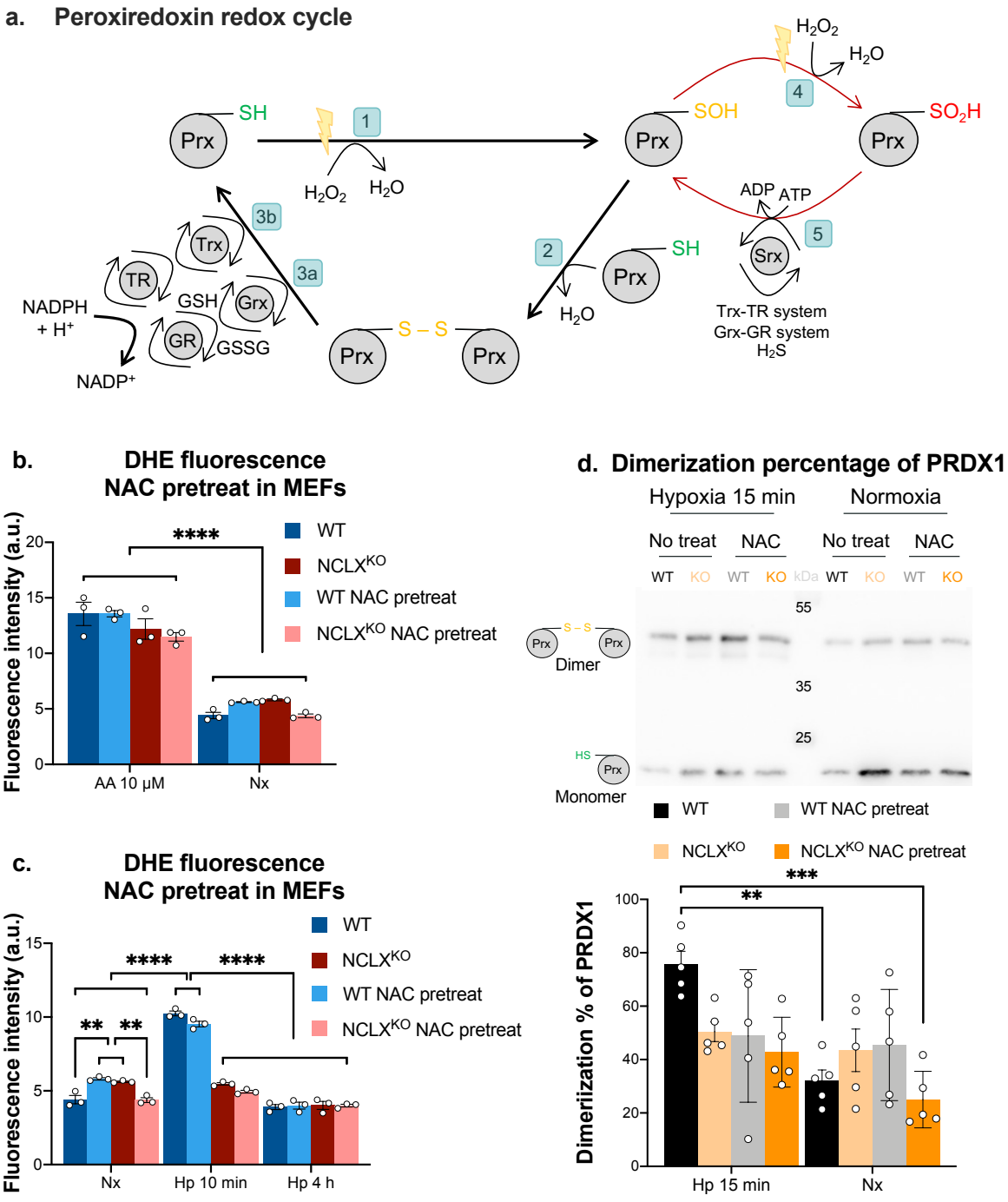

Figure 6. Effects of NAC pretreatment on cellular basal ROS in MEFs. (**a**) Scheme of the peroxiredoxins (prxs) redox cycle. By reducing H_2O_2 to water, reduced prx is oxidized by forming sulfenic acid in its peroxidatic cysteine (C_P) [1]. The interaction between the oxidized C_P and a reduced resolving cysteine (C_R) from other prx results in the prx dimer formation, by a sulfide bond genesis and a water molecule release [2]. The prx dimer can be reduced back to monomeric prx by the glutaredoxin-glutathione reductase (Grx-GR) system [3a] or by the thioredoxin-thioredoxin reductase (Trx-TR) system [3b]. Both systems use $NADPH+H^+$ as the final donor of reducing equivalents, but only grx-GR system needs glutathione (reduced (GSH) and oxidized (GSSG)) as an intermediate molecule [3a]. Prxs can be inactivated when oxidized C_P is again oxidized by H_2O_2, forming sulfinic acid in the C_P and water [4]. This sulfinic acid in the C_P can be reduced to sulfenic acid through an ATP-dependent reaction catalyzed by sulfiredoxin (Srx), which is, in turn, reduced by trx-GR system, grx-GR system or directly by H_2S [5]. (**b** and **c**) Detection of superoxide production by fluorescence microscopy in fixed MEFs. Some cells were treated for 2 hours with 1 mM NAC in normoxia. For normoxia conditions, cells were incubated with fresh media in normoxia for 4 hours (Nx) or, during the last 30 min of these 4 hours, some cells were treated with 10 μM AA. Then, DHE was added for 10 min and cells were fixed. For hypoxic conditions, media with or without NAC was replaced by pre-hypoxic-balanced media in the hypoxia chamber (1% oxygen) for 0 min (Hp 10 min) or for 4 hours (Hp 4 h). Then, 5 μM DHE was added for 10 min and cells were fixed inside the hypoxia chamber and fluorescence quantified by microscopy. (**d**) Dimerization percentage of PRDX1 (d%P1) measured by non-reducing western blotting in MEFs. Some cells were treated for 2 hours with 1 mM NAC in normoxia. Then, cells were incubated with fresh media in normoxia for 4 hours (Nx) or with pre-hypoxic-balanced media in the hypoxia chamber (1% oxygen) for 15 min (Hp 15 min) or 4 hours (data not shown). Samples were obtained thoughtfully as explained in materials and methods section and blotted against PRDX1 protein. The d%P1 was calculated through dividing the dimer band by the total PRDX1, which is the sum of dimer plus monomer bands. At least three independent experiments were done. **p<0.01, ****p<0.0001, by two-way ANOVA with Tukey's post-hoc test

Additionally, we decided to check a cytosolic redox indicator, the peroxiredoxin 1 (PRDX1) redox state. Peroxiredoxins (prxs) are ubiquitous family of cysteine-based peroxidases, whose rate constants for the reaction with H_2O_2 are the highest in cells (Alvarez et al., 2022). Also, prxs reduce hydroperoxides in other substrates, like oxidized proteins (Hall et al., 2011); thus, prxs are involved in both antioxidant protection and cellular signaling pathways. Taken together, prxs and all glutathione-related proteins explained above are the main cellular H_2O_2 detoxifying mechanisms (Alvarez et al., 2022).

The catalytic mechanism of prxs relies on two essential cysteines within them: the peroxidatic cysteine (C_P) and the resolving cysteine (C_R). During the hydroperoxide reduction, the C_P reacts with the hydroperoxide to form cysteine sulfenic acid (CSOH), which reacts with the C_R from other prx, forming an intermolecular disulfide bond. Then, this disulfide bond is usually reduced by the thioredoxin-thioredoxin reductase (Trx-TR) system or by Grx-GR system (**Figure 6a**). Besides, the C_P can be over-oxidized by other hydroperoxide, forming a cysteine sulfinic acid (CSO_2H), which inactivates the prx (**Figure 6a**). This inactivated form can be rescued through an ATP-dependent reaction catalyzed by sulfiredoxin (Srx) (**Figure 6a**). Therefore, the redox state of prxs is related to the intracellular redox state. Thus, the dimerization percentage of prxs is used to compare the intracellular redox state between different conditions (Cox et al., 2010). As prxs are very sensitive to H_2O_2 and its dimer is maintained through a disulfide bond, the samples were obtained carefully as specified in the materials and methods section and always without thiol-reducing agents such as 2-mercaptoethanol.

The dimerization percentage of PRDX1 (d%P1) in normoxia showed the same tendency as DHE fluorescence: while in WT MEFs pretreated with NAC the d%P1 tended to increase, in NCLX KO MEFs pretreated with NAC the d%P1 tended to decrease, compared to the non-pretreated cells respectively (**Figure 6d**). After subjecting cells to 15 minutes of hypoxia, whilst the d%P1 in WT MEFs was increased, in NCLX KO MEFs the d%P1 was kept similar to its normoxic level (**Figure 6d**), according to previous results (Hernansanz-Agustín, 2017; Hernansanz-Agustín et al., 2020) and DHE fluorescence (**Figure 6c**). However, during the first few minutes of hypoxia, in NAC-pretreated WT MEFs the d%P1 did not increase such as in non-pretreated WT cells (**Figure 6d**) and in NAC-pretreated NCLX KO MEFs the d%P1 was kept similar than non-pretreated NCLX KO cells (**Figure 6d**).

Since we observed that the hypoxic superoxide burst in WT MEFs is still occurring by DHE fluorescence (**Figure 6c**) and we missed to detect the consequent increase of d%P1 (**Figure 6d**), these results suggest that NAC pretreatment may rise the cellular thiol antioxidants systems, for example by increasing the GSH pool (Alvarez et al., 2022) or by increasing NADPH production. Thus, even though PRDX1 might be dimerizing due to the hypoxic superoxide burst, its reduction cycle may be speeded up (**Figure 6a**), rendering the increase of d%P1 undetectable.

1.3. NCLX KO MEFs pretreated with NAC or L-cysteine do not stabilize HIF-1α in hypoxia

After knowing the effect of 1 mM NAC pretreatment on intracellular ROS levels (**Figure 6**), we analyzed whether NAC pretreatment could affect HIF-1α stabilization. Both WT and NCLX KO MEFs without NAC pretreatment stabilized HIF-1α during hypoxia, as shown before (**Figure 7a**). However, while NAC-pretreated WT MEFs were able to stabilize HIF-1α (**Figure 7a**), NAC-pretreated NCLX KO MEFs were unable to stabilize HIF-1α during hypoxia (**Figure 7a**).

As the main effect of NAC in cells is releasing cysteine (Alvarez et al., 2022), to ensure these results, we decided to pretreat MEFs directly with 1 mM L-cysteine instead of NAC and similar results were obtained: only L-cysteine pretreatment prevented HIF-1α stabilization during hypoxia in NCLX KO MEFs (**Figure 7b**).

Accordingly, the same result was observed in a colorectal cancer mouse model (Pathak et al., 2020), HIF-1α stabilization in NCLX KO cells was prevented in presence of mitoTEMPO, a mitochondria-targeted ROS scavenger. Therefore, the increase in ROS production induced by chronic NCLX deletion is somehow predisposing cells to stabilize HIF-1α.

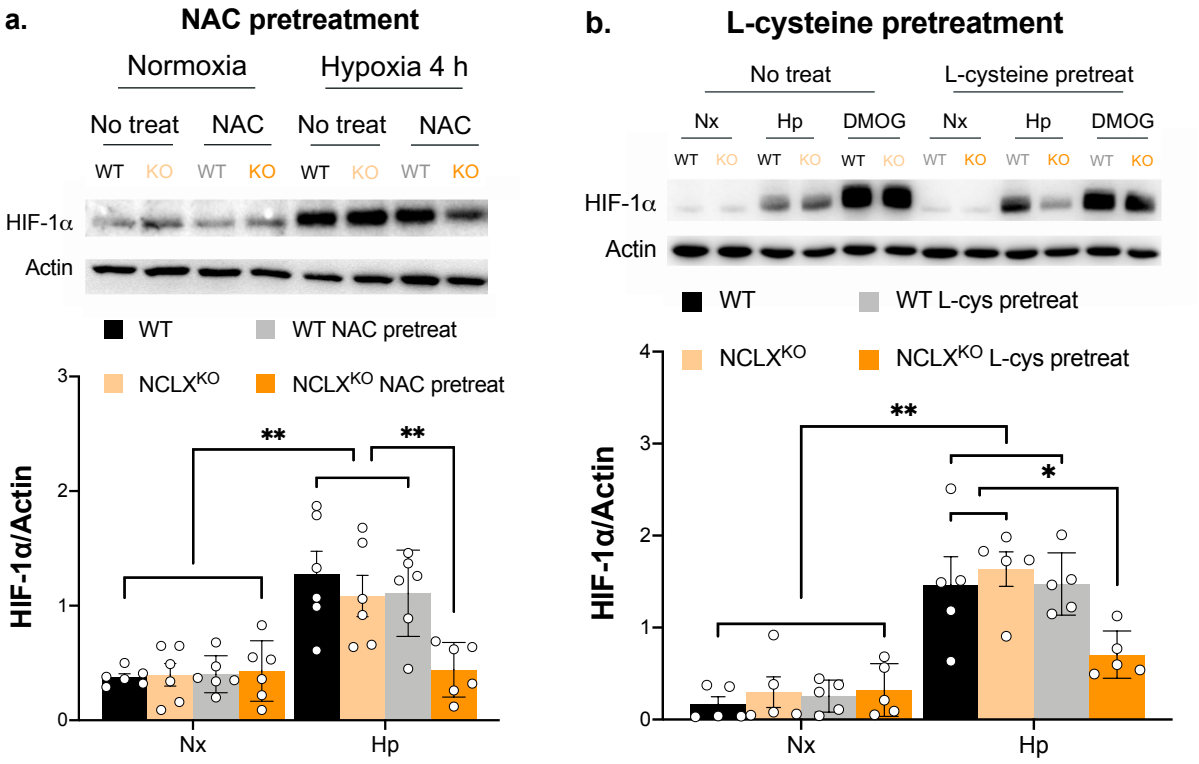

Figure 7. Effects of NAC and L-cysteine pretreatment on HIF-1α stabilization during hypoxia in MEFs. HIF-1α stabilization measured by Western blotting in MEFs. WT and NCLX KO MEFs were treated with 1 mM NAC (**a**) or 1 mM L-cysteine (**b**) for 2 hours in normoxia. Then, cells were incubated with fresh media in normoxia for 4 hours (Nx) or with pre-hypoxic-balanced media in the hypoxia chamber (1% oxygen) for 4 hours (Hp). Samples were extracted, blotted against HIF-1α protein and normalized with ß-actin protein. At least five independent experiments were done. *p<0.05, **p<0.01, by two-way ANOVA with Tukey's post-hoc test

Thus, the pretreatment with 1 mM NAC or L-cysteine restored the link between the presence of NCLX with HIF-1α stabilization, as we had observed in other cell types (Hernansanz-Agustín, 2017). Intriguingly, this effect did not correlate well with the appearance of the hypoxic superoxide burst alone (**Figure 6**). Taking in account all these results, it seems that the absence of HIF-1α stabilization after 4 hours of hypoxia correlates with the low basal levels of cellular ROS together with the absence of the hypoxic superoxide burst, as summarized in **Table 3**.

Table 3. Relationship between HIF-1α stabilization and ROS measurements in MEFs.

	WT No treat	NCLX^{KO} No treat	WT NAC pretreat	NCLX^{KO} NAC pretreat
Hypoxic HIF-1α stabilization	✓	✓	✓	✗
Superoxide burst (DHE) in hypoxia	✓	✗	✓	✗
High hypoxic d%PRX1	✓	✗	✗	✗
High basal d%PRX1	✗	✓	✓	✗
High basal superoxide (DHE)	✗	✓	✓	✗

1.4. NCLX inhibition prevents HIF-1α stabilization during hypoxia in mouse adult fibroblasts

However, these results did not explain why only MEFs needed to be pretreated with an enhancer of cellular antioxidant systems to recover the dependence of HIF-1α stabilization on NCLX activity, compared to other cell types previously analyzed, adult cells all of them (Hernansanz-Agustín, 2017). So, we wondered that the difference could be that those cell types presented adult origin, whereas MEFs were embryonic cells and therefore their antioxidant defenses may be compromising because the activity of some antioxidant proteins depends on development stage (Surai et al., 2016).

Thus, we analyzed basal ROS production in MEFs versus their isogenic adult cells version, mouse adult fibroblasts (MAFs), using Hyper7 cytosolic version (Pak et al., 2020). These experiments were carried out by Dr. Pablo Hernansanz-Agustín in the Centro Nacional de Investigaciones Cardiovasculares (CNIC). We observed that the cytosolic ROS were increased in WT MEFs compared to MAFs (**Figure 8a**). Hence, this high basal ROS levels in MEFs, even higher in NCLX KO MEFs (**Figure 6**), may be bypassing the NCLX-dependent hypoxic ROS and, thus, becoming the ROS source for inducing HIF-1α stabilization in hypoxia. Therefore, MEFs without a functional NCLX were still stabilizing HIF-1α in hypoxia (**Figure 5**), unless NCLX KO MEFs were pretreated with NAC or L-cysteine (**Figure 7**), which diminished the high basal ROS level (**Figure 6**), according to the observed results in other model of NCLX chronic deletion (Pathak et al., 2020).

Next, we studied if the hypoxic superoxide burst in MAFs would be NCLX-dependent. By using DHE fluorescence, we observed that MAFs produced a superoxide burst in response to acute hypoxia when NCLX was active, but they did not when NCLX was pharmacologically blocked with CGP (**Figure 8b**), like it was previously observed in other cell types (Hernansanz-Agustín et al., 2017, 2020).

Finally, we analyzed the HIF-1α stabilization in MAFs, through subjecting them to four hours to normoxia, hypoxia or DMOG. DMOG treatment induced a stabilization of HIF-1α in both CGP-treated and untreated cells (**Figure 8c**). However, only untreated cells were able to stabilize HIF-1α during hypoxia (**Figure 8c**). Also, we studied HIF-1α stabilization in MAFs overexpressing dnNCLX, and we observed that cells overexpressing dnNCLX were able to stabilize HIF-1α under DMOG treatment (**Figure 8d**), but HIF-1α stabilization was inhibited under hypoxia (**Figure 8d**). Hence, in MAFs the NCLX-dependent hypoxic-ROS production was linked to HIF-1α stabilization, as observed in other adult cells previously studied (Hernansanz-Agustín, 2017).

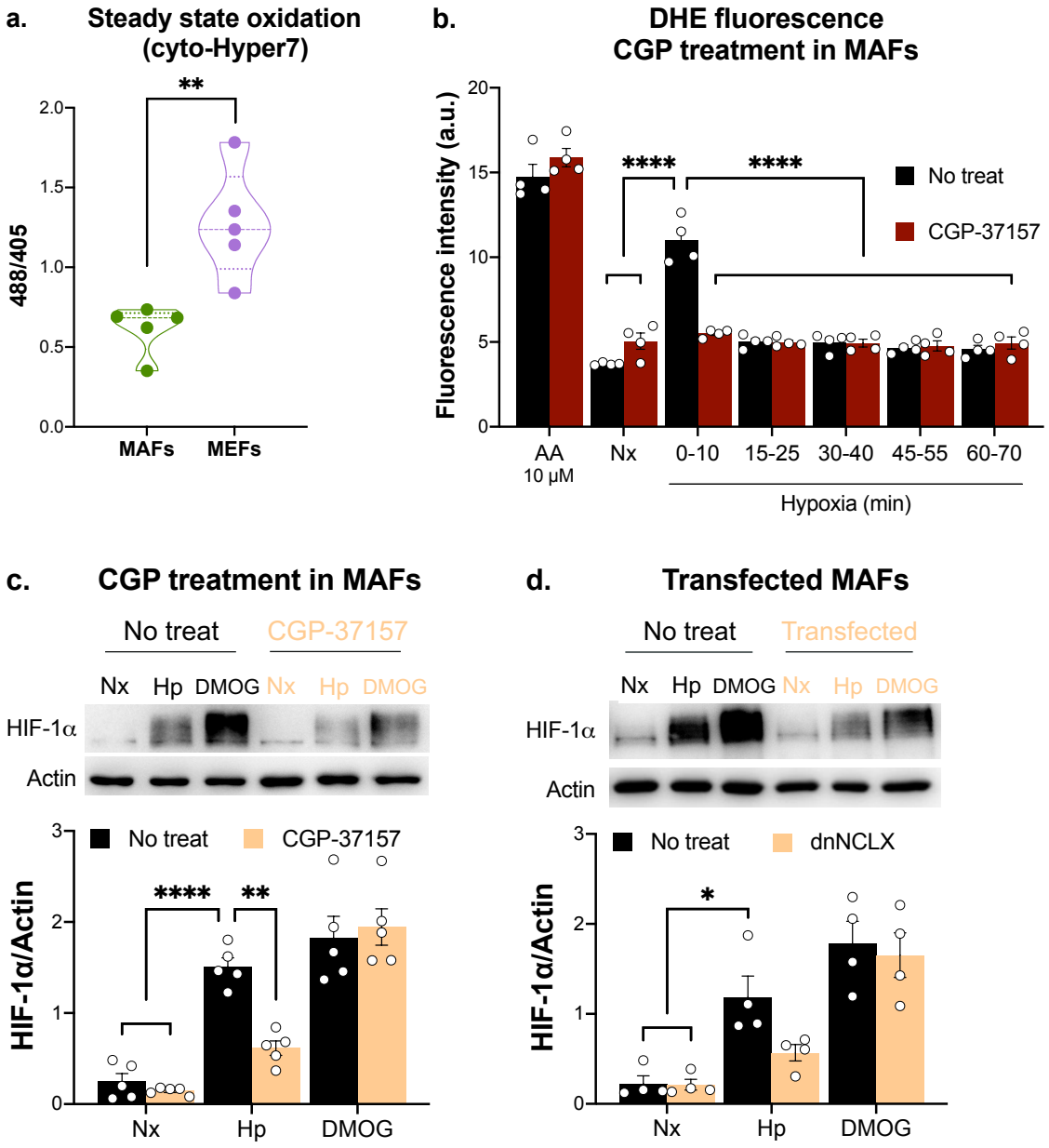

Figure 8. NCLX inhibition prevents HIF-1α stabilization during hypoxia in MAFs. (**a**) Detection of cytosolic basal ROS levels by live imaging confocal fluorescence microscopy in MEFs and MAFs transfected with the cytosolic version of Hyper7 (Pak et al., 2020). At least three images were taken per experiment and five independent experiments were performed. (**b**) Detection of superoxide production by fluorescence microscopy in fixed cells. Some cells were treated with 10 µM CGP for 30 min prior to experiment. For normoxia conditons, MAFs were incubated for 30 min with 10 µM antimycin A (AA) or without AA (Nx). Then, DHE was added for 10 min and cells were fixed. For hypoxic conditions, cells were transferred to hypoxia chamber (1% oxygen) and, inside it, media were replaced by pre-hypoxic-balanced media for 0, 15, 30, 45 or 60 min. Then 5 µM DHE was added for 10 min and cells were fixed inside hypoxia chamber and analyzed by fluorescence microscopy. (**c** and **d**) HIF-1α stabilization measured by Western blotting in MAFs. MAFs treated with 10 µM CGP (**c**) or transfected with dnNCLX (**d**) were exposed for 4 hours to normoxia (Nx), normoxia with 1 mM DMOG (DMOG) or hypoxia (1% oxygen, Hp). Proteins were extracted, blotted against HIF-1α protein and normalized with ß-actin protein. At least four independent experiments were done. *p<0.05, **p<0.005, ****p<0.0001, by Student's t test (**a**) or two-way ANOVA with Tukey's post-hoc test (**b-d**)

2. Lithium treatment affects mitochondrial metabolism

The effect of lithium in mitochondria has been studied since it was discovered that mitochondria were sensitive to sodium ions (Gear & Lehninger, 1968; Krall, 1967) and both, sodium and lithium, could trigger $_{m}Ca^{2+}$ efflux (Blaustein & Wiesmann, 1970). Many years later, the molecular identity of the mitochondrial sodium/calcium/lithium exchanger (NCLX) was discovered and its lithium sensibility was also demonstrated (Palty et al., 2010; Roy et al., 2017). However, lithium concentration in plasma patients has been established between 0.6 mM and 1.2 mM (Nolen et al., 2019) and lithium concentration used in several studies is much higher or, even, sodium ions are completely replaced by lithium ions (Blaustein & Wiesmann, 1970; Palty et al., 2010; Roy et al., 2017; Rysted et al., 2021; Shalbuyeva et al., 2007; Stepanova et al., 2015). This makes impossible to assess whether lithium ions are able to affect mitochondrial metabolism or, even, NCLX sensitivity to them at therapeutical concentration.

2.1. Mitochondrial lithium import depends on NCLX at therapeutical concentration

Taking into account the controversial results obtained by several groups and the different lithium concentrations used in that experiments (Maurer et al., 2009; Palty et al., 2010; Rysted et al., 2021; Shalbuyeva et al., 2007), we aimed to determine if NCLX is sensitive to lithium ions at therapeutical concentration.

Therefore, NCLX WT and KO MEFs were treated with 1 mM LiCl added to a regular DMEM, which contains 140 mM NaCl, for 30 minutes in normoxia (21% O_2 and 5% CO_2). As we had shown that NCLX is activated upon acute hypoxia (Hernansanz-Agustín et al., 2020), after those 30 minutes in normoxia some cells were transferred to the hypoxia chamber (1% O_2 and 5% CO_2), where medium was changed for one pre-equilibrated to hypoxia during the night before experiment, for 10 minutes. Then, mitochondrial isolation was done and $_{m}Li^{+}$ amount was measured by inductively coupled plasma mass spectrometry (ICP-MS) or by graphite furnace atomic absorption spectrometry (GF-AAS). To note both methods use acid buffer for sample dissolution.

2.1.1. Measurement of mitochondrial lithium by ICP-MS

These measurements were carried out in the Unidad de Técnicas Geológicas from the Universidad Complutense de Madrid by Teresa Benito Criado.

Due to the detectability threshold of ICP-MS, a large number of mitochondria was required, so isolated mitochondria from different experiments were pulled together and only one measurement of $_{m}Li^{+}$ was done (**Figure 9**). Besides, reagents used for ICP-MS technique were incompatibles with assay for mitochondrial protein measurement, so we could not normalize the data.

Despite these issues, a clear increase in $_{m}Li^{+}$ was observed in WT MEFs treated with 1 mM LiCl, both in normoxia and hypoxia (**Figure 9**). Since this increment was not observed in NCLX KO MEFs treated with 1 mM LiCl, we can assume that NCLX can import lithium into mitochondria when both lithium and sodium are at physiological concentration.

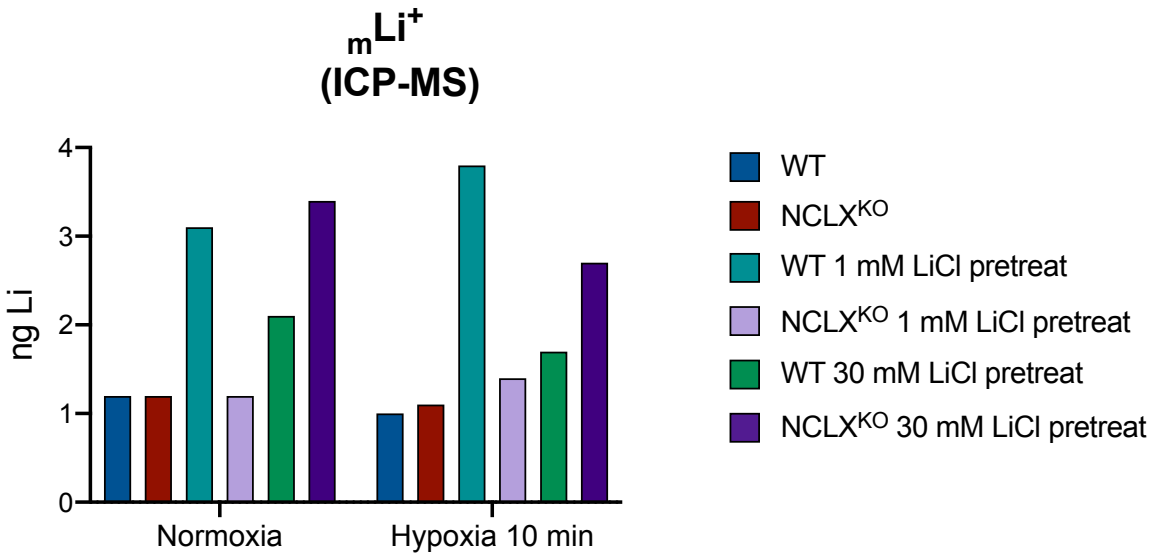

Figure 9. Mitochondrial lithium import relies on NCLX in a concentration-dependent manner. WT MEFs and NCLX KO MEFs were treated or not with 1 mM LiCl or 30 mM LiCl for 30 min in normoxia. Then, some cells were transferred to the hypoxia chamber (1% oxygen) where media was replaced by pre-balanced-hypoxic media for 10 minutes. After that incubation, plates were transferred to ice (in normoxia or inside the hypoxia chamber) and mitochondria were isolated. Mitochondria from different experiments made in different days were pooled together and to measure Li^{+} by ICP-MS.

We also measured lithium in isolated mitochondria from MEFs treated with 30 mM LiCl and, at this concentration, lithium was detected in WT and NCLX KO cells (**Figure 9**), suggesting that at higher extracellular lithium concentration, NCLX dependency is lost and lithium import into mitochondria is probably done by a different mechanism, for example the MPTP opening, which is known to be more frequent in NCLX KO cells (Assali et al., 2020; Luongo et al., 2017).

2.1.2. Measurement of mitochondrial lithium, sodium and calcium by GF-AAS

In order to confirm the results obtained with the ICP-MS and a as a pilot test, we decided to analyze $_{m}Li^{+}$ through GF-AAS. These measurements were carried out in the Departamento de Química Analítica y Análisis Instrumental at the Facultad de Ciencias from the Universidad Autónoma de Madrid by Dr. Beatriz Gómez Nieto.

Despite that it is only one independent experiment, we observed that, after 30 minutes of lithium incubation in normoxia, $_{m}Li^{+}$ concentration was higher in WT than NCLX KO MEFs (**Figure 10a**). Also, $_{m}Li^{+}$ could be more concentrated in untreated NCLX KO than untreated WT MEFs (**Figure 10a**). These results suggest that, while the main $_{m}Li^{+}$ import seems to be NCLX-dependent, it is plausible that NHE may be importing a small amount of lithium into mitochondria too or at least in cells without a functional NCLX, but more experiments should be done to ensure this finding.

In addition, we were able to measure $_{m}Na^{+}$ and $_{m}Ca^{2+}$ by GF-AAS in the same samples and we observed that both $_{m}Na^{+}$ and $_{m}Ca^{2+}$ concentrations were increased in NCLX KO compared to WT MEFs independently to lithium treatment (**Figure 10b and c**). This increase in $_{m}Ca^{2+}$ in NCLX KO MEFs has been noticed before as the main consequence of NCLX deletion (Luongo et al., 2017; Pathak et al., 2020). However, since $_{m}Na^{+}$ is not usually measured and sodium fluorescent dyes are not as sensitive as GF-AAS, its increase together with the increase in $_{m}Li^{+}$ concentration in untreated NCLX KO MEFs suggest that NCLX KO MEFs may have mitochondrial cation efflux impairment.

Also, $_{m}Ca^{2+}$ in NCLX KO MEFs seems to be more concentrated after lithium treatment (**Figure 10c**), suggesting that $_{m}Ca^{2+}$ uptake could be enhanced in presence of lithium as we will show bellow (section 2.10).

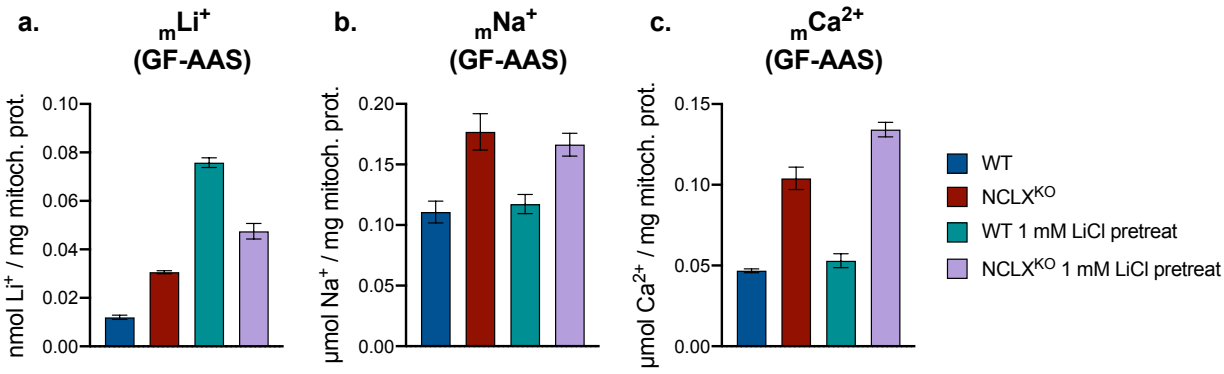

Figure 10. Effect of lithium treatment on $_{m}Li^{+}$, $_{m}Na^{+}$ and $_{m}Ca^{2+}$ in isolated mitochondria from WT and NCLX KO MEFs. WT MEFs and NCLX KO MEFs were treated or not with 1 mM LiCl for 30 min in normoxia. Then, plates were transferred to ice and mitochondria were isolated. Mitochondria from 3 plates per condition were pooled together and their dried pellets were stored at -80 ºC. Pellets were dissolved with ultrapure twice-filtered water and, while some microliters were used for protein determination assay, the most of them were used to measure three times each ion by GF-AAS. Mean ± SEM from the three measurements of one independent experiment is showed.

2.2. Lithium ions replace sodium ions in acute hypoxia response

Since NCLX is more sensitive to lithium ions than sodium ions (Roy et al., 2017) and we have observed that lithium is imported into mitochondria through NCLX at physiological concentration (**Figure 9 and 10c**), we wondered whether $_{m}Na^{+}$ import upon acute hypoxia (Hernansanz-Agustín et al., 2020) could be affected by lithium.

To measure $_{m}Na^{+}$ in isolated mitochondria, the same protocol as explained above was done. After treating cells with 1 mM LiCl for 30 minutes in normoxia, some plates were transferred to the hypoxia chamber (1% O_2 and 5% CO_2), where medium was changed for one pre-equilibrated to hypoxia during the night before experiment, for 10 minutes. Then, we isolated mitochondrial and quantified sodium amount by measuring sodium benzofuran isophthalate (SBFI) fluorescence.

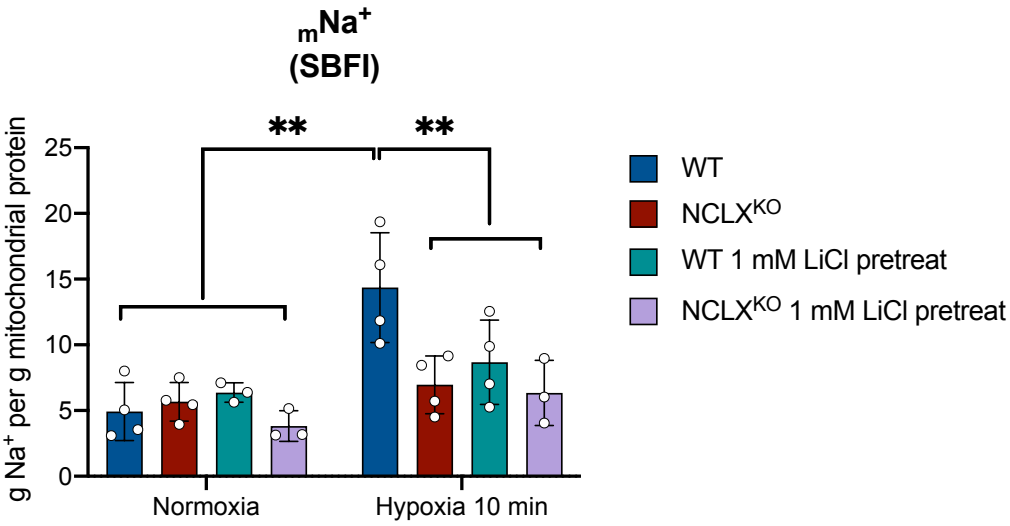

Figure 11. Effect of 1 mM LiCl on $_{m}Na^{+}$ content. WT MEFs and NCLX KO MEFs were treated or untreated with 1 mM LiCl for 30 min in normoxia. Then, some cells were transferred to the hypoxia chamber (1% oxygen) where media was replaced by pre-balanced-hypoxic media for 10 minutes. After, plates were transferred to ice (in normoxia or inside hypoxia chamber) and mitochondria isolation followed by sodium measurement using SBFI probe were done as described above. At least three independent experiments were done. **p<0.005, by two-way ANOVA with Tukey's post-hoc test

As we had previously described (Hernansanz-Agustín et al., 2020), acute hypoxia increased $_{m}Na^{+}$ in WT cells but not in NCLX KO cells (**Figure 11**). This hypoxia-dependent $_{m}Na^{+}$ increment was clearly reduced when WT MEFs were treated with 1 mM LiCl (**Figure 11**), while lithium treatment did not have an effect on NCLX KO MEFs (**Figure 11**). Although SBFI has not been ever tested in presence of lithium, all these results (**Figures 9 and 10b**) indicate that lithium treatment is not affecting $_{m}Na^{+}$ content in WT cells in normoxia (**Figures 10b and 11**), but it seems that lithium ions replace sodium ions during acute hypoxia response (**Figures 9 and 11**).

2.3. Lithium ions interact with phospholipids differently than sodium ions

Metal cations are known to interact with lipid membranes, according to each cation properties (Binder & Zschörnig, 2002), but, also, the interaction strength depends on lipid composition, as well as, the charge of phospholipids forming the bilayer (Javanainen et al., 2017). Indeed, several years ago it was demonstrated that, although all alkali ions increase the order in phosphatidylserine (PS) membranes, the interaction between sodium or potassium ions with PS bilayers was remarkably different to their interaction with lithium ions (Hauser & Shipley, 1983). To note, PS is an anionic phospholipid, like as CL, with cylindrical shape, like as PC, and is enriched in the nervous system membranes (Ma et al., 2022). Lithium ions increased the order in the tails of PS membranes and maintained the bilayer structure in a higher range of temperature (Hauser & Shipley, 1981), similarly to the effect of magnesium or calcium ions on that PS membranes (Binder & Zschörnig, 2002; Hauser & Shipley, 1984). Principally, charge and ionic radius of each cation are the responsible of this difference between lithium and the other monovalent cations. Lithium cation's small radius and single charge allows them to replace water molecules and go deeper into PS bilayers, dehydrating them and increasing the interaction lipid-lithium-lipid through stronger bounds, as observed in (López Cascales & Garcia de la Torre, 1997).

As one of the most abundant phospholipids in the IMM is PC (zwitterionic with cylindrical shape), we decided to analyze the effect of lithium ions on PC liposomes through infrared (IR) spectroscopy. These experiments were carried out by our collaborators Dr. Susana Carregal-Romero and Jesús Ruiz-Cabello in the CIC biomaGUNE. IR spectroscopy relies on the principle that molecules absorb specific frequencies based on their structure and that frequencies are associated with the strength of the bounds between the atoms forming the molecule. IR absorption spectrum of a sample is obtained by passing a beam of IR light through the sample and, when the frequency of the light is the same as the vibrational frequency of a bond, absorption occurs. Thus, we performed IR spectroscopy experiments on DPPC (1,2-dipalmitoyl-sn-glycero-3-phosphocholine) pure liposomes or after 2 hours of incubation at a ratio of 16 mM LiCl or NaCl per 0.5 mg/mL lipids. Comparing the spectra in presence of each cation with the pure liposome spectrum, we detected a shift in the carbonyl (CO) region of the spectrum (**Figure 12**). The attachment of cations to the oxygen of CO groups substantially reduces the corresponding bound stretch frequency of CO group itself due to the partial electron transfer from the CO group to the nearby cation. So, since CO stretching peaks generally fall between 1900 and 1600 cm^{-1} in wavenumber units, we observed that CO bond wavelength was strongly red shifted, which means that a new peak or peaks appeared at a lower wavelength (**Figure 12b and c**).

a. Infrared absorption spectrum of pure liposome

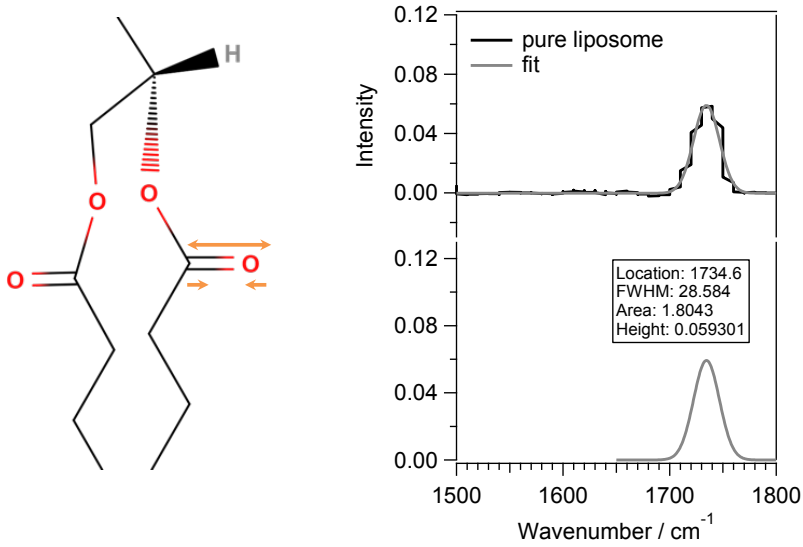

DPPC phospholipid

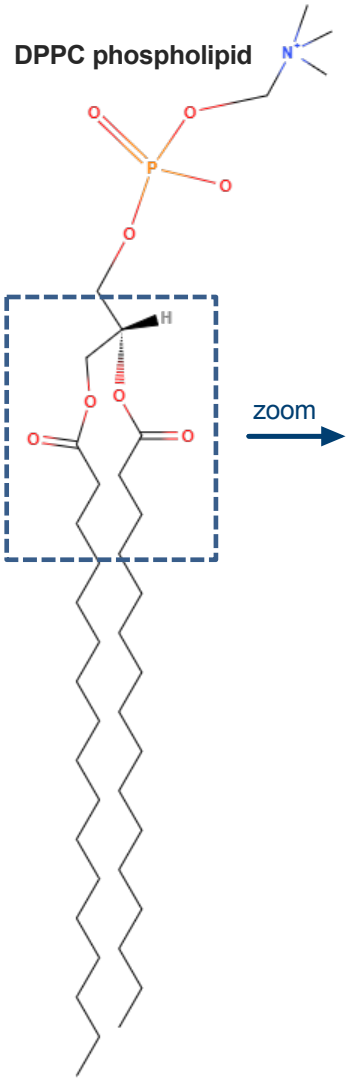

zoom

b. Infrared absorption spectrum in presence of Li^+

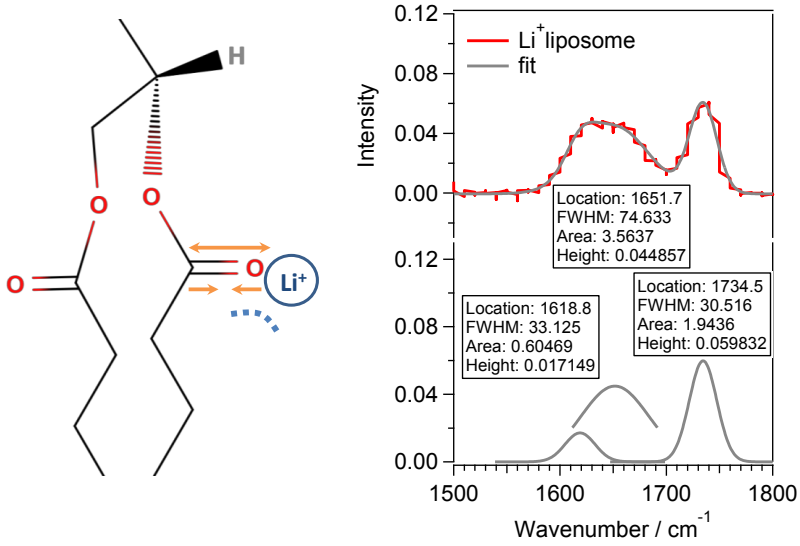

c. Infrared absorption spectrum in presence of Na^+

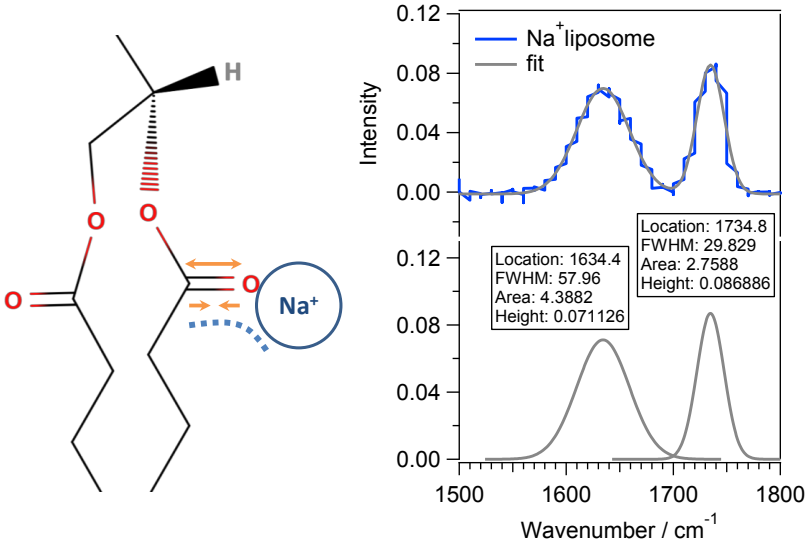

Figure 12. Infrared absorption spectra of the carbonyl group of DPPC liposomes alone or in presence of Li^+ or Na^+. Liposomes composed by DPPCs (structure showed in the left) were used for IR spectroscopy experiments after 2 h at 37 ºC in absence (**a**) or presence of 16 mM LiCl (**b**) or NaCl (**c**) per 0.5 mg/mL lipids. Schematic representation of CO group bound (**a**) and its interaction with Li^+ (**b**) or Na^+ (**c**). Representative absorption measurements obtained by IR spectroscopy are showed in black (**a**), red (**b**) or blue (**c**) with their correspondent fit-curve in grey and each peak features (location, FWHM (Full Width at Half Maximum, which informs about peak resolution), area and height. Three independent experiments were done.

In these IR spectroscopy experiments, we observed that both lithium and sodium ions interacted with the oxygen of the CO groups within PC, but in a slightly different way. In presence of both ions new peaks appeared, which means that there were oxygens of the CO groups interacting with them and free ones (**Figure 12b and c**). But in presence of lithium ions two overlapping peaks were detected, meaning that two different isomers were formed by the lithium-CO interaction (**Figure 12b**). This suggests that the different size of the alkali ion determines the strength of the metal-oxygen bond and the number of possible isomers and, both could make a difference on their effect on phospholipid bilayers.

2.4. Lithium treatment prevents the reduction of inner mitochondrial membrane fluidity upon acute hypoxia

Through IR experiments we have shown that lithium ions were able to interact with phospholipids (**Figure 12**), but would lithium ions be able to interact with phospholipids at physiological concentration and/or in presence of sodium ions?

Some years ago, a molecular dynamic study with PS membranes showed that when both lithium and sodium ions are present in the aqueous phase, lithium ions showed a special affinity for the PS membrane, displacing almost all the sodium ions toward the middle of the water layer (López Cascales & Garcia de la Torre, 1997). Accordingly, a range of physiological concentration of lithium was studied in healthy human erythrocytes in presence of sodium ions and the results showed that lithium ions were able to alter the electrostatic interactions of molecules close to the membrane surface, improving their motion and slightly reducing the membrane surface anisotropy (Pettegrew et al., 1987). Besides, long-term lithium treatment has been observed to affect lipid composition in brain membranes from rodent models (López-Corcuera et al., 1988; Zanni et al., 2017), increasing lipids which allow a higher level of fluidity in membranes.

Therefore, since $_{m}Li^{+}$ was increased in WT MEFs treated with 1 mM LiCl (**Figures 9 and 10a**), without affecting $_{m}Na^{+}$ (**Figures 10b and 11**), and lithium ions were able to interact with phospholipids (**Figure 12**), also in presence of sodium ions (López Cascales & Garcia de la Torre, 1997), we wondered whether the inner mitochondrial membrane (IMM) fluidity may be affected. We have previously observed that during the first minutes of hypoxia, through sodium ions and their interaction with phospholipids, the IMM fluidity decreased (Hernansanz-Agustín et al., 2020). Thus, we considered acute hypoxia treatment as the perfect scenario to test the effect of lithium ions on IMM fluidity.

WT MEFs were transfected with a plasmid which encodes a red fluorescent protein targeted to the IMM (mitoRFP) and fluorescence recovery after photobleaching (FRAP) experiment were performed, as previously described (Hernansanz-Agustín et al., 2020). By adding 1 mM LiCl before or at the same time with hypoxia induction, we observed that the presence of lithium ions inhibited the usual hypoxia-induced reduction of IMM fluidity (**Figure 13**), suggesting that the replacement of sodium ions by lithium ions (**Figures 9 and 11**) was also displacing the sodium ions from the IMM (**Figure 13**), as previously observed (López Cascales & Garcia de la Torre, 1997). Thus, the interaction between sodium ions and phospholipids was avoided and, as consequence, the hypoxic-dependent fluidity reduction of the IMM was prevented too (**Figure 13**) (Hernansanz-Agustín et al., 2020).

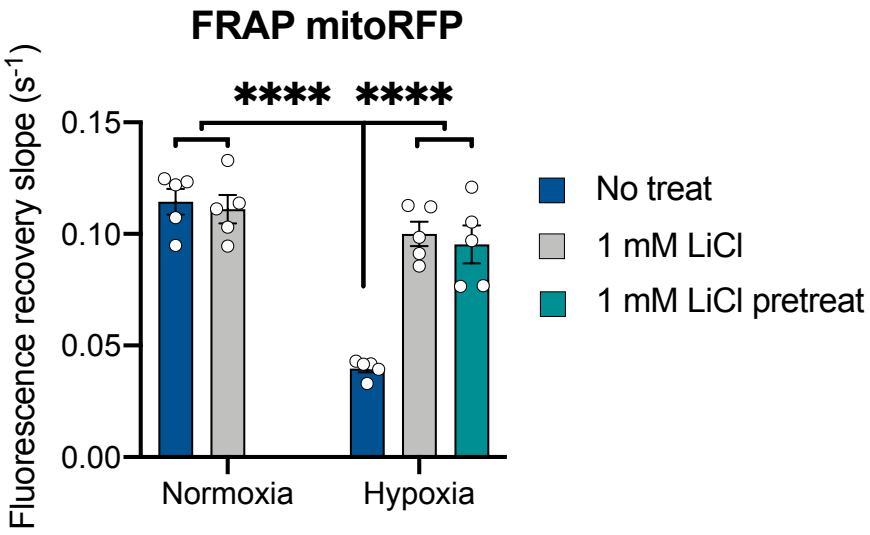

Figure 13. Effect of 1 mM LiCl on IMM fluidity. FRAP slope quantification of mitoRFP-expressing WT MEFs in normoxia or hypoxia (1% oxygen), untreated, treated with 1 mM LiCl or pretreated with 1 mM LiCl for 30 min in normoxia prior to hypoxia. 5 independent experiments with, at least, 5 replicates of each condition were performed. ****p<0.0001, by two-way ANOVA with Tukey's post-hoc test

2.5. Lithium treatment inhibits the hypoxic superoxide burst and induces superoxide production in normoxia

Since we have shown that one of the effects of NCLX activation upon acute hypoxia is an increase on superoxide production during the first few minutes due to the reduction of IMM fluidity (Hernansanz-Agustín et al., 2020), we wondered whether the addition of lithium could affect this superoxide burst. Thus, we measured intracellular superoxide levels using DHE after different time periods of hypoxia, with the fixed-cell microscopy method that we have previously described (Hernansanz-Agustín et al., 2021).

We observed that, during the first few minutes of hypoxia, the presence of lithium inhibited the NCLX-dependent superoxide burst in WT MEFs (**Figure 14**). Indeed, we measured the effect of lithium on ROS production through two different incubations: MEFs were pretreated with lithium for 30 min and then incubated with 5 μM DHE for 10 min (called "pretreat" on **Figure 14**) or MEFs were incubated with lithium and DHE at the same time for 10 min. NCLX KO MEFs did not produce superoxide burst in acute hypoxia, as we have previously described described (Hernansanz-Agustín et al., 2021), so, lithium addition did not have effect upon acute hypoxia (**Figure 14**).

However, regarding ROS production in normoxia, the addition of lithium increased DHE signal in normoxia in both WT and NCLX KO MEFs (**Figure 14**), suggesting that lithium ions may affect mitochondria beyond NCLX.

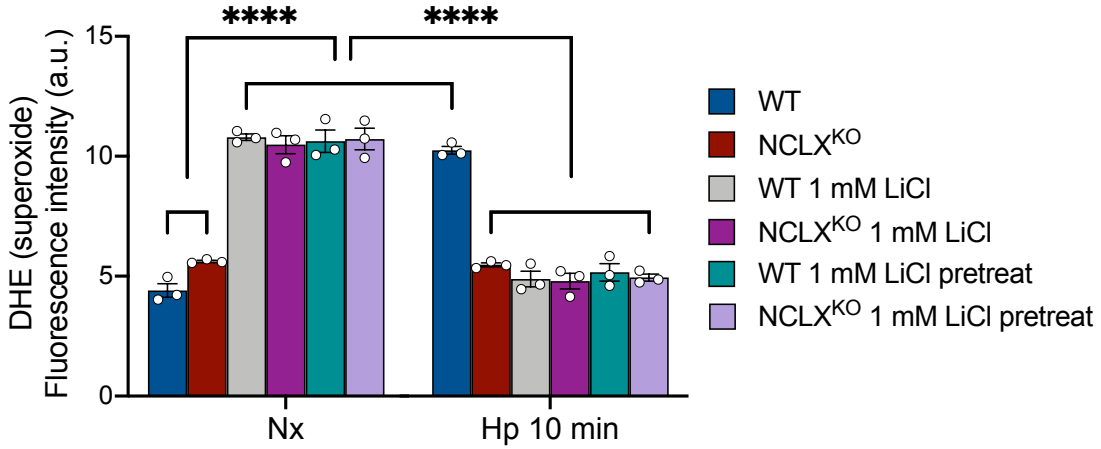

Figure 14. Effect of 1 mM LiCl on ROS production in MEFs. For normoxic condition (Nx), WT or NCLX KO MEFs were untreated, treated for 10 min with DHE or pretreated for 30 min prior to DHE incubation with 1 mM LiCl. Then, cells were incubated for 10 min with 5 μM DHE. For hypoxic condition, WT or NCLX KO MEFs were untreated, treated only in hypoxia or pretreated for 30 min in normoxia prior to hypoxia with 1 mM LiCl. Then, cells were quickly washed in the hypoxia chamber at 1% oxygen with pre-balanced hypoxic medium and were incubated with 5 μM DHE for 10 min. Then, cells were fixed inside hypoxia chamber. Quantification of three independent experiments is shown. ****p<0.0001, by two-way ANOVA with Tukey's post-hoc test

2.5.1. Lithium-induced ROS production does not require mitochondrial complex III

In order to assess the ROS source induced by lithium during normoxia, we treated MEFs with 1 μM myxothiazol, a CIII inhibitor at its Q_o site. Contrary to antimycin A, a CIII blocker at its Q_i site, myxothiazol incubation does not induce ROS production because, by blocking Q_o site, the Q cycle in CIII is completely inhibited which prevents electrons from being unpaired (Hernansanz-Agustín & Enríquez, 2021b).

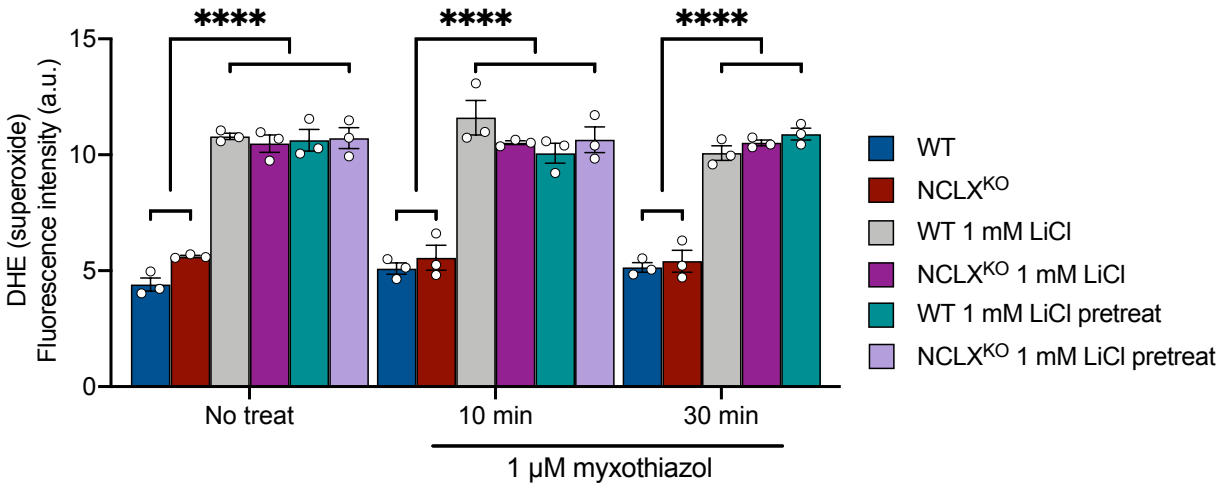

Figure 15. Effect of 1 μM myxothiazol on lithium-induced ROS production in MEFs. WT or NCLX KO MEFs were untreated, treated for 10 min with DHE incubation or pretreated for 30 min prior to DHE incubation with 1 mM LiCl and with 1 μM myxothiazol for 10 or 30 minutes. Then, cells were incubated for 10 min with 5 μM DHE and were fixed. Quantification of three independent experiments is shown. ****p<0.0001, by two-way ANOVA with Tukey's post-hoc test

However, myxothiazol treatment did not block lithium-induced ROS production, nor added for 10 minutes during the DHE incubation, neither after 30 minutes before the 10-minutes DHE incubation (**Figure 15**). Therefore, CIII is not the ROS source of lithium-induced ROS production in normoxia. Besides, cotreatment of 1 mM LiCl together with 1 μM myxothiazol for 30 minutes induces NCLX KO MEFs death (missing group in **Figure 15**), indicating that cells with NCLX chronic deletion were not able to handle the effect of lithium together with the CIII inhibition and, in turn, suggesting that NCLX chronic deletion is deeply disturbing mitochondrial metabolism as we will see below.

2.6. Lithium-induced ROS production involves mitochondrial complex I

In addition to CIII inhibition was not preventing the lithium-induced ROS production (**Figure 15**), the effect of lithium on superoxide production (**Figure 14**) reminded us of what was happening when mitochondrial CI is blocked (Hernansanz-Agustín et al., 2017). Similar to lithium treatment, CI inhibition, using small interference RNAs or rotenone, produced an increase of ROS in normoxia and abolished the superoxide burst induced by hypoxia (Hernansanz-Agustín et al., 2017).

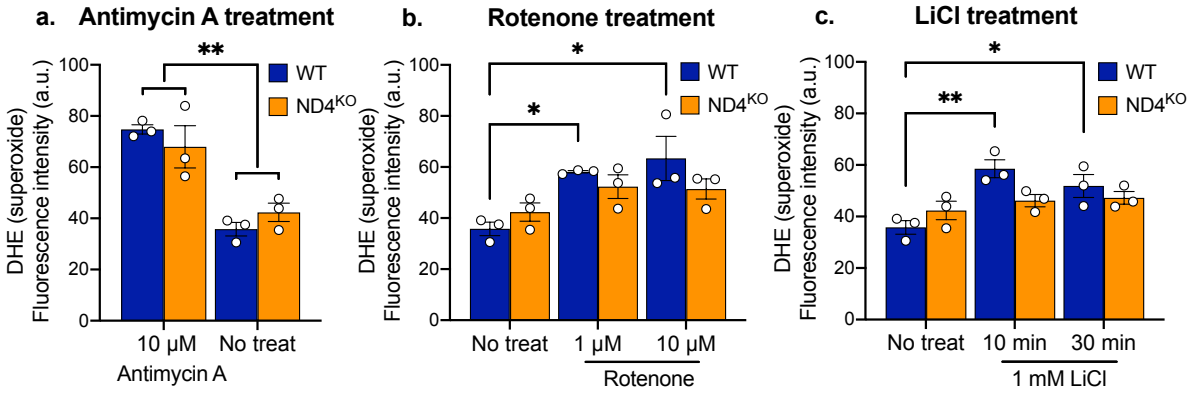

Figure 16. ROS production determination in FBalb cells. WT or ND4 KO FBalb cells were incubated with 10 µM antimycin A for 30 min (**a**), 1 µM or 10 µM rotenone for 30 min (**b**) or 1 mM LiCl for 0 or 30 min (**c**) and, then, 5 µM DHE was added for 10 min. Quantification of three independent experiments with at least 8 replicates measured per condition. *p<0.05, **p<0.005, by two-way ANOVA with Tukey's post-hoc test

Thus, we analyzed superoxide levels in cells without CI, specifically without ND4 protein (Hernansanz-Agustín et al., 2023). First, we saw that in presence of antimycin A (AA), WT and ND4 KO FBalb cells were able to increase superoxide levels (**Figure 16a**). We also checked the effect of rotenone on these cells and, as expected, WT FBalb cells presented an increase on superoxide production in presence of 1 µM or 10 µM rotenone while ND4 KO FBalb cells were not significatly affected by rotenone (**Figure 16b**). Similarly, we observed that the presence of 1 mM LiCl for 10 min, during the incubation with the tdye, or added 30 min before the incubation with the dye, induced an increase on superoxide exclusively in WT FBalb cells meanwhile ND4 KO FBalb cells did not seem to be affected by LiCl (**Figure 16c**); indicating that CI is involved in lithium-induced ROS production, so, in turn, lithium ions may be affecting mitochondrial CI.

2.7. Lithium treatment affects mitochondrial oxygen consumption

Since we have observed that CI is involved in the lithium effect on mitochondria (**Figure 16**), we wondered whether lithium treatment may impact on cellular respiration.

2.7.1. Lithium addition reduces mitochondrial maximal respiration in whole cells

A well-known approach to analyze bioenergetic features in cell cultures is the measurement of oxygen consumption rates (OCR) with subsequent injections of oligomycin, FCCP and antimycin A plus rotenone. After basal respiration is measured, oligomycin is injected, so the mitochondrial complex V is inhibited and, in turn, the respiration is diminished. The amount of oxygen consumed to produce ATP by OXPHOS is calculated from the difference between basal respiration and after oligomycin injection. Next, FCCP is injected, an OXPHOS uncoupler which transports protons from the intermembrane space to the mitochondrial matrix. Thus, the electron flux through the ETC is maximized which is translated into the cellular maximal respiration. The difference between the maximal respiratory capacity and the basal respiration is known as the reserve capacity, which is a measure of the ability of cells to respond to increased energy demand or under stress. Eventually, antimycin A and rotenone are complexes III and I inhibitors, respectively, so, their injection implies the inhibition of electron flux through the ETC. Therefore, the leftover value after the last injection corresponds to non-mitochondrial respiration, i.e., the oxygen consumed by other cellular enzymes. The difference between the oxygen consumed after oligomycin injection and the non-mitochondrial respiration is known as proton leak and is the respiration due to the proton translocation done by other molecules than complex V.

We modified the regular experiment described above by adding one more injection, before oligomycin, we injected 1 mM LiCl in some wells to analyze whether lithium ions could affect directly to cellular oxygen consumption (**Figure 17a**). We observed that the basal respiration was not changed in presence of lithium, both in WT and in NCLX KO MEFs (**Figure 17b**). However, by analyzing each time point, we saw that basal respiration was reduced in NCLX KO MEFs compared to WT (**Figure 17a**), as observed in another NCLX chronic deletion cells (Pathak et al., 2020). Additionally, we observed that, after FCCP injection, the OCR was reduced in WT MEFs treated with lithium and in NCLX KO MEFs, treated or not with lithium, compared to untreated WT MEFs (**Figure 17a**). According to this result, the maximal respiratory capacity and, in turn, the reserve capacity were also decreased in WT MEFs treated with lithium and in NCLX KO MEFs, treated or not with

lithium, compared to untreated WT MEFs (**Figure 17c and d**). Finally, other analyzed parameters were not affected by the presence of lithium nor by chronic NCLX ablation (**Figure 17e to g**).

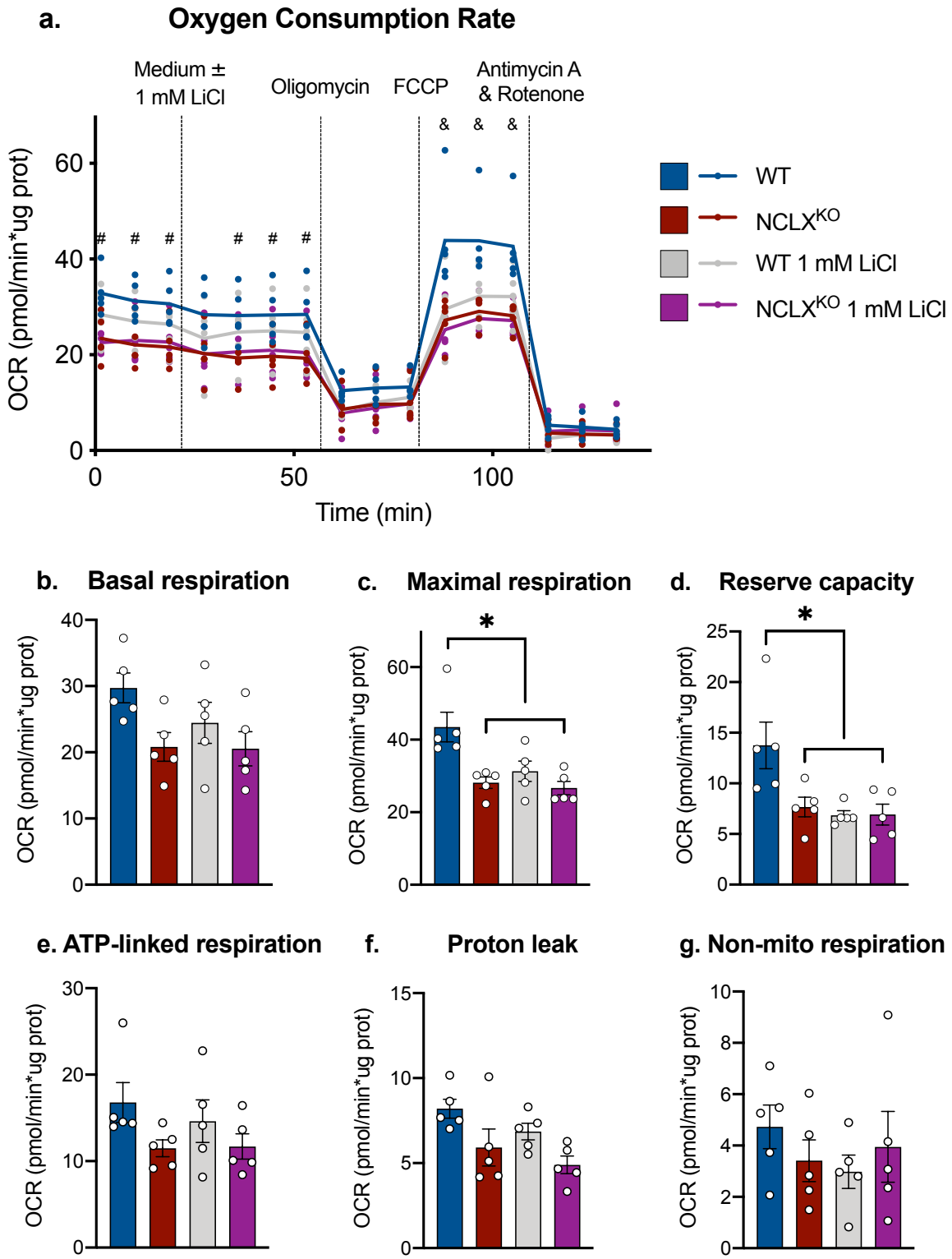

Figure 17. Effect of 1 mM LiCl and NCLX presence on oxygen consumption rate in MEFs. Oxygen consumption was measured in a Seahorse XF24 Analyzer in WT and NCLX KO MEFs and, after the experiment, total protein was measured in each well. (**a**) Normalized OCR plot indicating the sequential addition of medium with or without 1 mM LiCl, 5 µg/mL oligomycin, 300 nM FCCP, 1 µM antimycin A and 1 µM rotenone. Quantification of basal respiration (**b**), maximal respiration (**c**), reserve capacity (**d**), ATP-linked respiration (**e**), proton leak (**f**) and non-mitochondrial respiration (**g**) shown in (**a**). 5 independent experiments with, at least, 3 replicates of each condition were performed. # means *p<0.05 WT vs KO and & means **p<0.005 WT vs all other, by two-way ANOVA with Bonferroni's post-hoc test; *p<0.05, by one-way ANOVA with Tukey's post hoc test

2.7.2. Lithium addition increases oxygen consumption in permeabilized cardiomyocytes cell line

To directly measure the effect of lithium on mitochondrial complexes activity, during my stay in the laboratory of Dr. John W. Elrod we decided to permeabilize the cardiomyocytes AC16 cell line and measured oxygen consumption by Seahorse experiments using substrates for different ETC complexes as described (Salabei et al., 2014).

First, we analyzed the digitonin concentration required to permeabilize AC16 cells and maintain mitochondrial proteins by Western blot (**Figure 18**). Thus, we used 25 µg/mL digitonin immediately before to Seahorse experiments and 1 mM LiCl was added together with digitonin treatment in some wells.

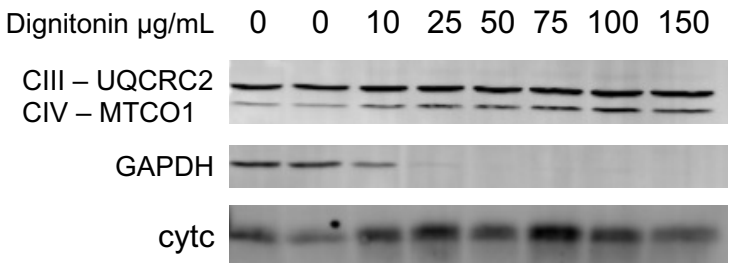

Figure 18. Effect of different digitonin concentrations on cytosolic and mitochondrial proteins analyzed by Western blotting. AC16 cells were incubated with different digitonin concentrations (in µg/mL: 0, 10, 25, 50, 75, 100, 150) dissolved in BSA-MAS buffer during 30 min at 37 ºC and 5% CO_2. Samples were extracted and blotted against ubiquinol-cytochrome *c* reductase core protein 2 (UQCRC2, from mitochondrial CIII) and cytochrome c oxidase I (MTCO1, from mitochondrial CIV), glyceralsehyde-3-phosphate dehydrogenase (GAPDH) and cytochrome c (cytc).

During the Seahorse experiment, successive injections were performed: firstly, ADP plus specific substrates to activate CI (pyruvate and malate, **Figure 19**) or CII (succinate, **Figure 20**), then, oligomycin to inhibit CV and, finally, antimycin A plus rotenone to block completely the ETC. Notably, FCCP was not injected because the ADP concentration used (1 mM) is enough to saturate mitochondrial complexes activity, inducing respiration state 3. After oligomycin injection, oxygen consumption is assumed to be comparable to respiration state 4, when all ADP has been transformed into ATP and, in turn, ETC function is inhibited. Bey dividing state 3 by state 4 we calculated the respiratory control ratio (RCR), which indicates mitochondrial coupling.

First, we analyzed the effect of different lithium concentrations (0.5, 0.75 and 1 mM LiCl) on oxygen consumption (**Figure 19**). Despite the fact that it is only one experiment, we saw that the oxygen consumption before substrates injection seemed to be increased in presence of lithium (**Figure 19a and b**). Besides, 0.5 mM and 0.75 mM LiCl tended to increase oxygen consumption after CI-dependent substrates injection (**Figure 19a and c**), as observed in isolated mitochondria from leukocytes of BD patients in presence of lithium (de Sousa et al., 2015) and also in cortex homogenate from postmortem human brain tissue of healthy individuals (Maurer et al., 2009). Oxygen consumption also seemed to be increased after oligomycin injection (**Figure 19d**), which may be related to the observed increment in OCR before substrate injection (**Figure 19a and b**), but more replicates should be done to ensure these results.

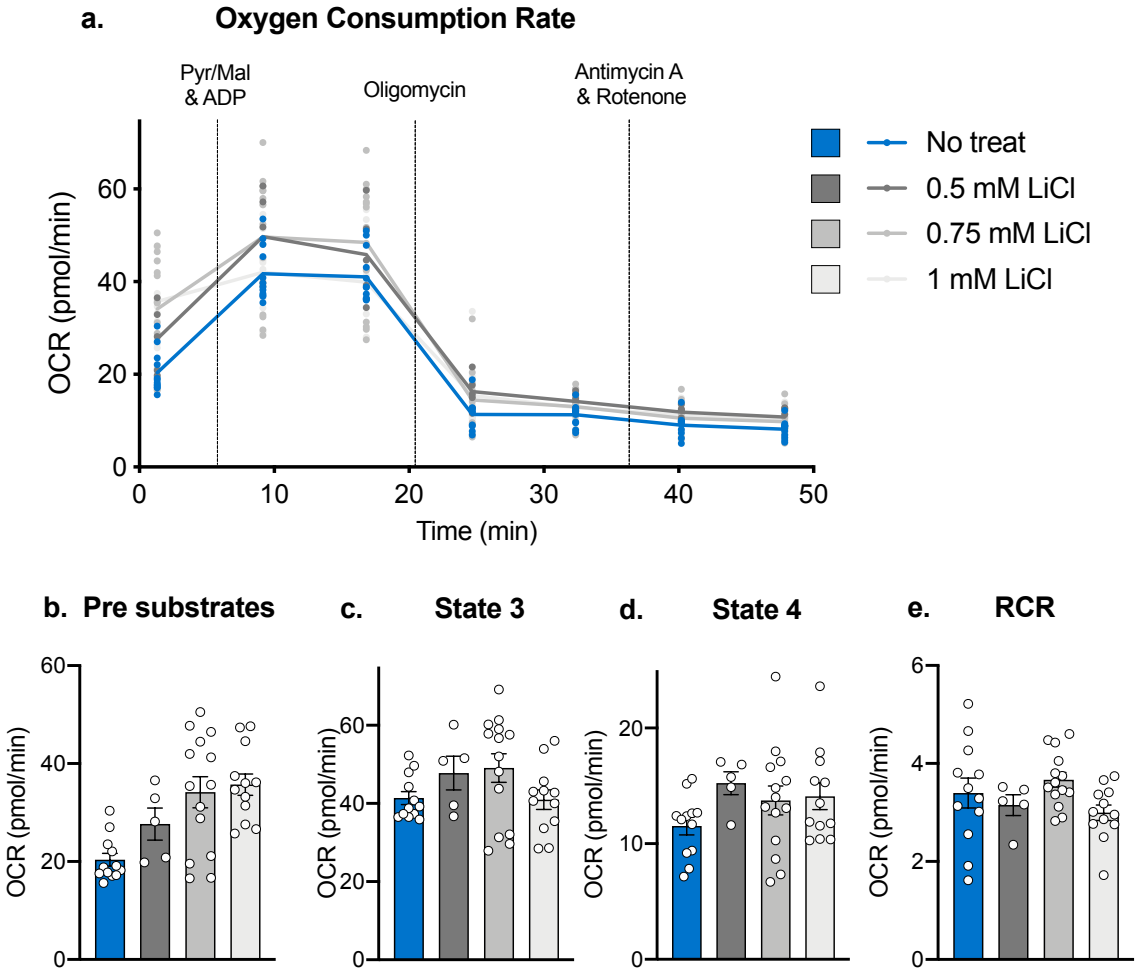

Figure 19. Effect of different lithium concentrations on oxygen consumption rate in permeabilized cardiomyocytes cell line. Oxygen consumption was measured in a Seahorse XF96 Analyzer in AC16 cells previously permeabilized with 25 µg/mL digitonin and treated or not with 0.5 mM, 0.75 mM or 1 mM LiCl, as indicated. (**a**) OCR plot indicating the sequential addition of substrates (5 mM pyruvate, 2.5 mM malate and 1 mM ADP), 1 µg/mL oligomycin, 1 µM antimycin A and 1 µM rotenone. Quantification of oxygen consumption before substrates injection (**b**), state 3 respiration (oxygen consumption after substrates injection) (**c**), state 4 respiration (oxygen consumption after oligomycin injection) (**d**) and respiratory control ratio (state 3 divided by state 4, RCR) (**e**) shown in (**a**). One independent experiment is shown. Each dot represents one well.

In order to analyze the effect of lithium on CII-dependent respiration, we performed the same experiment but injecting ADP plus succinate with or without rotenone, to assess at the same time the role of CI activity under succinate implementation. Although it is only one experiment, we saw that 0.75 mM LiCl again enhanced oxygen consumption before substrates injection (**Figure 20a and b**). Besides, the presence of rotenone seemed to decrease state 3 respiration (**Figure 20c**), while lithium addition tended to increase state 4 respiration (**Figure 20d**). Thus, RCR seemed to be decreased in presence of lithium (**Figure 20e**), suggesting that lithium addition may be impairing mitochondrial coupling under succinate induction with functional or non-functional CI. However, more replicates should be done to guarantee these results.

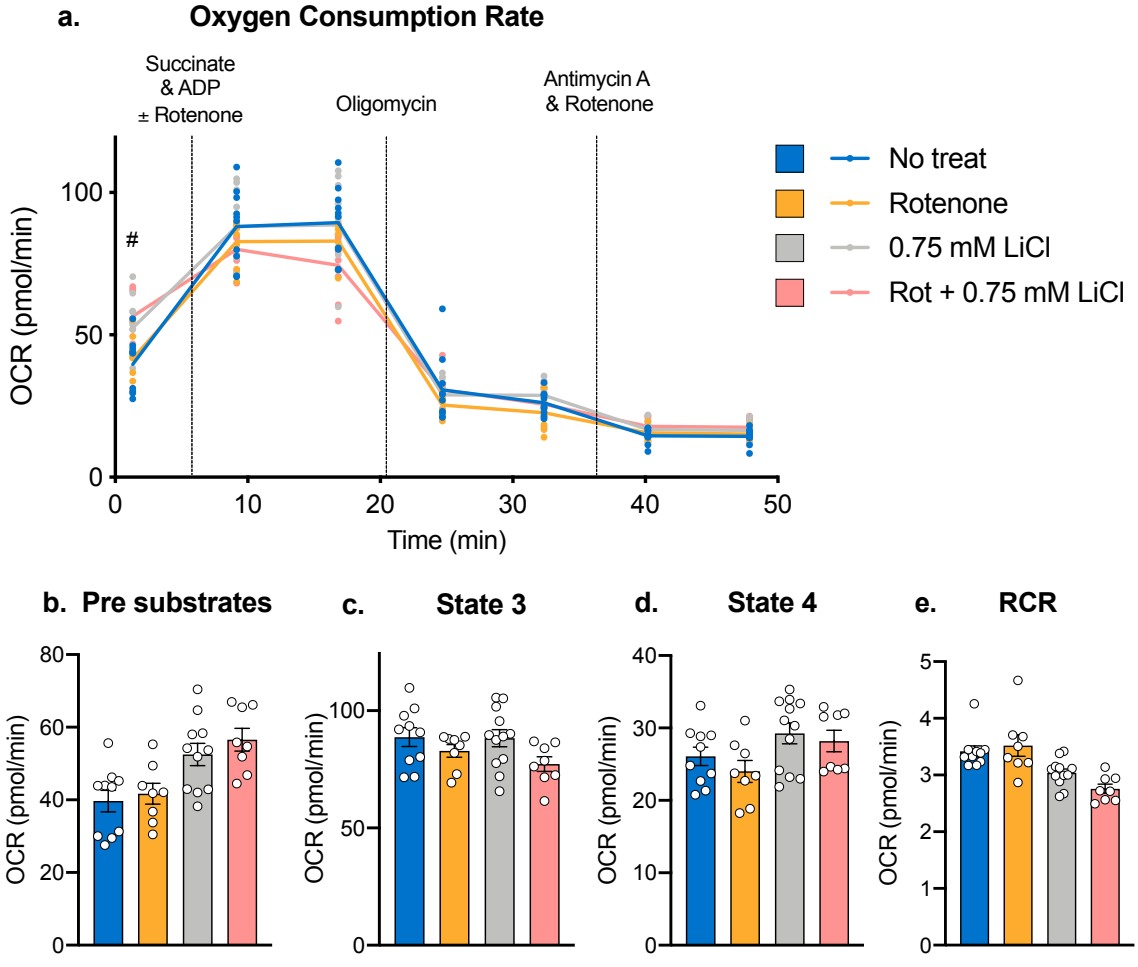

Figure 20. Effect of 0.75 mM LiCl on oxygen consumption rate in permeabilized cardiomyocytes cell line. Oxygen consumption was measured in a Seahorse XF96 Analyzer in AC16 cells previously permeabilized with 25 µg/mL digitonin and treated or not with 0.75 mM LiCl, as indicated. (**a**) OCR plot indicating the sequential addition of substrates (10 mM succinate, 1 mM ADP and, as indicated, 1 µM rotenone), 1 µg/mL oligomycin, 1 µM antimycin A and 1 µM rotenone. Quantification of oxygen consumption before substrates injection (**b**), state 3 respiration (oxygen consumption after substrates injection) (**c**), state 4 respiration (oxygen consumption after oligomycin injection) (**d**) and respiratory control ratio (state 3 divided by state 4, RCR) (**e**) shown in (**a**). One independent experiment is shown. Each dot represents one well.

Although the results in whole cells seem to be controversial with results in permeabilized cells, it is necessary to clarify that the conditions required to analyze oxygen consumption in permeabilized cells differ from regular cellular conditions, for example, the total absence of sodium and calcium ions in the permeabilized medium. Altogether these results would indicate that lithium ions may be impacting directly on OXPHOS (**Figures 17, 19 and 20**) and, specially, it would be directly related to CI (**Figures 16 and 19**).

2.8. Lithium treatment slightly breaks the mitochondrial network

During performing FRAP experiments, we realized that after lithium treatment addition in normoxia, something was happening to the mitochondrial network. Therefore, we decided to take photos of MEFs transfected with mitoRFP, which encodes a red fluorescence protein targeted into IMM, and we analyzed the mitochondrial network as described (Valente et al., 2017).

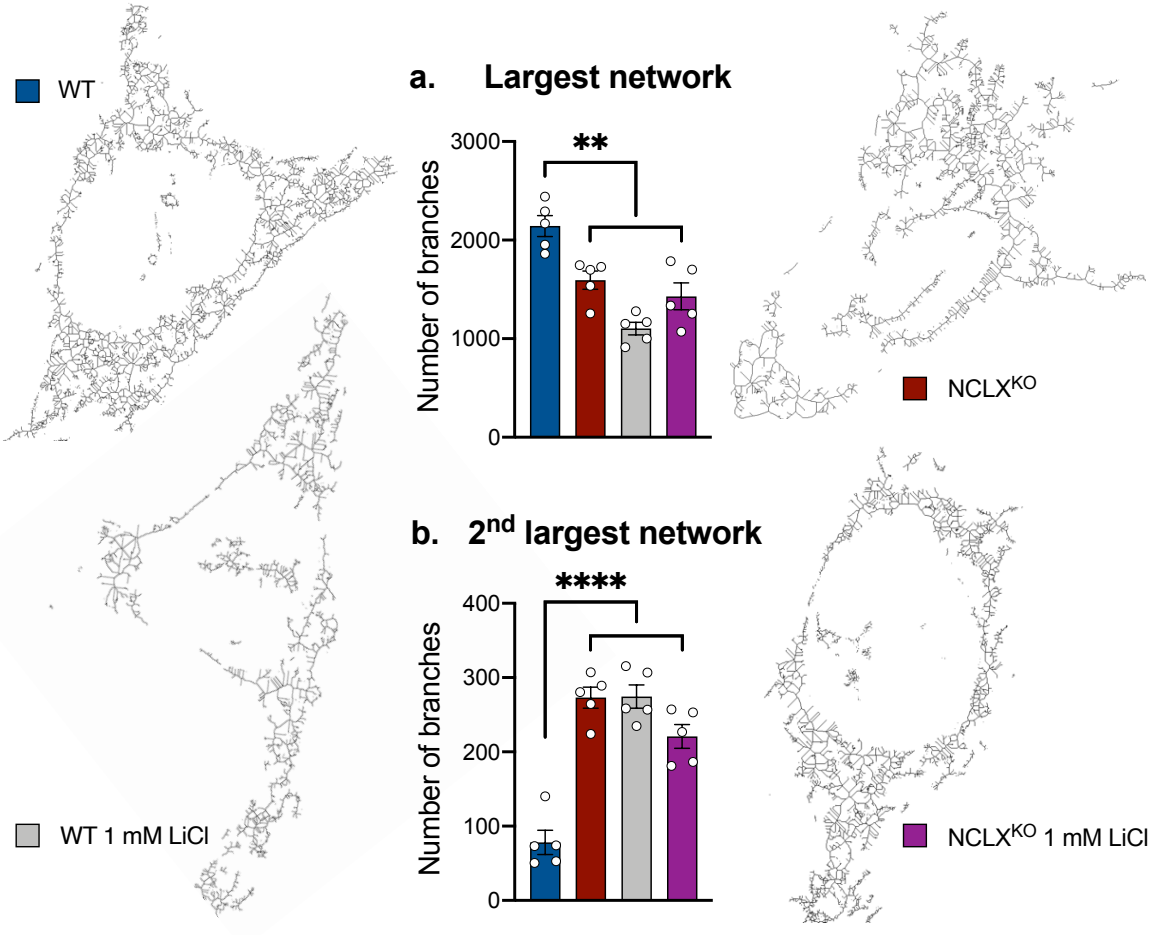

Figure 21. Effect of 1 mM LiCl and NCLX presence on mitochondrial network in normoxia. Representative images of mitochondrial network of mitoRFP-transfected WT or NCLX KO MEFs treated or untreated with 1 mM LiCl in normoxia. Quantification of the number of branches of the largest (**a**) or the second largest (**b**) mitochondrial network. 5 independent experiments with, at least, 5 replicates of each condition were performed. **p<0.005, ****p<0.0001, by one-way ANOVA with Tukey's post-hoc test

We observed that while the mitochondrial network of WT MEFs was mainly one and continuous network around the nucleus (**Figure 21**), the addition of lithium induced that mitochondrial network got broken into smaller networks (**Figure 21**). Thus, comparing the number of branches of the first largest network, the addition of lithium decreased its number in WT MEFs (**Figure 21a**). However, in NCLX KO MEFs the number of branches was smaller than in WT MEFs and the mitochondrial network remained practically unchanged in presence of lithium (**Figure 21a**). As a consequence, the number of branches of the second largest network was bigger in WT MEFs treated with lithium and in NCLX KO MEFs treated or untreated with lithium than in untreated WT MEFs (**Figure 21b**).

Furthermore, we tested the effect of lithium treatment on mitochondrial network during hypoxia. However, hypoxia *per se* induced the breakdown and reduction of mitochondrial network (**Figure 22**), eventually resulting in cells becoming a circle and mitochondria becoming dots. This strong and time-dependent effect of hypoxia made impossible to assess if lithium ions were worsening, ameliorating or unaffecting the effect of hypoxia on mitochondrial network.

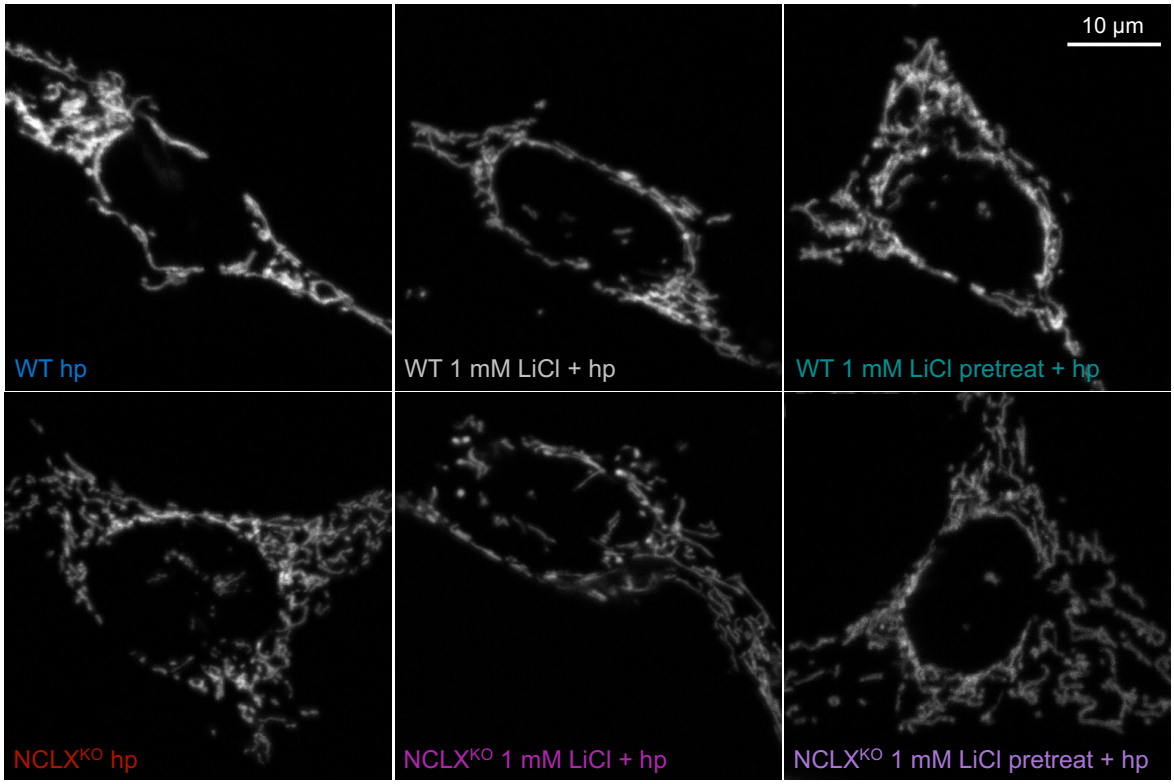

Figure 22. Representative images of hypoxia effect on mitochondrial network. WT and NCLX KO MEFs were transfected with mitoRFP and, after 30 minutes of hypoxia (1% O_2 and 5% CO_2), images were taken using confocal microscopy. Left panels show untreated cells, central panels show cells subjected to hypoxia and treated with 1 mM LiCl at the same time (indicated as 1 mM LiCl + hp) and right panel show cells pretreated with 1 mM LiCl in normoxia during 30 minutes before hypoxia (indicated as 1 mM LiCl pretreat hp).

2.9. Lithium treatment induces mitochondrial hyperpolarization independently of NCLX

Due to the different effects of lithium on mitochondrial metabolism that we had observed (**Figures 14 to 21**), we wondered whether the IMM potential ($\Delta\Psi_{mt}$) may be affected. Therefore, by using TMRM fluorescent dye, we analyzed $\Delta\Psi_{mt}$ in MEFs through live imaging using a confocal microscopy with temperature and gas control.

Firstly, we analyzed the maximal and minimal values of $\Delta\Psi_{mt}$, by adding 1 µM oligomycin and subsequently 1 µM FCCP, respectively (**Figure 23**). We observed that both WT and NCLX KO MEFs were able to respond to both compounds similarly (**Figure 23**).

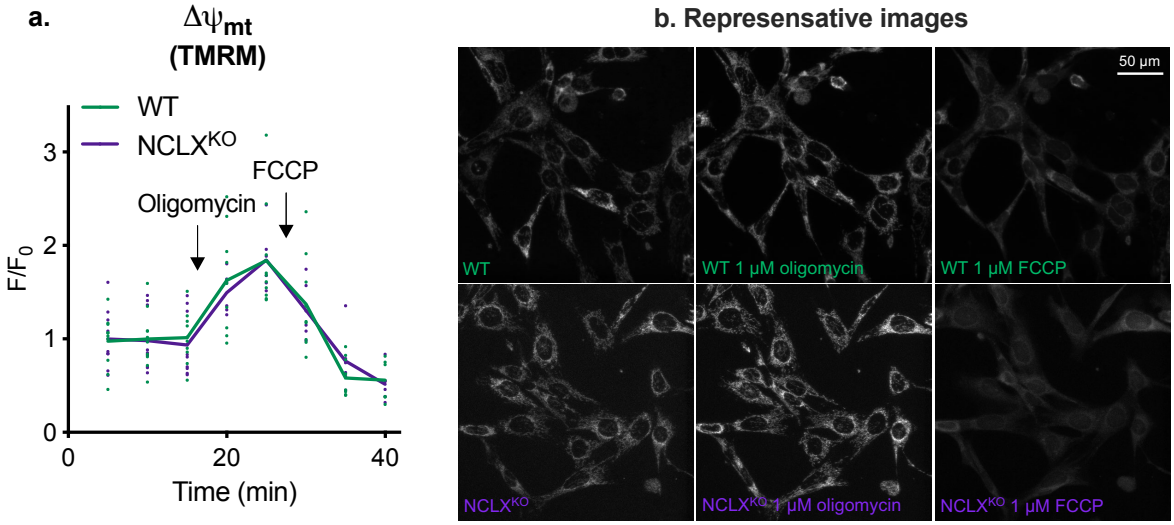

Figure 23. Effect of oligomycin and FCCP on $\Delta\Psi_{mt}$ in MEFs. WT and NCLX MEFs were incubated with 20 nM TMRM during all experiment long. After setting the baseline, 1 µM oligomycin was injected and, then, 1 µM FCCP was added too. Pooled and normalized traces from 3 independent experiments are shown in (**a**) and representative images of each treatment are showed in (**b**).

Next, we analyzed the effect of lithium addition on $\Delta\Psi_{mt}$. After some cycles to set the baseline, we added 1 mM LiCl in normoxia which induces an increase in $\Delta\Psi_{mt}$ in both, WT and NCLX KO MEFs (**Figure 24a to c**). Interestingly, the transition to hypoxia itself induced hyperpolarization only in WT MEFs (**Figure 24a, d and e**) and adding lithium before the transition to hypoxia inhibited the hypoxia-dependent hyperpolarization in WT MEFs (**Figure 24a**). Besides, we analyzed the lithium effect together with hypoxia and we saw the same result than in normoxia, a hyperpolarization in both genotypes (**Figure 24d to f**), showing that adding lithium with hypoxia bypassed the NCLX deletion regarding $\Delta\Psi_{mt}$ in MEFs (**Figure 24d and e**).

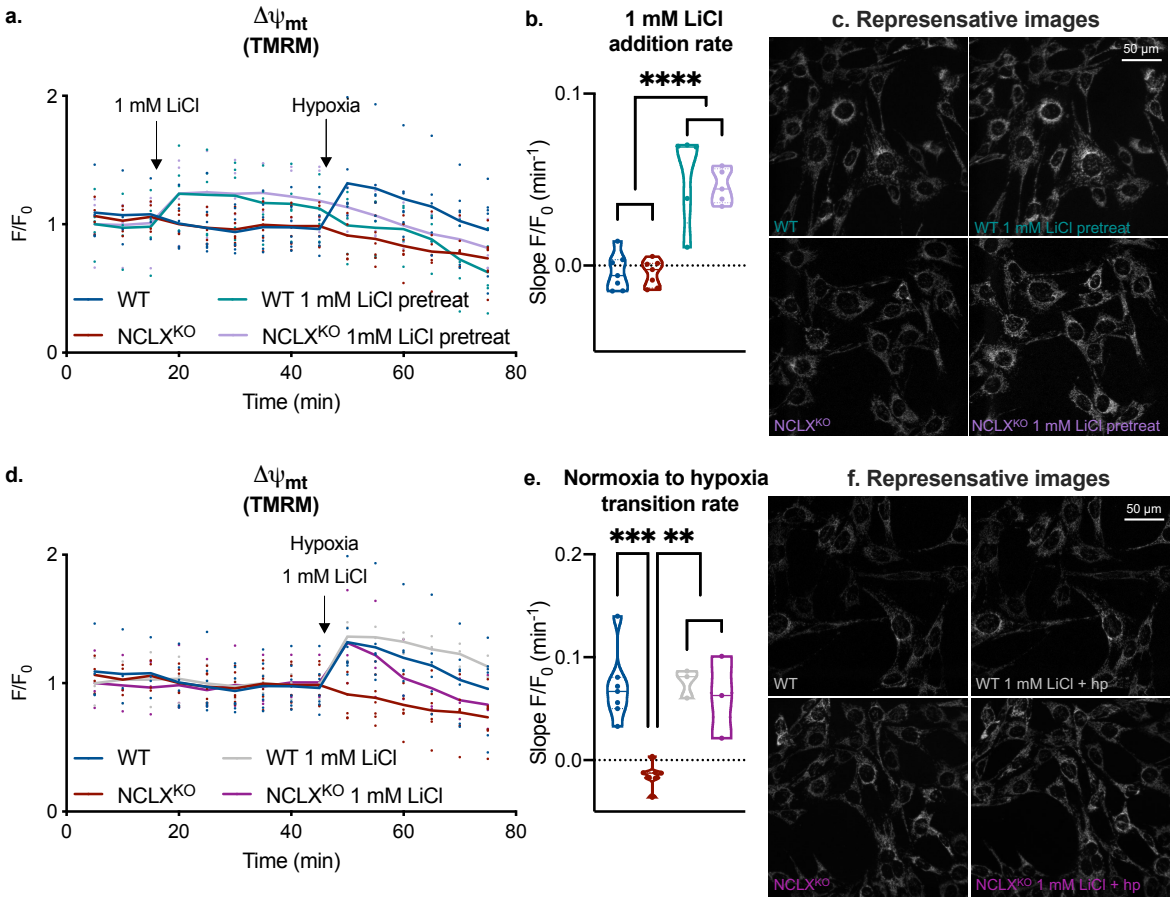

Figure 24. Effect of 1 mM LiCl on $\Delta\Psi_{mt}$ in MEFs. WT and NCLX KO MEFs were incubated with 20 nM TMRM during all experiment long. In some wells, 1 mM LiCl was injected in normoxia (**a**) or together with hypoxia (1% oxygen) (**d**). Pooled and normalized traces showed (**a** and **d**) were used to calculate the lithium injection rate (**b**) and hypoxia induction rate (**e**), respectively. Representative images of before and after lithium injection are showed in (**c**) and (**f**). Quantification of at least three independent experiments with three replicates measured per condition. **p<0.01, ***p<0.001, ****p<0.0001, by two-way ANOVA with Tukey's post-hoc test

Therefore, as observed in lithium-induced ROS production (**Figure 14**), the effect of lithium on mitochondrial metabolism is beyond NCLX, but, as we have observed (**Figures 16 and 19**), Cl may also be mediating this effect of lithium on $\Delta\Psi_{mt}$, as it has been recently observed (Hernansanz-Agustín et al., 2023).

2.9.1. Acute hypoxia produces NCLX-dependent mitochondrial hyperpolarization through mitochondrial sodium import

Surprisingly, we observed that acute hypoxia induced IMM hyperpolarization in WT MEFs, but did not affect $\Delta\Psi_{mt}$ of NCLX KO MEFs (**Figure 25**). This result may seem contradictory to our previous data because we had demonstrated that mitochondrial matrix is acidified after inducing acute hypoxia in a CI-dependent manner (Hernansanz-Agustín et al., 2017). Thus, we decided to go further and try to explain this unexpected result.

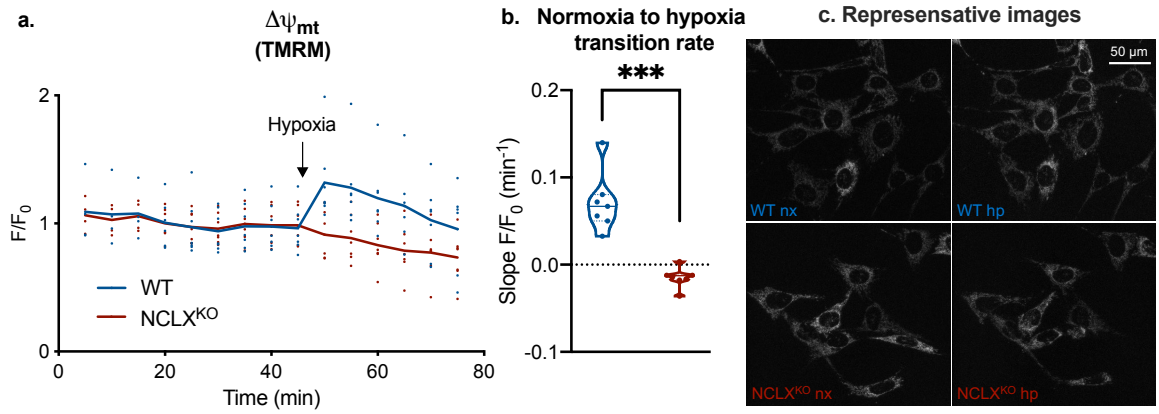

Figure 25. Effect of acute hypoxia on $\Delta\Psi_{mt}$ in MEFs. WT and NCLX MEFs were incubated with 20 nM TMRM during all experiment long. Pooled and normalized traces from 7 independent experiments are shown in (**a**) and, using these data, the hypoxia induction slope (**b**) was calculated. Representative images of hypoxia transition are showed in (**c**). ***p<0.001, by Student's t test

Since NCLX KO MEFs did not present NCLX, the main difference between them and WT MEFs after inducing hypoxia is that $_{m}Na^{+}$ import does not occur (Hernansanz-Agustín et al., 2020) (**Figure 11**). Hence, in order to find out why acute hypoxia is inducing NCLX-dependent mitochondrial hyperpolarization, we decided to increase $_{m}Na^{+}$ import by increasing extracellular sodium content. As cell culture media buffers usually have 140 mM NaCl, we tried different extra-sodium concentrations (50 mM and 100 mM) to make sure that cells were able to sense it. We observed that concentrations higher than 25 mM of extra-NaCl disrupted the $\Delta\Psi_{mt}$ completely (**Figure 26**).

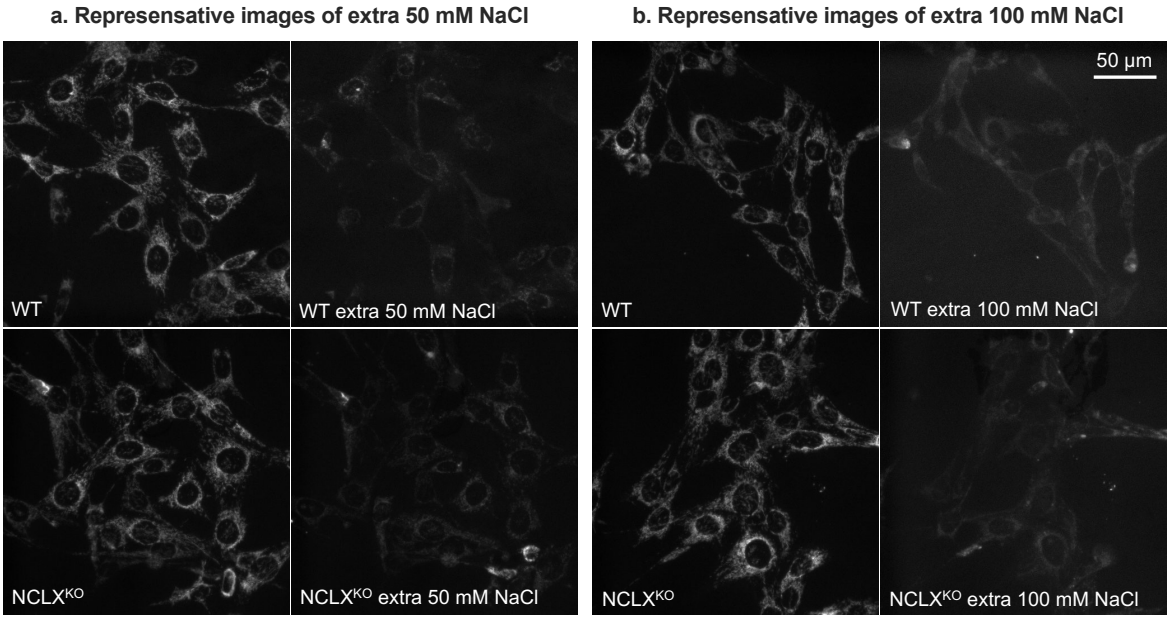

Figure 26. Effect of extra NaCl on $\Delta\Psi_{mt}$ in MEFs. WT and NCLX MEFs were incubated with 20 nM TMRM during all experiment long. Representatives images of extra 50 mM NaCl (**a**) or 100 mM NaCl (**b**) addition on TMRM fluorescence.

However, by adding 25 mM NaCl in the extracellular media, the $\Delta\Psi_{mt}$ was increased in WT MEFs and was not affected or, even, seemed to decrease in NCLX KO MEFs (**Figure 27**). This $\Delta\Psi_{mt}$ control induced by sodium ions has been recently noticed independently to these experiments and, interestingly, CI is involved in the mechanism (Hernansanz-Agustín et al., 2023).

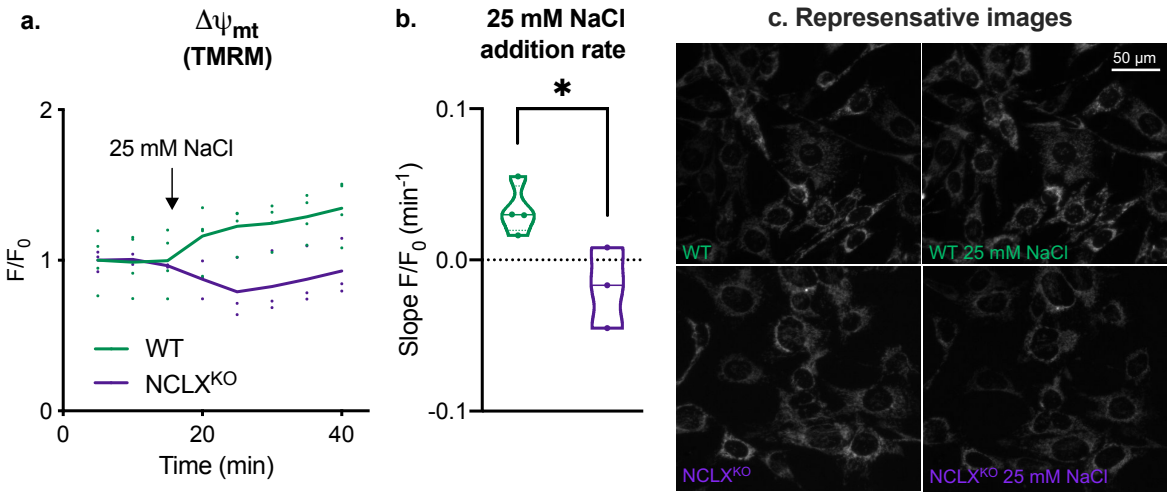

Figure 27. Effect of extra 25 mM NaCl on $\Delta\Psi_{mt}$ in MEFs. WT and NCLX MEFs were incubated with 20 nM TMRM during all experiment long. Pooled and normalized traces from at least 3 independent experiments are shown in (**a**) and, using these data, the sodium injection slope (**b**) was calculated. Representative images of before and after sodium addition are showed in (**c**). *p<0.001, by Student's t test

Altogether, these results indicate that monovalent cations are able to control the $\Delta\Psi_{mt}$ (**Figures 24 and 27**) and as observed with sodium by CI-NHE activity (Hernansanz-Agustín et al., 2023), but more experiments are required to fully unravel the exact role of NCLX and CI and the effect of lithium on their delicate relationship.

2.10. Lithium treatment affects mitochondrial calcium dynamics

Finally, NCLX function is generally measured by analyzing mitochondrial calcium ($_mCa^{2+}$) dynamics by using probes sensitive to either cytosolic or extramitochondrial calcium ($_iCa^{2+}$) or $_mCa^{2+}$ after a stimulus that provokes $_mCa^{2+}$ import and the subsequent NCLX-depdendent $_mCa^{2+}$ efflux. Thus, since we have observed that $_mLi^{+}$ import is a NCLX-dependent effect of lithium addition (**Figures 9 and 10a**) and $_mCa^{2+}$ seems to be more concentrated in NCLX KO MEFs after 30 minutes of lithium treatment in normoxia (**Figure 10c**), we have analyzed $_mCa^{2+}$ dynamics using different cell types and technique approaches, as described in (Luongo et al., 2017; Rozenfeld et al., 2022).

2.10.1. Lithium ions enhance NCLX-dependent mitochondrial calcium efflux in permeabilized cardiomyocytes cell line

To directly measure NCLX function and avoiding plasma membrane calcium transporters, during my stay in the laboratory of Dr. John W. Elrod we decided to permeabilize cells and measured $_{m}Ca^{2+}$ transients with the technique they have used (Garbincius et al., 2023; Luongo et al., 2017). Notably, the buffer used in these experiments contained 11 mM NaCl in lithium-free conditions and 10 mM NaCl plus 1 mM LiCl in lithium conditions.

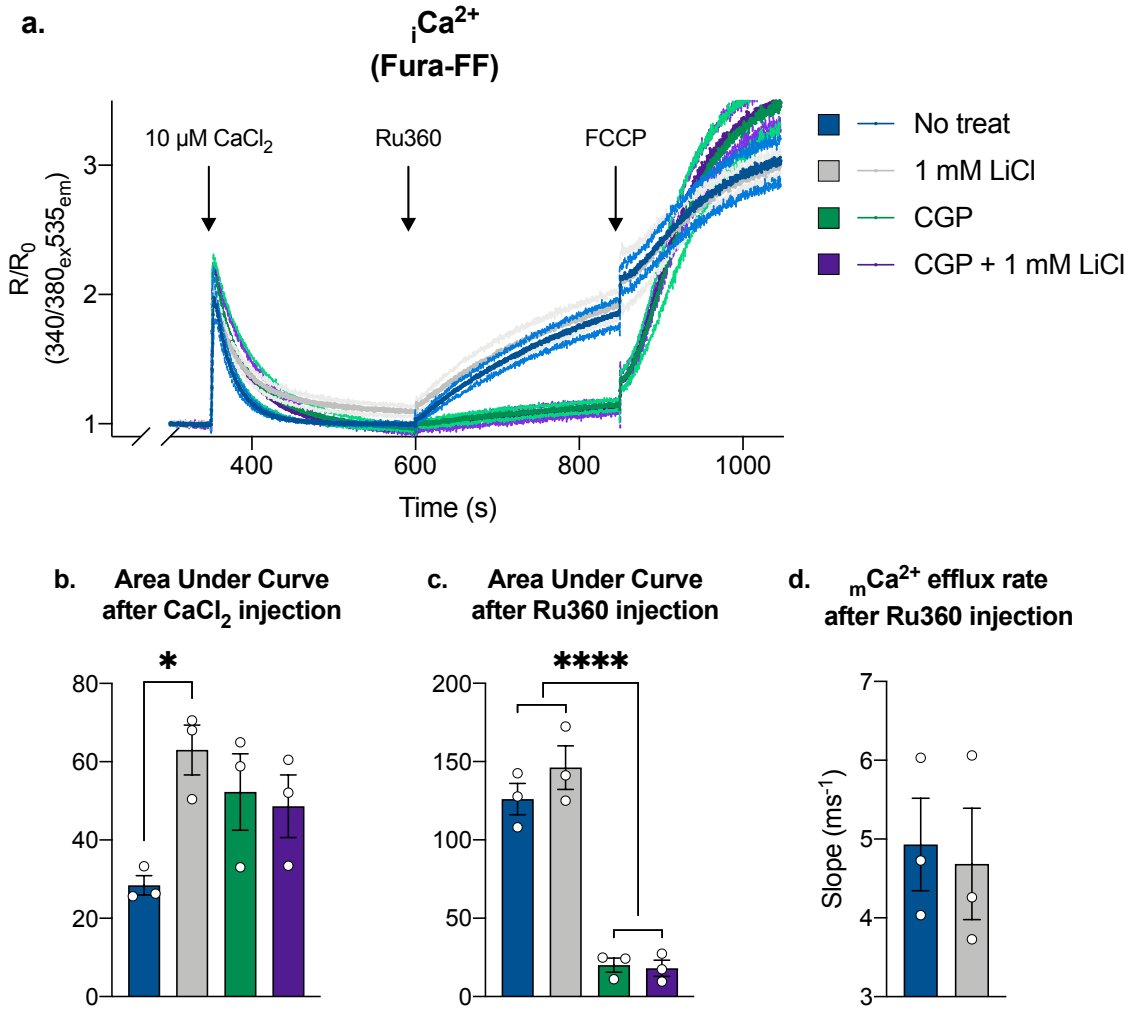

Figure 28. Effect of 1 mM LiCl on $_{m}Ca^{2+}$ dynamics in permeabilized AC16 cells. (**a**) Pooled traces from 3 independent experiments of AC16 cardiomyocytes in the presence or absence of 1 mM LiCl and/or NCLX inhibitor CGP-37157 (CGP), representing extramitochondrial bath Ca^{2+} ($_{i}Ca^{2+}$) measured with Fura-FF. 4 million cells were permeabilized with digitonin in the presence of thapsigargin (SERCA inhibitor), then administered a single 10 µM Ca^{2+} bolus, with subsequent additions of the mtCU inhibitor Ru360 and ETC uncoupler FCCP as indicated. Quantification of area under the curve (AUC) after Ca^{2+} bolus (**b**) or after Ru360 injection (**c**) and quantification of the fluorescence slope from 25 seconds after Ru360 injection (**d**) shown in (**a**). *p< 0.05, ****p< 0.0001, by one-way ANOVA with Tukey's post-hoc test

Using 1 μM Fura-FF dye, $_{i}Ca^{2+}$ was measured in permeabilized cardiomyocytes cell line, AC16 cells, with 80 μg/mL digitonin in presence of 6 μM thapsigargin, for avoiding the ER calcium uptake, and in presence of 5 mM succinate, for energizing mitochondria. After some seconds, a unique bolus of 10 μM $CaCl_2$ was injected in the cuvette and, consequently, the fluorescence increased (**Figure 28a**); but quickly, fluorescence decreased because calcium was taken up by mitochondria (**Figure 83a**). However, a resting amount of $_{i}Ca^{2+}$ was kept in lithium-treated mitochondria compared with non-treated ones (**Figure 28a and b**), suggesting $_{m}Ca^{2+}$ efflux was increased when lithium was present. Then, 10 μM Ru360 was injected to inhibit mtCU, thereby $_{m}Ca^{2+}$ uptake was inhibited and, consequently, fluorescence was gradually increasing because $_{i}Ca^{2+}$ could not be taken up by mitochondria (**Figure 28a**). Quantitative analysis was performed comparing the area under the curve (AUC), calculated from calcium bolus injection until seconds before RU360 injection, and the slope, calculated from the 25 seconds after Ru360 injection (**Figure 28a, to d**). As a result, while the AUC trended to be increased in presence of lithium (**Figure 28c**), the slope trended to be decreased (**Figure 28d**), suggesting that the initial faster $_{m}Ca^{2+}$ efflux after Ru360 injection was already out. Finally, to prove that mitochondria were functional, 10 μM FCCP was added, inducing the mitochondrial potential disruption and, consequently, solubilization and release of $_{m}Ca^{2+}$.

To ensure that $_{m}Ca^{2+}$ efflux was performed by NCLX, 10 μM CGP was added from the beginning of some experiments in the cuvette (**Figure 28a**). Although after calcium bolus injection, $_{m}Ca^{2+}$ uptake was slowed down in presence of CGP (**Figure 28a**) and, thus, the AUC is increased (**Figure 28b**), before Ru360 injection, all $_{i}Ca^{2+}$ was completely taken up by mitochondria, indicating that $_{m}Ca^{2+}$ uptake was compromised due to NCLX inhibition by CGP. Besides, after Ru360 injection, $_{m}Ca^{2+}$ efflux was almost entirely blocked by CGP (**Figure 28a and c**), showing that NCLX was the main $_{m}Ca^{2+}$ efflux pathway. No difference between lithium-treated and non-treated mitochondria in presence of CGP was observed (**Figure 28a to c**), pointing out that the effect of lithium on $_{m}Ca^{2+}$ was lost by blocking NCLX.

Besides, through this technique we were also able to measure the $\Delta\Psi_{mt}$, but, due to some technical issues, we could not get enough replicates neither in presence of CGP. Nevertheless, we saw that, depending on cell number and lithium concentration, the presence of lithium increased the $\Delta\Psi_{mt}$, as we have observed in whole cells (**Figure 24**), but more replicates are needed to confirm this result.

2.10.2. Lithium treatment activates mitochondrial calcium efflux after depolarization independently of NCLX phosphorylation at Ser258 in primary neurons culture

Since brain tissue from rodents treated with lithium salts is known to be enriched by lithium ions (López-Corcuera et al., 1988; Zanni et al., 2017), we wondered whether the presence of lithium could affect $_{m}Ca^{2+}$ in primary neurons culture.

Therefore, we decided to measure $_{m}Ca^{2+}$ as previously described by the group of Dr. Israel Sekler (Rozenfeld et al., 2022). After cellular depolarization with a high potassium concentration buffer (high K^{+}), primary neurons loaded with rhodamine-2 acetoxymethyl (Rhod2, a fluorescent $_{m}Ca^{2+}$ indicator) showed an increase in $_{m}Ca^{2+}$ and this calcium stayed inside the mitochondria in both WT and NCLX KO neurons, unless NCLX was previously activated in WT cells (Rozenfeld et al., 2022).

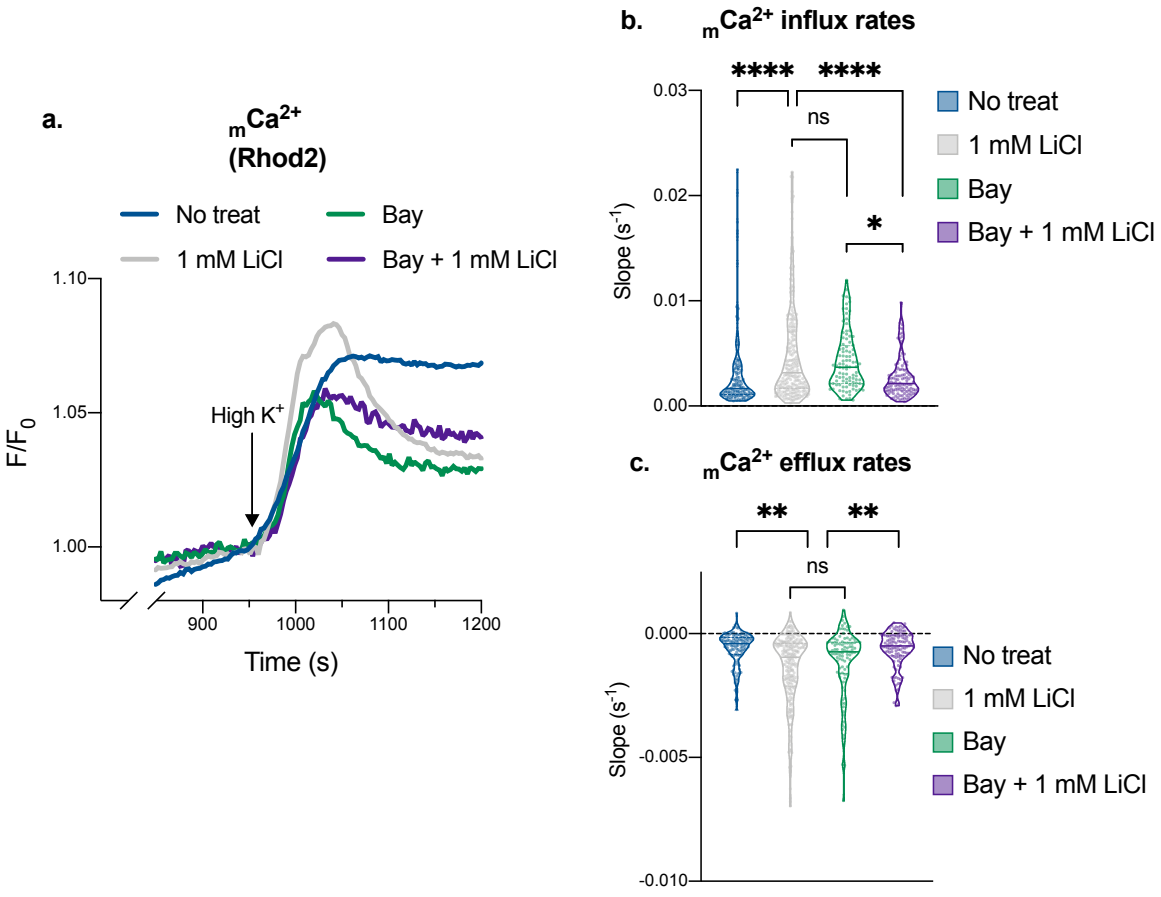

Figure 29. Effect of 1 mM LiCl treatment and Bay pretreatment on $_{m}Ca^{2+}$ after depolarization in primary cultured hippocampal neurons. WT neurons were loaded with 1 µM rhod-2 during 30 min and, at the same time, pretreated or not with 10 µM Bay. Then, neurons were treated or untreated with 1 mM LiCl and, after 10 min, were depolarized using the high K^{+} buffer. (**a**) Pooled and normalized traces of $_{m}Ca^{2+}$ changes monitored in neurons from at least 3 independent experiments. Quantification of $_{m}Ca^{2+}$ influx rates (**b**) $_{m}Ca^{2+}$ and efflux rates (**c**) shown in (**a**). *p<0.05, **p<0.005, ****p<0.0001, by one-way ANOVA with Tukey's post-hoc test

During my stay in the laboratory of Dr. Israel Sekler and using the same technique approach, we observed that in primary neurons without lithium treatment, loaded with 1 µM Rhod2 and depolarized with high K^+ buffer, calcium was imported into mitochondria and stayed mainly inside them (**Figure 29a**). However, when this procedure was performed after 10 minutes of 1 mM LiCl treatment, $_mCa^{2+}$ increased and then decreased (**Figure 29a**). The quantitative analysis showed that both $_mCa^2$ efflux rates and influx rates were increased in neurons treated with lithium compared with untreated cells (**Figure 29b and c**). The increment of $_mCa^2$ efflux rates indicates NCLX activation, as observed in permeabilized cells (**Figure 28**), and the increment of $_mCa^2$ influx rate may be caused by the lithium-dependent mitochondrial hyperpolarization (**Figure 24a to c**), due to mtCU activity is related to mitochondrial potential. This increase in the $_mCa^2$ influx rate also explains the higer $_mCa^2$ concentration observed in isolated mitochondria (**Figure 10c**).

Additionally, NCLX presents a phosphokinase A (PKA) phosphorylation site at Ser258 (Kostic et al., 2015) and, though this PKA-dependent phosphorylation, NCLX is activated (Assali et al., 2020; Kostic et al., 2015). The cyclic adenosine monophosphate (cAMP) is known to activate PKA and the phosphodiesterases (PDEs) are a superfamily of enzymes that catalyze the hydrolysis of cAMP. Besides, PKA (Technikova-Dobrova et al., 2001), cAMP (Acin-Perez et al., 2009; Rozenfeld et al., 2022) and PDE2 (Acin-Perez et al., 2011) have been detected inside mitochondria. Thus, when neurons were treated with a PDE2 inhibitor, such as caffeine or BAY 60-7550 (Bay), cAMP was accumulated into mitochondria and, through PKA phosphorylation, NCLX was activated, decreasing $_mCa^{2+}$ after its increase induced by depolarization with high K^+ buffer (Rozenfeld et al., 2022).

However, using this same technique approach, the presence of 1 mM LiCl for 10 minutes, added after 30 min with Bay, reduced the $_mCa^{2+}$ efflux compared to treatment only with Bay or treatment only with lithium (**Figure 29a**), suggesting that lithium ions did not activate NCLX through its phosphorylation. Accordingly, analyzing the $_mCa^{2+}$ efflux, the double treatment was more similar to untreated neurons, and independently Bay treatment and lithium treatment were equivalent (**Figure 29c**). Furthermore, the $_mCa^{2+}$ influx rates of the double treatment were similar to control influx rates (**Figure 29b**), and the $_mCa^{2+}$ influx rates of independent Bay treatment and lithium treatment were similar, too.

DISCUSSION

This Thesis has been focused on the role of NCLX in the long-term response to hypoxia, through the analysis of HIF-1α stabilization, and in the mitochondrial effects of lithium addition, due to the NCLX sensitivity to lithium ions. However, some controversial results need to be discussed.

1. NCLX- activity is involved in HIF-1α stabilization depending on cellular ROS context

Our results showed that MEFs, cells with high ROS basal levels, were able to bypass the NCLX-dependent ROS burst induced by acute hypoxia and stabilize HIF-1α during hypoxia (**Figure 5**). However, NCLX-dependent hypoxic ROS must happen to induce HIF-1α stabilization during hypoxia (**Figure 7**) by decreasing these high ROS basal levels using NAC or L-cysteine (**Figure 6**), as we observed in cells with low ROS basal levels, like MAFs (**Figure 8**), and in previous results (Hernansanz-Agustín, 2017). Therefore, the HIF-1α stabilization during hypoxia needs the NCLX-induced superoxide burst during the first few minutes of hypoxia depending on the redox cellular context (**Figure 30**).

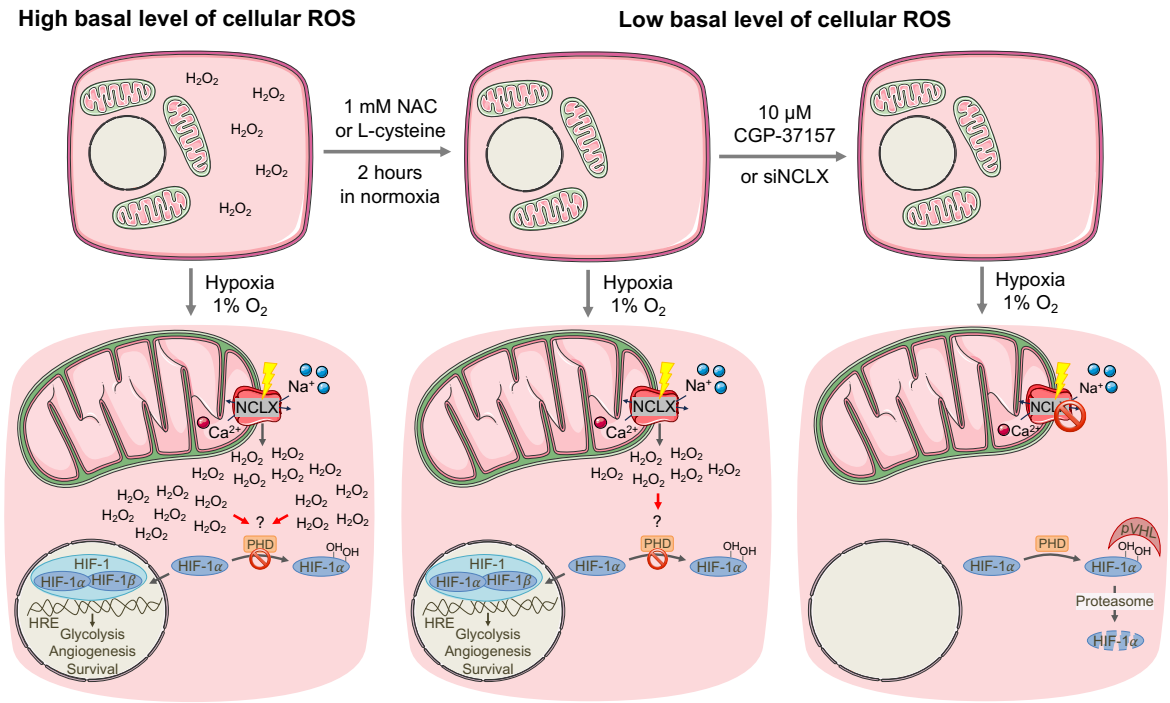

Figure 30. NCLX-dependent hypoxic ROS are needed for HIF-1α stabilization depending on cellular ROS context. Cells with high basal level of ROS (such as MEFs) subjected to hypoxia (1% oxygen) present enough cytosolic ROS to inactivate the prolyl hydroxylases (PHDs) in hypoxia and induce HIF-1α stabilization; meaning that the hypoxic NCLX-dependent ROS production is unnecessary for HIF-1α stabilization. After its stabilization, HIF-1α together with β subunit are bound to the hypoxia response elements (HREs), inducing the genetic responses related to glycolysis and angiogenesis, among others. In cells with low basal level of ROS (such as MAFs) or after decreasing basal level of ROS, by treating cells with 1 mM NAC or 1 mM L-cysteine for 2 hours in normoxia prior to hypoxia, the hypoxic NCLX-dependent ROS production is recovered as the source of ROS for PHDs inactivation and, in turn, HIF-1α stabilization occurs. Therefore, by blocking NCLX with 10 μM CGP-37157 or with a siRNA against NCLX (siNCLX), hypoxic ROS production is also inhibited and, thus, PHDs are active and hydroxylate HIF-1α. The Von Hippel-Lindau tumor suppressor (pVHL) recognizes HIF-1α hydroxylated which, eventually, tags HIF-1α to be degraded through proteasome and, thus, hypoxic HIF-1α stabilization is avoided when NCLX is inhibited. Question mark means that the ROS-dependent PHD inhibition may be mediated by a redox target and prohibition sign means protein activity inhibition. Scheme made using illustrations available on Elsevier Medical Art.

As HIF-1α stabilization takes part in many physiological and pathological mechanisms, the HIF pathway and related proteins have been thoroughly studied. Although PHDs are directly sensitive to oxygen concentration, other mechanisms have been proposed to affect PHDs and, in turn, allowing or preventing HIF-1α stabilization (Iommarini et al., 2017). Consistent with these ideas, various studies, even prior to the discovery of PHDs (Chandel et al., 1998), demonstrated that the production of mitochondrial ROS acts as an inductor of HIF-1α stabilization. Subsequent research has attributed this effect to the inhibition of PHDs (Brunelle et al., 2005; Guzy et al., 2005; Kim et al., 2006; Mansfield et al., 2005).

Recently, we showed that NCLX activity was necessary for producing a superoxide burst in acute hypoxia, highlighting the role of $_{m}Na^{+}$ import as the main player in our mechanism hypothesis (Hernansanz-Agustín et al., 2020). Thus, our research group focused on the role of NCLX on the HIF pathway activation demonstrating that, the blockage of NCLX in several cell types such as bovine aortic endothelial cells, human umbilical vein endothelial cells, HT-22 mouse hippocampal neuronal cells and mouse hippocampal slices, prevents the HIF-1α stabilization (Hernansanz-Agustín, 2017). The results of the present thesis using MAFs are also consistent with these data (**Figure 8**). In line with this role of sodium in signaling, elevation of $_{i}Na^{+}$ has recently been demonstrated to produce a major metabolic reprogramming of cardiac metabolism increasing glycolysis (Aksentijević et al., 2020). This metabolic switch directed towards improved glycolysis is a signature of HIF-driven metabolic adaptation (Semenza, 2013) and, even though the authors did not analyze the HIF pathway in their conditions, they showed that by blocking NCLX the glycolytic shift was inhibited (Aksentijević et al., 2020). Therefore, these data lead us to hypothesize that, by shifting mitochondrial activity toward glycolytic metabolism (Aksentijević et al., 2020) and increasing ROS production (Hernansanz-Agustín et al., 2020), NCLX-dependent $_{m}Na^{+}$ import may be the link between mitochondrial metabolism and HIF-1α stabilization.

However, the results collected in this thesis show that a particular cell type, MEFs, were able to stabilize HIF-1α with or without functional NCLX (**Figure 5**), while in all the other studied cell types NCLX activity was necessary. The main difference between MEFs and the other analyzed cell types is that MEFs were the only embryonic cells studied, and they showed higher basal ROS levels compared with the adult MAFs (**Figure 8a**). During embryonic development hypoxia and, in turn, the HIF pathway have been demonstrated to be essential for a correct morphogenesis (Dunwoodie, 2009). Also, the antioxidant defenses are known to be mainly provided by the yolk sac during the earliest stages (Deluao et al., 2022; Surai et al., 2016) and they later increase gradually within the embryo (Zaken et al., 2000). Therefore, the difference in basal ROS levels between MEFs and MAFs may be explained due to the different stages when they were isolated from mice. Besides, the relationship between the HIF pathway and redox levels has been demonstrated before (Nytko et al., 2011), showing an increase in PHD activity at higher concentrations of GSH. Accordingly, we saw that in MEFs the dependency of HIF-1α stabilization upon NCLX activity was restored after pretreatment with NAC or L-cysteine (**Figure 7**), two well-known intracellular antioxidant defense enhancers. Thus, NAC or L-cysteine pretreatment decreased the higher basal ROS levels in NCLX KO MEFs (**Figure 6**), reversing a rather pro-oxidant cellular environment which made MEFs insensitive to hypoxic NCLX-dependent ROS production. In line with this, in a colorectal cancer mouse model (Pathak et al., 2020), chronic NCLX deletion induced HIF-1α stabilization without hypoxic stimulus and it was prevented by adding mito-TEMPO, a mitochondria-targeted ROS scavenger. Thus, it seems that the increase in ROS production induced by the NCLX loss of function leads to HIF-1α stabilization. Moreover, chronic NCLX ablation induced other changes in mitochondrial metabolism (Pathak et al., 2020), such as the decrease in oxygen consumption (**Figure 17**) or the increase in $_{m}Ca^{2+}$ (**Figure 10c**), which may be the cause and/or the consequence of the increase in ROS production. However, another hypothesis is that the increase in $_{m}Na^{+}$ content observed in NCLX KO MEFs (**Figure 10b**) may be producing the metabolic shift, observed in (Aksentijević et al., 2020) and reducing the reduction of oxygen consumption (**Figure 17**). Therefore, the inherent consequences related to NCLX chronic deletion may be preconditioning HIF-1α stabilization even without hypoxic stimulus (Pathak et al., 2020).

Additionally, intracellular cysteine level has been shown to work as a PHD regulator (Briggs et al., 2016). The authors revealed that specific intramolecular cysteine residues of PHD are able to auto-oxidate, inducing an auto-inhibition of PHD, and the treatment with free cysteine reversed that auto-oxidation. Accordingly, NAC or L-cysteine pretreatment in MEFs may be recovering the regulatory role of cysteine levels towards PHD activity and, thus, reverting MEFs to a NCLX-dependent HIF-1α stabilization. Besides, since one of the most known effects of NAC is to increase GSH levels through a rise of the L-cysteine levels

(Alvarez et al., 2022), and the GSH levels have been demonstrated to increase PHD activity (Nytko et al., 2011), it seems very possible that NAC or L-cysteine pretreatment may be enhancing PHD activity by keeping low the ROS basal levels. However, we have not identified if this effect on ROS levels is directly impacting on PHD or if it is due to some redox-sensitive transductor.

Nevertheless, NAC or L-cysteine pretreatment may be inducing ROS-independent effects which can be participating in this mechanism. For instance, the intracellular cysteine depletion observed in (Briggs et al., 2016) was a consequence of the excessive glutamate export by cells, which in turn inhibited their own xCT glutamate-cystine antiporter. Consequently, pretreatment with NAC or L-cysteine might be altering some metabolic pathways in MEFs, thereby reinstating the NCLX-dependency of HIF-1α stabilization.

Altogether, these results highlight the redox dependence of HIF-1α stabilization and how tiny differences between different cell types lead to distinct responses to the same stimulus. Besides, we have demonstrated that the role of NCLX during acute hypoxia is also impacting in the long-term response to hypoxia, suggesting that both responses are intimately linked.

2. Lithium treatment alters mitochondrial metabolism

We have explored the effects of lithium on mitochondria by administering and acute treatment of 1 mM LiCl to cell cultures. This concentration falls within the range of blood concentration in patients under lithium treatment. We observed that this lithium addition is directly altering mitochondrial functioning in several ways, summarized in **Figure 31**.

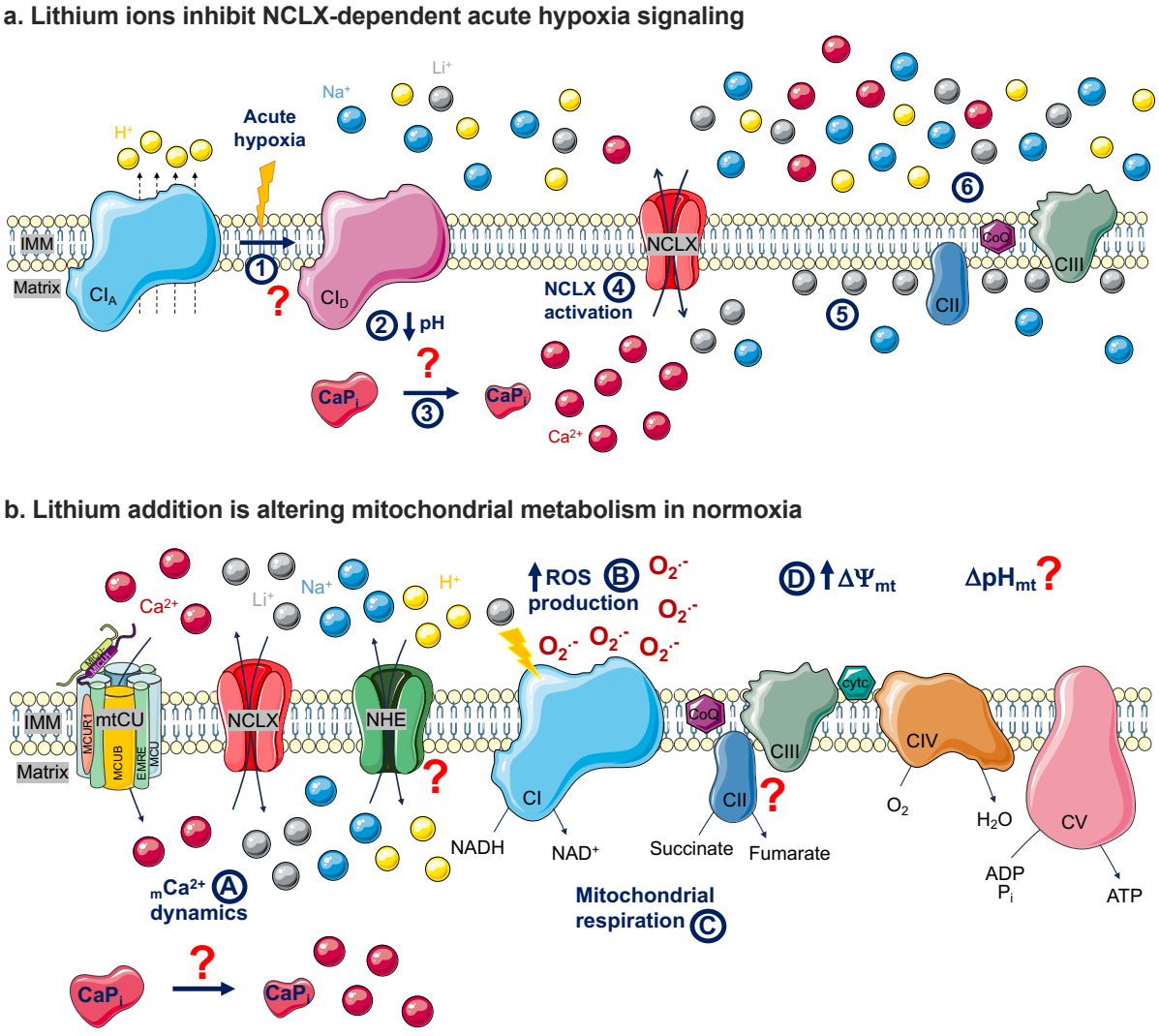

Figure 31. Summarized effects of lithium on mitochondrial metabolism. (**a**) **Effect of lithium on acute hypoxia signaling**. While we have not analyzed whether lithium ions may affect CI deactivation upon acute hypoxia **(1)**, nor the mitochondrial matrix acidification **(2)**, or the partial dissolution of calcium-phosphate granules **(3)**, our observations indicate that lithium ions are imported into mitochondrial matrix by NCLX replacing sodium ions **(4)**. By their own interaction with the inner leaflet of IMM, lithium ions do not alter IMM fluidity **(5)** which, in turn, inhibits the hypoxia-induced superoxide burst that is produced when $_{m}Na^{+}$ is imported **(6)**. (**b**) **Effect of lithium on mitochondrial metabolism in normoxia**. We have seen that lithium ions enhance $_{m}Ca^{2+}$ dynamics **(A)**, induce CI-dependent ROS production **(B)**, alter mitochondrial respiration **(C)** and increase $\Delta\Psi_{mt}$ **(D)**. Question mark means non-analyzed plausible alterations in presence of lithium. Scheme made using illustrations available on Elsevier Medical Art

On the one hand (**Figure 31a**), we propose that, by replacing sodium ions (**Figure 11**), lithium ions would be imported into mitochondrial matrix by NCLX (**Figure 9**) during the first few minutes of hypoxia. Since the interaction of sodium and lithium with phospholipids was slightly different (**Figure 12**), the hypoxia-dependent reduction of IMM fluidity induced by $_{m}Na^{+}$ import (Hernansanz-Agustín et al., 2020) was prevented in presence of lithium (**Figure 13**) and, in turn, NCLX-induced superoxide burst during the first few minutes of hypoxia was blocked (**Figure 14**)

On the other hand (**Figure 31b**), we saw that NCLX also imported lithium ions into the mitochondrial matrix in normoxia (**Figures 9 and 10a**). Consequently, we observed that not only NCLX-dependent $_{m}Ca^{2+}$ efflux was enhanced in presence of lithium (**Figures 10c, 28 and 29**), but also $_{m}Ca^{2+}$ influx was improved (**Figures 29**), an effect that could be derived from the increase in $\Delta\Psi_{mt}$ observed after lithium addition (**Figure 24**). However, in the presence of lithium, the $\Delta\Psi_{mt}$ (**Figure 24**) and the normoxic ROS production (**Figure 14**) were increased in both WT and NCLX KO MEFs, suggesting that the effects of lithium ions on mitochondria are not only mediated by NCLX, but also by other factors, such as CI (**Figure 16 and 19**). In line with this, we observed that mitochondrial respiration (**Figures 17, 19 and 20**) and mitochondrial network (**Figure 21**) were affected after lithium addition too. We have not dilucidated the whole mechanism induced by acute addition of lithium, but we can discuss several aspects regarding our results.

2.1. Lithium addition inhibits NCLX-dependent acute hypoxia signaling

2.1.1. Mitochondrial lithium uptake versus mitochondrial sodium uptake through NCLX

We recently demonstrated that NCLX-dependent $_{m}Na^{+}$ import was a major player in the acute hypoxia response in non-specialized cells (Hernansanz-Agustín et al., 2020) and we also know that NCLX is able to transport to lithium ions (Palty et al., 2010; Roy et al., 2017). Thus, we wondered how the presence of lithium could affect the response to hypoxia.

Although we have not been able to perform several replicates, we saw that $_{m}Li^{+}$ import depends on NCLX when we added 1 mM LiCl in the cell culture (**Figure 9**), which is in the range of desirables concentrations for patients under lithium treatment. At that lithium concentration, $_{m}Na^{+}$ import in acute hypoxia was almost abolished (**Figure 11**). Thus, we can hypothesize that lithium ions may be substituting sodium ions in NCLX import activity. However, the results in **Figures 9 and 10** showed a huge difference between the scales of each ion; while the $_{m}Li^{+}$ was measured in the nanograms range, $_{m}Na^{+}$ was detected in the grams range. To explain this difference is necessary to consider that sodium concentration

in extracellular and intracellular contents is also higher than lithium. While extracellular NaCl content is 140 mM and $_{i}Na^{+}$ concentration is around 10 mM, we added 1 mM LiCl in the extracellular medium and, consequently, we can assume that $_{i}Li^{+}$ concentration should be less than 1 mM. Accordingly, the $_{i}Li^{+}$ concentration is known to be the half of lithium concentration in the plasma (Mendels & Frazer, 1973). Besides, when we increased the extracellular lithium concentration to 30 mM, we saw that $_{m}Li^{+}$ import was not dependent on NCLX (**Figure 9**), notably this extracellular concentration was 15 times higher than the toxic lithium concentration in the plasma of lithium patients (McKnight et al., 2012). Therefore, due to the limited technical procedures for measuring lithium in cells, to ensure the NCLX sensitivity to lithium ions we measured $_{m}Ca^{2+}$ dynamics. We observed in permeabilized cells that the $_{m}Ca^{2+}$ efflux was enhanced in a NCLX-dependent manner when the alkali ions concentration in the buffer was 10 mM NaCl plus 1 mM LiCl compared to 11 mM NaCl (**Figure 28**). However, when all sodium ions were replaced by lithium ions, the lithium-induced $_{m}Ca^{2+}$ efflux improvement was sometimes lost (Rysted et al., 2021). Therefore, the differences between $_{m}Na^{+}$ and $_{m}Li^{+}$ ranges seem to be a direct consequence of their extracellular concentration. These data also indicate that each cation has its specific role in mitochondrial metabolism due to their inherent features beyond to NCLX activity. Thus, by changing the lithium concentration and, in turn, its proportion regarding sodium concentration, the onset of lithium toxicity occurs, and the sensitivity of NCLX to lithium ions diminishes.

Furthermore, although to our knowledge there has been no description of the mitochondrial sodium/proton exchanger (NHE) being sensitive to lithium ions, it could potentially be the perfect candidate to mediate $_{m}Li^{+}$ efflux, by replacing sodium ions in a similar manner to that observed in NCLX and other sodium exchangers. Given the high activity of mitochondrial NHE (Douglas & Cockrell, 1974; Murphy & Eisner, 2009) and the higher NCLX-sensitivity to lithium ions than sodium ions, attributed to specific residues within its sequence (Roy et al., 2017), it is plausible that even low concentration of $_{i}Li^{+}$ would be enough to activate NCLX, leading to the uptake of $_{m}Li^{+}$. This $_{m}Li^{+}$ would then be released to the cytosol by NHE, initiating this recurrent cycle. It is important to note that if these two exchangers work as a coupled tandem as a consequence of $_{m}Li^{+}$ import mediated by NCLX, two effects might occur: (i) an efflux of $_{m}Ca^{2+}$ could be induced and, subsequently, would enhance $_{m}Ca^{2+}$ uptake by mtCU, which is aligned with our observations that $_{m}Ca^{2+}$ dynamics were amplified in the presence of lithium (**Figures 10c and 29**). (ii) Simultaneously, $_{m}Li^{+}$ efflux mediated by NHE could lead to a mitochondrial matrix acidification. This pH change would further promote the $_{m}Ca^{2+}$ loop by partially dissolving the mitochondrial calcium-phosphate precipitates, as shown before (Hernansanz-Agustín et al., 2020), and may also contribute to the observed lithium-induced hyperpolarization (**Figure 24**).

Moreover, apart from the well-known $_mCa^{2+}$ impairment caused by NCLX deletion; it is reasonable to presume that NCLX KO cells may present $_mNa^+$ impairment too. In line with this, even though we only performed one experiment, we saw that $_mNa^+$ concentration in NCLX KO was increased compared to WT MEFs independently to lithium treatment (**Figure 10b**). In addition, we observed that $_mLi^+$ content was elevated in untreated NCLX KO compared to WT MEFs and a slight $_mLi^+$ increase was observed after treating NCLX KO MEFs with 1 mM LiCl during 30 minutes in normoxia (**Figure 10a**). These results suggest that lithium and sodium are imported into mitochondria and, as NCLX is not present, some other possible mechanisms could be behind them. Since NCLX deletion is known to increase the susceptibility to MPTP opening (Assali et al., 2020; Luongo et al., 2017), these cations may be reaching mitochondrial matrix through this nonspecific channel opening and, as NCLX is not present, NHE activity may be decreased. Thus, sodium and lithium would be accumulated inside mitochondria (**Figures 10a and b**). Another possibility is that NHE may be slowly working in reverse mode (meaning one sodium is imported into mitochondrial matrix while one proton is exported) and, since there is no other way to get out from mitochondria, sodium and lithium are gradually accumulating inside. Consequently, in NCLX KO MEFs, the basal levels of $_mNa^+$ and $_mLi^+$ are elevated and the acute addition of lithium cannot be imported into mitochondria as fast as in WT cells due to the absence of NCLX. However, this lithium import still occurs in NCLX KO MEFs, but to a lesser extent it occurs as well (**Figures 10a**).

Considering everything, it seems plausible to propose that the activities of NCLX and NHE, being the main $_mNa^+$ transporters, might be coupled to maintain mitochondrial function. This hypothesis is specially compelling when considering the newly identified role of $_mNa^+$ to control the $\Delta\Psi_{mt}$ through NHE-CI activity (Hernansanz-Agustín et al., 2023) as will be commented in further detail. Therefore, additional experiments are required to find out the whole mechanism, particularly the NCLX-NHE dynamics and its plausible disturbance in NCLX KO models and/or in presence of lithium. Moreover, we need to keep in mind that in the plasmatic NHE lithium ions were observed to replace protons (Busch et al., 1995), so this possibility also needs to be explored.

2.1.2. Lithium ions and their interaction with phospholipids

Through infrared (IR) spectroscopy experiments we confirmed that lithium ions and sodium ions were able to interact with the oxygen of CO of PC in liposomes (**Figure 12**), but in a slightly different way. We observed that while lithium ions are able to form two different isomers with the CO of PC, sodium ions only formed one (**Figure 12**). As a consequence of this interaction, we saw that whilst $_mNa^+$ import in acute hypoxia induces a

reduction of the IMM fluidity (Hernansanz-Agustín et al., 2020), lithium treatment avoided that reduction (**Figure 13**), probably because $_{m}Li^{+}$ import would be replacing sodium ions, as we have previously discussed.

However, after analyzing the literature regarding alkali ions and their interaction with phospholipids, we found that, although it was known that lithium ions interact with phospholipids in a different way than sodium ions do, all of them increase the order in the membranes (Hauser & Shipley, 1983). Nevertheless, some details need to be explained.

First, the concentration of lithium used in experiments to see the membrane crystallization was 0.5 M LiCl (Hauser & Shipley, 1981). However, using the same high concentration of other alkali ions (including sodium), the obtained results were not the same (Hauser & Shipley, 1983). Interestingly, similar results were observed when the same concentration of calcium and specially magnesium was used (Hauser & Shipley, 1984). While the monovalent ions, except lithium, kept the temperature of the transition from gel to liquid-crystal around 40 ºC, the divalent cations and lithium ions increased the transition temperature to 90 ºC (lithium and magnesium) and 105 ºC (calcium). These results suggest that, since lithium ions stablish similar interactions to divalent cations, the interaction between lithium ions and phospholipids is stronger than that interaction with sodium ions. This enhanced interaction is likely due to the smaal size of lithium ions, which enables them to penetrate deepen into the membrane by replacing water molecules and establishing stronger interactions with the phospholipids, as previously postulated (López Cascales & Garcia de la Torre, 1997).

Second, in addition to the non-therapeutical lithium concentration used, the results summarized above were performed in artificial bilayers formed by only one type of phospholipid. Thus, when the effect of lithium on healthy human erythrocytes was tested at a therapeutical concentration range using two different probes (one for the membrane surface and the other one for the hydrocarbon core), the authors showed that lithium ions alter the electrostatic interactions of molecules close to the membrane surface, increasing their motion and slightly decreasing the membrane surface anisotropy (Pettegrew et al., 1987). No lithium effect on the membrane core was detected and, notably, these experiments were carried out in presence of sodium ions too. Besides, lithium chronic treatment in rodents has been observed to affect lipid composition in brain membranes (López-Corcuera et al., 1988; Zanni et al., 2017), increasing lipids which allow a higher level of fluidity in membranes. However, this long-term effect of lithium ions could be related to the metabolic changes induced by chronic lithium treatment, or even could be a compensation to the direct effect of lithium addition.

Finally, the IMM is a membrane with specific features, presenting presents a higher ratio of proteins versus lipids and is formed by special lipids which confer crucial features

to the membrane. The unique characteristics of cardiolipin (CL) structure, being twice the size of any other phospholipid and, above all, its two negative charges, could make it particularly sensitive to cations. However, we could not find any work that analyzed the effect of lithium ions on CL bilayers.

Altogether, our results showed that the differences between sodium and lithium ions in both the interaction phospholipid-cation (**Figure 12**) and the IMM fluidity during acute hypoxia response (**Figure 13**) highlight the fact observed in all previous works explained above: lithium behavior with membranes is slightly different than sodium behavior and this difference is due to the intrinsic differences between both ions.

2.1.3. Lithium addition inhibits acute hypoxia-induced ROS production

We observed that the superoxide burst induced during the first few minutes of hypoxia was inhibited as a consequence of lithium presence (**Figure 14**). This result is pointing out that the ROS production induced because of the reduction of IMM fluidity is clearly specific to NCLX-dependent $_{m}Na^{+}$ import (**Figure 1**) and can be easily bypassed without blocking NCLX-dependent $_{m}Ca^{2+}$ efflux, just by adding some lithium ions. Thus, in situations of controlled hypoxias, such as those occurring in organ transplantation or programmed surgery, it could be worthy to assess the possible use of lithium salts as an additive to minimize side effects.

2.2. Lithium treatment is altering mitochondrial metabolism in normoxia

In addition, our observations included the impact of lithium treatment on mitochondrial metabolism in normoxic cultures, with effects that were either dependent or independent of NCLX activity.

2.2.1. Mitochondrial complex I is involved in lithium-induced ROS production

Although lithium was inhibiting the NCLX-dependent superoxide burst in acute hypoxia, we simultaneously saw that lithium increased the superoxide production in WT and NCLX KO MEFs in normoxia (**Figure 14**). Furthermore, we observed that in the presence of myxothiazol, a CIII inhibitor, the lithium-induced ROS production was still occurring (**Figure 15**). However, this ROS production was blocked in ND4 KO FBalb cells compared with their WT (**Figure 16**), indicating that CI is involved in that ROS production. Since one of the main mechanisms of mitochondrial ROS production is RET (**Figure 4**) and it is concomitant with

mitochondrial hyperpolarization, which has been also observed in presence of lithium (**Figure 24**), it is very plausible that the lithium-induced ROS production is occurring by RET. Thus, lithium ions would be impairing CI activity by promoting RET instead of FET and, in turn, inducing ROS production. Therefore, to corroborate this hypothesis, it would be pertinent to analyze ROS production in the presence of FCCP, to dissipate the $\Delta\Psi_{mt}$, and/or in presence of dimethylmalonate, a CII inhibitor.

2.2.2. Oxygen consumption is altered in the presence of lithium

Lithium has been demonstrated to enhance mitochondrial metabolism by improving mitochondrial complexes activity in human brain tissue (Maurer et al., 2009; Scola et al., 2014), as well as in leukocytes (de Sousa et al., 2015). However, in whole cells we saw that lithium injection did not affect basal respiration and, after FCCP injection, the maximal respiration was decreased in WT MEFs treated with lithium compared with non-treated cells (**Figure 17**). However, we also measured independent-complexes respiration in permeabilized AC16 cardiomyocytes by Seahorse (**Figures 19 and 20**), as described (Salabei et al., 2014). We saw that the basal OCR tends to increase in presence of lithium (**Figures 19 and 20**) and CI-dependent respiration seemed to increase in presence of 0.75 mM LiCl (**Figure 19**). Although these experiments have been performed in single individual experiments, these results (**Figures 19 and 20**) together with previous studies (de Sousa et al., 2015; Maurer et al., 2009; Scola et al., 2014) suggest that lithium ions are able to improve mitochondrial complexes activity. Therefore, experiments in isolated mitochondria would help to determine the possible lithium direct effect on mitochondrial complexes and to clarify whether these effects are dependent on NCLX. However, it is essential to note that possible differences in isolated mitochondria versus whole cells experiments may be explained due to the differences in the standard conditions used in isolated mitochondria experiments, such as substrates concentration or total absence of sodium and calcium ions, which would directly impact on NCLX activity.

Furthermore, in earlier findings, we observed that blocking NCLX with a small interference RNA led to an increase in the maximal respiration and, in turn, the reserve in comparison with control cells (Hernansanz-Agustín et al., 2020). This contrasts with the current result in NCLX KO MEFs (**Figure 17**) and in other model of chronic NCLX deletion (Pathak et al., 2020). Although these results are initially opposites, it is known that an acute increase in $_{m}Ca^{2+}$ implies an increase in OXPHOS activity (Rizzuto et al., 2012), by the direct active effect of calcium on some enzymes of the Krebs cycle (Glancy & Balaban, 2012). However, an increased $_{m}Ca^{2+}$ sustained over time has been observed to be counterproductive and, even, lethal (Assali et al., 2020; Luongo et al., 2017). Thus, acute

NCLX inhibition could increase the maximal OXPHOS activity through an acute $_{m}Ca^{2+}$ increment (Hernansanz-Agustín et al., 2020), but chronic $_{m}Ca^{2+}$ increment would decrease OXPHOS activity, even in basal conditions (**Figure 17**) (Pathak et al., 2020). Therefore, it is essential to note that $_{m}Ca^{2+}$ metabolism and OXPHOS are not independent events occurring in mitochondria: changes on $_{m}Ca^{2+}$ metabolism impacts on OXPHOS and *vice versa*.

Finally, it is uncertain to what extent the NCLX-dependency of lithium effect on OCR observed in cells is due to the underlying differences between WT and NCLX KO MEFs in basal respiration (**Figure 17**) or mitochondrial cation concentrations (**Figure 10**). Does the effect of lithium on OCR really depend on NCLX activity (meaning $_{m}Li^{+}$ import through NCLX) or do the mitochondria from NCLX KO cells, due to chronic inhibition of NCLX, lack the capability to respond to lithium? We could try to answer this question by analyzing OCR in cells with acute NCLX inhibition treated with lithium, but acute NCLX inhibition increases maximal respiration by itself (Hernansanz-Agustín et al., 2020). Also, we should deeply analyze whether the expression/activity of ETC proteins may be affected in NCLX KO MEFs and/or in presence of lithium.

Therefore, although it seems that lithium ions are affecting mitochondrial oxygen consumption, not only in our experiments (**Figures 17, 19 and 20**) but also in (de Sousa et al., 2015; Maurer et al., 2009; Scola et al., 2014), more experiments are required to explain how this is happening and why the results are different in whole cells compared to isolated mitochondria.

2.2.3. Lithium addition slightly disrupts the mitochondrial network

Given that mitochondrial ultrastructure is linked to mitochondrial function (Mishra & Chan, 2016) and in light of the observed impacts of lithium on mitochondria, we examined the mitochondrial network. Our analysis revealed that, in the presence of lithium, the mitochondrial network in WT MEFs fragmented into smaller networks (**Figure 21**). We also observed that this effect of lithium did not affect the mitochondrial network in NCLX KO MEFs, but, again, their mitochondrial network was slightly broken in basal conditions compared to WT MEFs (**Figure 21**). Accordingly, mitochondrial fragmentation is associated to ETC dysfunction or cationic dysregulations (Mishra & Chan, 2016), which is exactly what we observed in NCLX KO MEFs (**Figures 17 and 10**). However, this is another track which indicates that the chronic deletion of NCLX affects mitochondria and, in turn, is collaborating to hinder whether the effect of lithium on mitochondria is fully NCLX-dependent. Additionally, since the mitochondrial ultrastructure is controlled by several proteins, it is also possible that their balance could be disrupted in NCLX KO cells or in presence of lithium. One of the

most important proteins is Opa1, which presents different isoforms and different proteolytic cleavages, that are induced as a response to mitochondrial stress. Thus, the long isoforms (l-Opa1) promote mitochondrial fusion, but, when they are transformed into the short ones (s-Opa1), mitochondrial fission is stimulated (Quintana-Cabrera & Scorrano, 2023). Therefore, according to the ratio of both isoforms, the mitochondrial ultrastructure can be inferred. However, we tried to analyze the Opa1 isoforms by western blot in NCLX KO MEFs as well as in presence of lithium (data not shown) without reaching a solid conclusion.

2.2.4. Lithium ions induce hyperpolarization

The $\Delta\Psi_{mt}$ together with the mitochondrial pH gradient (ΔpH_{mt}) result in the mitochondrial proton-motive force ($\Delta\mu_{mt}$), which represents the accumulated energy that may be converted into energy store by allowing the ATP formation. However, the $\Delta\Psi_{mt}$ and the ΔpH_{mt} do not contribute equally to the $\Delta\mu_{mt}$, with approximately 80% of its value attributed to $\Delta\Psi_{mt}$ (Nicholls, 1974). This huge difference makes sense considering that $\Delta\Psi_{mt}$ represents the electrical difference of all charges between the both sides of IMM whereas the ΔpH_{mt} solely represents the difference in proton concentration on either side of the IMM.

After increasing extracellular sodium concentration, we saw that the $\Delta\Psi_{mt}$ was increased in WT MEFs but was not affected in NCLX KO MEFs (**Figure 27**), indicating that $_mNa^+$ import induces mitochondrial hyperpolarization. Accordingly, the role of sodium on the $\Delta\Psi_{mt}$ control has been recently demonstrated and, surprisingly, the authors showed that NHE activity is performed by the P-module of CI (Hernansanz-Agustín et al., 2023). This CI-NHE activity is independent to the CI-oxidoreductase activity and it even allows sodium ions to create the $\Delta\Psi_{mt}$ at low proton gradient. This finding together with the CI involvement in lithium's mechanism of action (**Figures 16 and 19**) would explain the NCLX-independent mitochondrial hyperpolarization in presence of lithium (**Figure 24**). Therefore, additional experiments in WT MEFs are required to demonstrate the exact role of each protein and to determine whether the CI-NHE activity could also be involved following the addition of lithium, as well as in NCLX KO MEFs.

Besides, the relationship between NCLX and the $\Delta\Psi_{mt}$ has been also indicated in (Garbincius et al., 2023), showing that modifications in TMEM65 expression, a protein that allows NCLX activity, impairs the $\Delta\Psi_{mt}$. Both the NLCX-dependent inhibition of $_mCa^{2+}$ efflux (TMEM65 KO cells) and the NLCX-dependent enhancement of $_mCa^{2+}$ efflux (cells overexpressing (OE) TMEM65) resulted in a reduction of the resting $\Delta\Psi_{mt}$. While the deletion of TMEM65 decreased the expression of some OXPHOS proteins, potentially accounting for the observed reduction in the $\Delta\Psi_{mt}$, the disruption of $_mNa^+$ dynamics might

also contribute both observed phenotypes. On the one hand, in TMEM65 KO cells, the inhibition of NCLX-dependent $_{m}Na^{+}$ import could directly lead to a reduction in the $\Delta\Psi_{mt}$ due to $_{m}Na^{+}$'s role in controlling the $\Delta\Psi_{mt}$ (**Figure 27**). On the other hand, in TMEM65 OE cells, the enhancement of NCLX activity might not be immediately balanced by NHE, potentially diminishing the sodium gradient across IMM and resulting in the observed reduction of $\Delta\Psi_{mt}$. Moreover, TMEM65 OE cells seemed to never reach the $\Delta\Psi_{mt}$ collapse after several calcium bolus injections, suggesting that their exacerbated NCLX activity coupled to NHE function would be increasing the sodium movement between both sides of IMM and thus, avoiding the collapse.

Furthermore, considering that mitochondria play a significant role in cellular energy balance, it is important to remember that when CI is affected, CII activity may increase to compensate the loss of CI activity (Acín-Pérez et al., 2014). Therefore, exploring the potential role of CII in this pathway should also be in the roadmap, especially in light of observations that mitochondrial coupling is decreased in CII-dependent oxygen consumption in presence of lithium (**Figure 20**).

2.2.5. Calcium dynamics are enhanced in the presence of lithium

Finally, although we demonstrated that NCLX is sensitive to lithium by directly measuring $_{m}Li^{+}$ import (**Figures 9 and 10a**), the NCLX activity is generally measured by analyzing $_{m}Ca^{2+}$ efflux. Thus, we observed that the presence of lithium at therapeutical concentration enhances $_{m}Ca^{2+}$ dynamics, improving $_{m}Ca^{2+}$ efflux (**Figures 28 and 29**) as well as $_{m}Ca^{2+}$ uptake (**Figure 29**). Accordingly, we saw that $_{m}Ca^{2+}$ concentration was increased after lithium treatment compared to untreated in NCLX KO MEFs (**Figure 10c**), probably because $_{i}Li^{+}$ import may be also increasing $_{i}Ca^{2+}$ concentration.

These findings are a promising result because $_{m}Ca^{2+}$ overload is known as a mediator of disease progression and, in worst scenarios, a potent inducer of cell death. Indeed, NCLX overexpression is known to be protective in some pathologies such as heart failure (Garbincius et al., 2022; Luongo et al., 2017) or Alzheimer's disease (AD) (Jadiya et al., 2019). In human samples, NCLX expression is reduced in AD brains, contributing with its progression, and the rescue of NCLX in neurons protected from AD pathology in a mouse model (Jadiya et al., 2019). In addition, NCLX deletion in neurons was enough to induce AD-like pathology in a mouse model (Jadiya, Cohen, et al., 2023) and an independent study also demonstrated that NCLX deletion impairs neuronal plasticity and, in turn, learning and memory processes (Stavsky et al., 2021). Accordingly, lithium has been proposed, and even tested (Kessing et al., 2008; Nunes et al., 2007), as a treatment for some neurodegenerative diseases such as AD and other dementias, showing a correlation between cognitive decline

rate and continued lithium treatment. Therefore, these results indicate that lithium treatment could be an effective, easy, and safe treatment in diseases correlating with $_{m}Ca^{2+}$ overload, by enhancing $_{m}Ca^{2+}$ efflux through NCLX, such as AD.

Additionally, the results collected in this Thesis regarding lithium can explain some effects of lithium as treatment for BD. Although our experimental settings consist of acute addition of lithium and the treatment for BD patients is chronic, it is plausible that lithium treatment could be reverting some altered features in BD patients, such as intracellular calcium concentration (Harrison et al., 2021) or OXPHOS activity (Scaini et al., 2021). Therefore, as summarized in (**Figure 31**), the effects of lithium directly on mitochondria may be ameliorating the mitochondrial dysfunction observed in BD patients subjected to chronic treatment. Additionally, due to its features as mood stabilizer, one of the most important beneficial effects of lithium on BD is that it inhibits maniac episodes (Bach & Gallicchio, 1990), which are characterized by elevated arousal and energy levels. Indeed, a meta-analysis including 36 studies found that lithium was an effective treatment for acute mania and it was also more effective than placebo (McKnight et al., 2019). Therefore, it is very possible that the acute effects of lithium on mitochondria observed in this Thesis may be responsible of its beneficial effects on maniac episodes.

Taken together, despite of the technical limitations for measuring both $_{m}Na^{+}$ and $_{m}Li^{+}$, we have demonstrated that NCLX is sensitive to lithium ions at therapeutical concentration by directly measuring them in isolated mitochondria. While the quantification of lithium amount is a regular analysis in some fields like environmental toxicity or blood tests, it is a pioneering analysis in cellular biology because of NCLX activity is routinely measured through $_{m}Ca^{2+}$ dynamics solely. However, our results pointed out that the effects of lithium on mitochondrial metabolism are beyond to NCLX activity, highlighting the fact that lithium ions are not simply replacing sodium ions in some exchangers. Certainly, the ability of lithium ions to replace magnesium ions is another line that needs to be explore, especially due to the essential role of magnesium as a cofactor in ATP reactions and the central implication of mitochondria in ATP synthesis. This study is the start of the road to find out the lithium's mechanism of action regarding mitochondrial metabolism and, thus, it may explain why lithium is toxic at that low plasma concentration compared with sodium. Accordingly, we showed that 1 mM LiCl added into cell culture media is enough to inhibit the $_{m}Na^{+}$-dependent response to acute hypoxia, suggesting a newly potential pharmacological use of lithium salts.

In addition, all these results demonstrate that NCLX deletion is deeply disturbing mitochondrial metabolism. Therefore, even though the effects of NCLX deletion on $_{m}Ca^{2+}$ dynamics are well stablished, it seems unreasonable to pretend that $_{m}Na^{+}$ impairment due to NCLX deletion is innocuous to mitochondrial metabolism when it is not taken into account and, thus, unknown. Indeed, the mitochondrial alterations observed in the presence of lithium precisely highlight that fact: lithium ions impact mitochondrial metabolism beyond $_{m}Ca^{2+}$ efflux, similar to emerging evidence regarding the effects of sodium on mitochondrial functions.

CONCLUSIONS

The results obtained in this Thesis led to the following conclusions:

1. In mouse fibroblasts subjected to hypoxia the relationship between NCLX activity and HIF-1α stabilization depends on cellular ROS context and is not always related to the superoxide burst observed during the first few minutes of hypoxia produced by NCLX activation.
   1.1. In mouse embryonic fibroblasts, where cellular ROS basal levels are high, HIF-1α is stabilized in hypoxia independently of NCLX activation, unless they have been pretreated with L-cysteine or N-acetyl-L-cysteine.
   1.2. In mouse adult fibroblasts, where cellular ROS basal levels are low, HIF-1α stabilization in hypoxia only occurs after NCLX activation.

2. Lithium addition impedes mitochondrial sodium import during acute hypoxia, blocking also the alteration of inner mitochondrial membrane fluidity and the superoxide burst characteristic of the acute transition to hypoxia.

3. Superoxide production is increased by lithium addition, which depends on mitochondrial complex I but it is independent of NCLX and CIII.

4. Lithium addition alters mitochondrial function by decreasing maximal mitochondrial respiration and disrupting mitochondrial network.

5. Mitochondrial membrane potential is increased by lithium addition independently of NCLX.

6. The presence of lithium enhances mitochondrial calcium dynamics through NCLX.

CONCLUSIONES

Los resultados obtenidos en esta Tesis Doctoral llevan a las siguientes conclusiones:

1. En fibroblastos de ratón sometidos a hipoxia, la relación entre la actividad de NCLX y la estabilización de HIF-1α depende del contexto oxidativo celular y no siempre está relacionada con el estallido de superóxido observado durante los primeros minutos de hipoxia producido por la activación de NCLX.
   1.1. En fibroblastos embrionarios de ratón, en los que los niveles basales de ROS celulares son altos, HIF-1α se estabiliza en hipoxia independientemente de la activación de NCLX, excepto si las células han sido pretratradas con L-cisteína o N-acetil-cisteína.
   1.2. En fibroblastos adultos de ratón, en los que niveles basales de ROS celulares son bajos, la estabilización de HIF-1α en hipoxia ocurre sólo tras la activación de NCLX.

2. La adición de litio impide el importe de sodio a la mitocondria en hipoxia aguda, bloqueando también la alteración de la fluidez de la membrana mitocondrial interna y el estallido de superóxido característico de la transición aguda a la hipoxia.

3. La producción de superóxido se ve aumentada al añadir litio, lo que depende del complejo mitocondrial I, pero es independiente de NCLX y del complejo mitocondrial III.

4. La adición de litio altera la función mitocondrial, disminuyendo la respiración máxima y rompiendo la red mitocondrial.

5. El potencial de la membrana mitocondrial aumenta al añadir litio independientemente de NCLX.

6. La presencia de litio estimula las dinámicas de calcio mitocondrial mediante NCLX.

REFERENCES

Aaltonen, M. J., Friedman, J. R., Osman, C., Salin, B., di Rago, J.-P., Nunnari, J., Langer, T., & Tatsuta, T. (2016). MICOS and phospholipid transfer by Ups2–Mdm35 organize membrane lipid synthesis in mitochondria. *Journal of Cell Biology*, *213*(5), 525–534. https://doi.org/10.1083/jcb.201602007

Abe, H., Semba, H., & Takeda, N. (2017). The Roles of Hypoxia Signaling in the Pathogenesis of Cardiovascular Diseases. *Journal of Atherosclerosis and Thrombosis*, *24*(9), 884–894. https://doi.org/10.5551/jat.RV17009

Achleitner, G., Zweytick, D., Trotter, P. J., Voelker, D. R., & Daum, G. (1995). Synthesis and Intracellular Transport of Aminoglycerophospholipids in Permeabilized Cells of the Yeast, Saccharomyces cerevisiae. *Journal of Biological Chemistry*, *270*(50), 29836–29842. https://doi.org/10.1074/jbc.270.50.29836

Acin-Perez, R., Benincá, C., Fernandez del Rio, L., Shu, C., Baghdasarian, S., Zanette, V., Gerle, C., Jiko, C., Khairallah, R., Khan, S., Rincon Fernandez Pacheco, D., Shabane, B., Erion, K., Masand, R., Dugar, S., Ghenoiu, C., Schreiner, G., Stiles, L., Liesa, M., & Shirihai, O. S. (2023). Inhibition of <scp>ATP</scp> synthase reverse activity restores energy homeostasis in mitochondrial pathologies. *The EMBO Journal*, *42*(10). https://doi.org/10.15252/embj.2022111699

Acín-Pérez, R., Carrascoso, I., Baixauli, F., Roche-Molina, M., Latorre-Pellicer, A., Fernández-Silva, P., Mittelbrunn, M., Sanchez-Madrid, F., Pérez-Martos, A., Lowell, C. A., Manfredi, G., & Enríquez, J. A. (2014). ROS-Triggered Phosphorylation of Complex II by Fgr Kinase Regulates Cellular Adaptation to Fuel Use. *Cell Metabolism*, *19*(6), 1020–1033. https://doi.org/10.1016/j.cmet.2014.04.015

Acin-Perez, R., Russwurm, M., Günnewig, K., Gertz, M., Zoidl, G., Ramos, L., Buck, J., Levin, L. R., Rassow, J., Manfredi, G., & Steegborn, C. (2011). A Phosphodiesterase 2A Isoform Localized to Mitochondria Regulates Respiration. *Journal of Biological Chemistry*, *286*(35), 30423–30432. https://doi.org/10.1074/jbc.M111.266379

Acin-Perez, R., Salazar, E., Kamenetsky, M., Buck, J., Levin, L. R., & Manfredi, G. (2009). Cyclic AMP Produced inside Mitochondria Regulates Oxidative Phosphorylation. *Cell Metabolism*, *9*(3), 265–276. https://doi.org/10.1016/j.cmet.2009.01.012

Acín-Pérez, R., Bayona-Bafaluy, M. P., Fernández-Silva, P., Moreno-Loshuertos, R., Pérez-Martos, A., Bruno, C., Moraes, C. T., & Enríquez, J. A. (2004). Respiratory Complex III Is Required to Maintain Complex I in Mammalian Mitochondria. *Molecular Cell*, *13*(6), 805–815. https://doi.org/10.1016/S1097-2765(04)00124-8

Aksentijević, D., Karlstaedt, A., Basalay, M. V., O'Brien, B. A., Sanchez-Tatay, D., Eminaga, S., Thakker, A., Tennant, D. A., Fuller, W., Eykyn, T. R., Taegtmeyer, H., & Shattock, M. J. (2020). Intracellular sodium elevation reprograms cardiac metabolism. *Nature Communications*, *11*(1), 4337. https://doi.org/10.1038/s41467-020-18160-x

Almeida, O. P., Singulani, M. P., Ford, A. H., Hackett, M. L., Etherton-Beer, C., Flicker, L., Hankey, G. J., De Paula, V. J. R., Penteado, C. T., & Forlenza, O. V. (2022). Lithium and Stroke Recovery: A Systematic Review and Meta-Analysis of Stroke Models in Rodents and Human Data. *Stroke*, *53*(9), 2935–2944. https://doi.org/10.1161/STROKEAHA.122.039203

Almendro-Vedia, V., Natale, P., Valdivieso González, D., Lillo, M. P., Aragones, J. L., & López-Montero, I. (2021). How rotating ATP synthases can modulate membrane structure. *Archives of Biochemistry and Biophysics*, *708*, 108939. https://doi.org/10.1016/j.abb.2021.108939

Alvarez, B., Comini, M. A., Salinas, G., & Trujillo, M. (2022). *Redox Chemistry and Biology of Thiols*. Elsevier Netherlands. ISBN: 978-0-323-90219-9. https://doi.org/10.1016/C2020-0-01315-0

Andrási, E., Páli, N., Molnár, Z., & Kösel, S. (2005). Brain aluminum, magnesium and phosphorus contents of control and Alzheimer-diseased patients. *Journal of Alzheimer's Disease*, *7*(4), 273–284. https://doi.org/10.3233/JAD-2005-7402

Antony, A. N., Paillard, M., Moffat, C., Juskeviciute, E., Correnti, J., Bolon, B., Rubin, E., Csordás, G., Seifert, E. L., Hoek, J. B., & Hajnóczky, G. (2016). MICU1 regulation of mitochondrial Ca2+ uptake dictates survival and tissue regeneration. *Nature Communications*, *7*(1), 10955. https://doi.org/10.1038/ncomms10955

Arnold, P. K., & Finley, L. W. S. (2023). Regulation and function of the mammalian tricarboxylic acid cycle. *Journal of Biological Chemistry*, *299*(2), 102838. https://doi.org/10.1016/j.jbc.2022.102838

Assali, E. A., Jones, A. E., Veliova, M., Acín-Pérez, R., Taha, M., Miller, N., Shum, M., Oliveira, M. F., Las, G., Liesa, M., Sekler, I., & Shirihai, O. S. (2020). NCLX prevents cell death during adrenergic activation of the brown adipose tissue. *Nature Communications*, *11*(1), 3347. https://doi.org/10.1038/s41467-020-16572-3

Assali, E. A., & Sekler, I. (2021). Sprinkling salt on mitochondria: The metabolic and pathophysiological roles of mitochondrial Na+ signaling mediated by NCLX. *Cell Calcium*, *97*, 102416. https://doi.org/10.1016/j.ceca.2021.102416

Bach, R. O., & Gallicchio, V. S. (1990). *Lithium and Cell Physiology*. Springer-Verlag New York. ISBN: 978-1-4612-7967-9. https://doi.org/10.1007/978-1-4612-3324-4

Bae, Y. S., Oh, H., Rhee, S. G., & Yoo, Y. Do. (2011). Regulation of reactive oxygen species generation in cell signaling. *Molecules and Cells*, *32*(6), 491–509. https://doi.org/10.1007/s10059-011-0276-3

Ban, T., Ishihara, T., Kohno, H., Saita, S., Ichimura, A., Maenaka, K., Oka, T., Mihara, K., & Ishihara, N. (2017). Molecular basis of selective mitochondrial fusion by heterotypic action between OPA1 and cardiolipin. *Nature Cell Biology*, *19*(7), 856–863. https://doi.org/10.1038/ncb3560

Ban, T., Kohno, H., Ishihara, T., & Ishihara, N. (2018). Relationship between OPA1 and cardiolipin in mitochondrial inner-membrane fusion. *Biochimica et Biophysica Acta (BBA) - Bioenergetics*, *1859*(9), 951–957. https://doi.org/10.1016/j.bbabio.2018.05.016

Barth, P. G., Scholte, H. R., Berden, J. A., Van Der Klei-Van Moorsel, J. M., Luyt-Houwen, I. E. M., Van'T Veer-Korthof, E. Th., Van Der Harten, J. J., & Sobotka-Plojhar, M. A. (1983). An X-linked mitochondrial disease affecting cardiac muscle, skeletal muscle and neutrophil leucocytes. *Journal of the Neurological Sciences*, *62*(1–3), 327–355. https://doi.org/10.1016/0022-510X(83)90209-5

Beurel, E., Grieco, S. F., & Jope, R. S. (2015). Glycogen synthase kinase-3 (GSK3): Regulation, actions, and diseases. *Pharmacology & Therapeutics*, *148*, 114–131. https://doi.org/10.1016/j.pharmthera.2014.11.016

Binder, H., & Zschörnig, O. (2002). The effect of metal cations on the phase behavior and hydration characteristics of phospholipid membranes. *Chemistry and Physics of Lipids*, *115*(1–2), 39–61. https://doi.org/10.1016/S0009-3084(02)00005-1

Blaustein, M. P., & Wiesmann, W. P. (1970). Effect of Sodium Ions on Calcium Movements in Isolated Synaptic Terminals. *Proceedings of the National Academy of Sciences*, *66*(3), 664–671. https://doi.org/10.1073/pnas.66.3.664

Blomeyer, C. A., Bazil, J. N., Stowe, D. F., Dash, R. K., & Camara, A. K. S. (2016). Mg2+ differentially regulates two modes of mitochondrial Ca2+ uptake in isolated cardiac mitochondria: implications for mitochondrial Ca2+ sequestration. *Journal of Bioenergetics and Biomembranes*, *48*(3), 175–188. https://doi.org/10.1007/s10863-016-9644-1

Brand, M. D. (2016). Mitochondrial generation of superoxide and hydrogen peroxide as the source of mitochondrial redox signaling. *Free Radical Biology and Medicine*, *100*, 14–31. https://doi.org/10.1016/j.freeradbiomed.2016.04.001

Briggs, K. J., Koivunen, P., Cao, S., Backus, K. M., Olenchock, B. A., Patel, H., Zhang, Q., Signoretti, S., Gerfen, G. J., Richardson, A. L., Witkiewicz, A. K., Cravatt, B. F., Clardy, J., & Kaelin, W. G. (2016). Paracrine Induction of HIF by Glutamate in Breast Cancer: EglN1 Senses Cysteine. *Cell*, *166*(1), 126–139. https://doi.org/10.1016/j.cell.2016.05.042

Brunelle, J. K., Bell, E. L., Quesada, N. M., Vercauteren, K., Tiranti, V., Zeviani, M., Scarpulla, R. C., & Chandel, N. S. (2005). Oxygen sensing requires mitochondrial ROS but not oxidative phosphorylation. *Cell Metabolism*, *1*(6), 409–414. https://doi.org/10.1016/j.cmet.2005.05.002

Bschor, T. (2014). Lithium in the Treatment of Major Depressive Disorder. *Drugs*, *74*(8), 855–862. https://doi.org/10.1007/s40265-014-0220-x

Busch, S., Burckhardt, B.-C., & Siffert, W. (1995). Expression of the human sodium/proton exchanger NHE-1 in Xenopus laevis oocytes enhances sodium/proton exchange activity and establishes sodium/lithium countertransport. *Pfl□gers Archiv European Journal of Physiology*, *429*(6), 859–869. https://doi.org/10.1007/BF00374811

Cabral-Costa, J. V., Vicente-Gutiérrez, C., Agulla, J., Lapresa, R., Elrod, J. W., Almeida, Á., Bolaños, J. P., & Kowaltowski, A. J. (2023). Mitochondrial sodium/calcium exchanger <scp>NCLX</scp> regulates glycolysis in astrocytes, impacting on cognitive performance. *Journal of Neurochemistry*, *165*(4), 521–535. https://doi.org/10.1111/jnc.15745

Cade, J. F. J. (1949). Lithium salts in the treatment of psychotic excitement. *Medical Journal of Australia*, 349–352.

Calvo, E., Cogliati, S., Hernansanz-Agustín, P., Loureiro-López, M., Guarás, A., Casuso, R. A., García-Marqués, F., Acín-Pérez, R., Martí-Mateos, Y., Silla-Castro, JC., Carro-Alvarellos, M., Huertas, J. R., Vázquez, J., & Enríquez, J. A. (2020). Functional role of respiratory supercomplexes in mice: SCAF1 relevance and segmentation of the Q_{pool}. *Science Advances*, *6*(26). https://doi.org/10.1126/sciadv.aba7509

Cao, J., Liu, Y., Lockwood, J., Burn, P., & Shi, Y. (2004). A Novel Cardiolipin-remodeling Pathway Revealed by a Gene Encoding an Endoplasmic Reticulum-associated Acyl-CoA:Lysocardiolipin Acyltransferase (ALCAT1) in Mouse. *Journal of Biological Chemistry*, *279*(30), 31727–31734. https://doi.org/10.1074/jbc.M402930200

Chakrabarti, R., Ji, W.-K., Stan, R. V., de Juan Sanz, J., Ryan, T. A., & Higgs, H. N. (2018). INF2-mediated actin polymerization at the ER stimulates mitochondrial calcium uptake, inner membrane constriction, and division. *Journal of Cell Biology*, *217*(1), 251–268. https://doi.org/10.1083/jcb.201709111

Chandel, N. S., Maltepe, E., Goldwasser, E., Mathieu, C. E., Simon, M. C., & Schumacker, P. T. (1998). Mitochondrial reactive oxygen species trigger hypoxia-induced transcription. *Proceedings of the National Academy of Sciences*, *95*(20), 11715–11720. https://doi.org/10.1073/pnas.95.20.11715

Chandel, N. S., McClintock, D. S., Feliciano, C. E., Wood, T. M., Melendez, J. A., Rodriguez, A. M., & Schumacker, P. T. (2000). Reactive Oxygen Species Generated at Mitochondrial Complex III Stabilize Hypoxia-inducible Factor-1α during Hypoxia. *Journal of Biological Chemistry*, *275*(33), 25130–25138. https://doi.org/10.1074/jbc.M001914200

Chen, B., Zhang, M., Ji, M., Zhang, D., Chen, B., Gong, W., Li, X., Zhou, Y., Dong, C., Wen, G., Zhan, X., Wu, X., Yuan, H., Xu, E., Xia, M., Verkhratsky, A., & Li, B. (2022). The neuroprotective mechanism of lithium after ischaemic stroke. *Communications Biology*, *5*(1), 105. https://doi.org/10.1038/s42003-022-03051-2

Chen, W., Zhao, H., & Li, Y. (2023). Mitochondrial dynamics in health and disease: mechanisms and potential targets. *Signal Transduction and Targeted Therapy*, *8*(1), 333. https://doi.org/10.1038/s41392-023-01547-9

Chouchani, E. T., Pell, V. R., Gaude, E., Aksentijević, D., Sundier, S. Y., Robb, E. L., Logan, A., Nadtochiy, S. M., Ord, E. N. J., Smith, A. C., Eyassu, F., Shirley, R., Hu, C.-H., Dare, A. J., James, A. M., Rogatti, S., Hartley, R. C., Eaton, S., Costa, A. S. H., … Murphy, M. P. (2014). Ischaemic accumulation of succinate controls reperfusion injury through mitochondrial ROS. *Nature*, *515*(7527), 431–435. https://doi.org/10.1038/nature13909

Cogliati, S., Calvo, E., Loureiro, M., Guaras, A. M., Nieto-Arellano, R., Garcia-Poyatos, C., Ezkurdia, I., Mercader, N., Vázquez, J., & Enriquez, J. A. (2016). Mechanism of super-assembly of respiratory complexes III and IV. *Nature*, *539*(7630), 579–582. https://doi.org/10.1038/nature20157

Connerth, M., Tatsuta, T., Haag, M., Klecker, T., Westermann, B., & Langer, T. (2012). Intramitochondrial Transport of Phosphatidic Acid in Yeast by a Lipid Transfer Protein. *Science*, *338*(6108), 815–818. https://doi.org/10.1126/science.1225625

Cooper, G. M. (2019). *The cell: a molecular approach* (Eighth edition). Sinauer Associates, an imprint of Oxford University Press.

Côrte-Real, B. F., Hamad, I., Arroyo Hornero, R., Geisberger, S., Roels, J., Van Zeebroeck, L., Dyczko, A., van Gisbergen, M. W., Kurniawan, H., Wagner, A., Yosef, N., Weiss, S. N. Y., Schmetterer, K. G., Schröder, A., Krampert, L., Haase, S., Bartolomaeus, H., Hellings, N., Saeys, Y., … Kleinewietfeld, M. (2023). Sodium perturbs mitochondrial respiration and induces dysfunctional Tregs. *Cell Metabolism*, *35*(2), 299-315.e8. https://doi.org/10.1016/j.cmet.2023.01.009

Cox, A. G., Winterbourn, C. C., & Hampton, M. B. (2010). *Measuring the Redox State of Cellular Peroxiredoxins by Immunoblotting* (pp. 51–66). https://doi.org/10.1016/S0076-6879(10)74004-0

Daum, G., & Vance, J. E. (1997). Import of lipids into mitochondria. *Progress in Lipid Research*, *36*(2–3), 103–130. https://doi.org/10.1016/S0163-7827(97)00006-4

de Baaij, J. H. F., Hoenderop, J. G. J., & Bindels, R. J. M. (2015). Magnesium in Man: Implications for Health and Disease. *Physiological Reviews*, *95*(1), 1–46. https://doi.org/10.1152/physrev.00012.2014

de Brito, O. M., & Scorrano, L. (2008). Mitofusin 2 tethers endoplasmic reticulum to mitochondria. *Nature*, *456*(7222), 605–610. https://doi.org/10.1038/nature07534

de Sousa, R. T., Streck, E. L., Zanetti, M. V., Ferreira, G. K., Diniz, B. S., Brunoni, A. R., Busatto, G. F., Gattaz, W. F., & Machado-Vieira, R. (2015). Lithium increases leukocyte mitochondrial complex I activity in bipolar disorder during depressive episodes. *Psychopharmacology*, *232*(1), 245–250. https://doi.org/10.1007/s00213-014-3655-6

Deluao, J. C., Winstanley, Y., Robker, R. L., Pacella-Ince, L., Gonzalez, M. B., & McPherson, N. O. (2022). Oxidative stress and reproductive function: Reactive oxygen species in the mammalian pre-implantation embryo. *Reproduction*, *164*(6), F95–F108. https://doi.org/10.1530/REP-22-0121

Denton, R. M. (2009). Regulation of mitochondrial dehydrogenases by calcium ions. *Biochimica et Biophysica Acta (BBA) - Bioenergetics*, *1787*(11), 1309–1316. https://doi.org/10.1016/j.bbabio.2009.01.005

De-Paula, V. J., Gattaz, W. F., & Forlenza, O. V. (2016). Long-term lithium treatment increases intracellular and extracellular brain-derived neurotrophic factor (<scp>BDNF</scp>) in cortical and hippocampal neurons at subtherapeutic concentrations. *Bipolar Disorders*, *18*(8), 692–695. https://doi.org/10.1111/bdi.12449

Doeppner, T. R., Kaltwasser, B., Sanchez-Mendoza, E. H., Caglayan, A. B., Bähr, M., & Hermann, D. M. (2017). Lithium-induced neuroprotection in stroke involves increased miR-124 expression, reduced RE1-silencing transcription factor abundance and decreased protein deubiquitination by GSK3β inhibition-independent pathways. *Journal of Cerebral Blood Flow & Metabolism*, *37*(3), 914–926. https://doi.org/10.1177/0271678X16647738

Douglas, M. G., & Cockrell, R. S. (1974). Mitochondrial Cation-Hydrogen Ion Exchange. *Journal of Biological Chemistry*, *249*(17), 5464–5471. https://doi.org/10.1016/S0021-9258(20)79751-6

Dudek, J., Cheng, I.-F., Balleininger, M., Vaz, F. M., Streckfuss-Bömeke, K., Hübscher, D., Vukotic, M., Wanders, R. J. A., Rehling, P., & Guan, K. (2013). Cardiolipin deficiency affects respiratory chain function and organization in an induced pluripotent stem cell model of Barth syndrome. *Stem Cell Research*, *11*(2), 806–819. https://doi.org/10.1016/j.scr.2013.05.005

Dunwoodie, S. L. (2009). The Role of Hypoxia in Development of the Mammalian Embryo. *Developmental Cell*, *17*(6), 755–773. https://doi.org/10.1016/j.devcel.2009.11.008

Epand, R. F., Schlattner, U., Wallimann, T., Lacombe, M.-L., & Epand, R. M. (2007). Novel Lipid Transfer Property of Two Mitochondrial Proteins that Bridge the Inner and Outer Membranes. *Biophysical Journal*, *92*(1), 126–137. https://doi.org/10.1529/biophysj.106.092353

Fernández-Agüera, M. C., Gao, L., González-Rodríguez, P., Pintado, C. O., Arias-Mayenco, I., García-Flores, P., García-Pergañeda, A., Pascual, A., Ortega-Sáenz, P., & López-Barneo, J. (2015). Oxygen Sensing by Arterial Chemoreceptors Depends on Mitochondrial Complex I Signaling. *Cell Metabolism*, *22*(5), 825–837. https://doi.org/10.1016/j.cmet.2015.09.004

Frezza, C., Cipolat, S., Martins de Brito, O., Micaroni, M., Beznoussenko, G. V., Rudka, T., Bartoli, D., Polishuck, R. S., Danial, N. N., De Strooper, B., & Scorrano, L. (2006). OPA1 Controls Apoptotic Cristae Remodeling Independently from Mitochondrial Fusion. *Cell*, *126*(1), 177–189. https://doi.org/10.1016/j.cell.2006.06.025

Gaigg, B., Simbeni, R., Hrastnik, C., Paltauf, F., & Daum, G. (1995). Characterization of a microsomal subfraction associated with mitochondria of the yeast, Saccharomyces cerevisiae. Involvement in synthesis and import of phospholipids into mitochondria. *Biochimica et Biophysica Acta (BBA) - Biomembranes*, *1234*(2), 214–220. https://doi.org/10.1016/0005-2736(94)00287-Y

Gao, L., Ortega-Sáenz, P., Moreno-Domínguez, A., & López-Barneo, J. (2022). Mitochondrial Redox Signaling in O2-Sensing Chemoreceptor Cells. *Antioxidants & Redox Signaling*, *37*(4–6), 274–289. https://doi.org/10.1089/ars.2021.0255

Garbincius, J. F., & Elrod, J. W. (2022). Mitochondrial calcium exchange in physiology and disease. *Physiological Reviews*, *102*(2), 893–992. https://doi.org/10.1152/physrev.00041.2020

Garbincius, J. F., Luongo, T. S., Jadiya, P., Hildebrand, A. N., Kolmetzky, D. W., Mangold, A. S., Roy, R., Ibetti, J., Nwokedi, M., Koch, W. J., & Elrod, J. W. (2022). Enhanced NCLX-dependent mitochondrial Ca2+ efflux attenuates pathological remodeling in heart failure. *Journal of Molecular and Cellular Cardiology*, *167*, 52–66. https://doi.org/10.1016/j.yjmcc.2022.03.001

Garbincius, J. F., Salik, O., Cohen, H. M., Choya-Foces, C., Mangold, A. S., Makhoul, A. D., Schmidt, A. E., Khalil, D. Y., Doolittle, J. J., Wilkinson, A. S., Murray, E. K., Lazaropoulos, M. P., Hildebrand, A. N., Tomar, D., & Elrod, J. W. (2023). TMEM65 regulates NCLX-dependent mitochondrial calcium efflux. *Biorxiv*. https://doi.org/10.1101/2023.10.06.561062

García-Poyatos, C., Cogliati, S., Calvo, E., Hernansanz-Agustín, P., Lagarrigue, S., Magni, R., Botos, M., Langa, X., Amati, F., Vázquez, J., Mercader, N., & Enríquez, J. A. (2020). Scaf1 promotes respiratory supercomplexes and metabolic efficiency in zebrafish. *EMBO Reports*, *21*(7). https://doi.org/10.15252/embr.202050287

Garlid, K. D., & Paucek, P. (2001). The Mitochondrial Potassium Cycle. *IUBMB Life*, *52*(3–5), 153–158. https://doi.org/10.1080/15216540152845948

Garrido, C., Galluzzi, L., Brunet, M., Puig, P. E., Didelot, C., & Kroemer, G. (2006). Mechanisms of cytochrome c release from mitochondria. *Cell Death & Differentiation*, *13*(9), 1423–1433. https://doi.org/10.1038/sj.cdd.4401950

Gear, A. R. L., & Lehninger, A. L. (1968). Rapid, Respiration-independent Binding of Alkali Metal Cations by Rat Liver Mitochondria. *Journal of Biological Chemistry*, *243*(14), 3953–3962. https://doi.org/10.1016/S0021-9258(18)92036-3

Giacomello, M., Pyakurel, A., Glytsou, C., & Scorrano, L. (2020). The cell biology of mitochondrial membrane dynamics. *Nature Reviews Molecular Cell Biology*, *21*(4), 204–224. https://doi.org/10.1038/s41580-020-0210-7

Gitler, D., Xu, Y., Kao, H.-T., Lin, D., Lim, S., Feng, J., Greengard, P., & Augustine, G. J. (2004). Molecular Determinants of Synapsin Targeting to Presynaptic Terminals. *The Journal of Neuroscience*, *24*(14), 3711–3720. https://doi.org/10.1523/JNEUROSCI.5225-03.2004

Glancy, B., & Balaban, R. S. (2012). Role of Mitochondrial Ca^{2+} in the Regulation of Cellular Energetics. *Biochemistry*, *51*(14), 2959–2973. https://doi.org/10.1021/bi2018909

Greenawalt, J. W., Rossi, C. S., & Lehninger, A. L. (1964). Effect of active accumulation of calcium and phosphate ions on the structure of rat liver mitochondria. *The Journal of Cell Biology*, *23*(1), 21–38. https://doi.org/10.1083/jcb.23.1.21

Grimes, C. A., & Jope, R. S. (2001). The multifaceted roles of glycogen synthase kinase 3β in cellular signaling. *Progress in Neurobiology*, *65*(4), 391–426. https://doi.org/10.1016/S0301-0082(01)00011-9

Guzy, R. D., Hoyos, B., Robin, E., Chen, H., Liu, L., Mansfield, K. D., Simon, M. C., Hammerling, U., & Schumacker, P. T. (2005). Mitochondrial complex III is required for hypoxia-induced ROS production and cellular oxygen sensing. *Cell Metabolism*, *1*(6), 401–408. https://doi.org/10.1016/j.cmet.2005.05.001

Hajek, T., & W. Weiner, M. (2016). Neuroprotective Effects of Lithium in Human Brain? Food for Thought. *Current Alzheimer Research*, *13*(8), 862–872. https://doi.org/10.2174/1567205013666160219112712

Hall, A., Nelson, K., Poole, L. B., & Karplus, P. A. (2011). Structure-based Insights into the Catalytic Power and Conformational Dexterity of Peroxiredoxins. *Antioxidants & Redox Signaling*, *15*(3), 795–815. https://doi.org/10.1089/ars.2010.3624

Harari, F., Bottai, M., Casimiro, E., Palm, B., & Vahter, M. (2015). Exposure to Lithium and Cesium Through Drinking Water and Thyroid Function During Pregnancy: A Prospective Cohort Study. *Thyroid*, *25*(11), 1199–1208. https://doi.org/10.1089/thy.2015.0280

Harrison, P. J., Hall, N., Mould, A., Al-Juffali, N., & Tunbridge, E. M. (2021). Cellular calcium in bipolar disorder: systematic review and meta-analysis. *Molecular Psychiatry*, *26*(8), 4106–4116. https://doi.org/10.1038/s41380-019-0622-y

Harrison, P. J., & Luciano, S. (2021). Incidence of Parkinson's disease, dementia, cerebrovascular disease and stroke in bipolar disorder compared to other psychiatric disorders: An electronic health records network study of 66 million people. *Bipolar Disorders*, *23*(5), 454–462. https://doi.org/10.1111/bdi.13022

Hauser, H., & Shipley, G. G. (1981). Crystallization of phosphatidylserine bilayers induced by lithium. *The Journal of Biological Chemistry*, *256*(22), 11377–11380.

Hauser, H., & Shipley, G. G. (1983). Interactions of monovalent cations with phosphatidylserine bilayer membranes. *Biochemistry*, *22*(9), 2171–2178. https://doi.org/10.1021/bi00278a018

Hauser, H., & Shipley, G. G. (1984). Interactions of divalent cations with phosphatidylserine bilayer membranes. *Biochemistry*, *23*(1), 34–41. https://doi.org/10.1021/bi00296a006

Hernansanz-Agustín, P. (2017). *Deactive complex I triggers a superoxide signal through NCLX in acute hypoxia*. Doctoral Thesis. Universidad Autónoma de Madrid.

Hernansanz-Agustín, P., Choya-Foces, C., Carregal-Romero, S., Ramos, E., Oliva, T., Villa-Piña, T., Moreno, L., Izquierdo-Álvarez, A., Cabrera-García, J. D., Cortés, A., Lechuga-Vieco, A. V., Jadiya, P., Navarro, E., Parada, E., Palomino-Antolín, A., Tello, D., Acín-Pérez, R., Rodríguez-Aguilera, J. C., Navas, P., … Martínez-Ruiz, A. (2020). Na+ controls hypoxic signalling by the mitochondrial respiratory chain. *Nature*, *586*(7828), 287–291. https://doi.org/10.1038/s41586-020-2551-y

Hernansanz-Agustín, P., Choya-Foces, C., & Martínez-Ruiz, A. (2021). Measurement of Superoxide Production in Acute Hypoxia by Fixed-Cell Microscopy. *Methods in molecular biology* (pp. 43–50)*. Humana-Press (Springer Nature) New York.* ISBN: 978-1-0716-0895-1. https://doi.org/10.1007/978-1-0716-0896-8_3

Hernansanz-Agustín, P., & Enríquez, J. A. (2021a). Functional segmentation of CoQ and cyt c pools by respiratory complex superassembly. *Free Radical Biology and Medicine*, *167*, 232–242. https://doi.org/10.1016/j.freeradbiomed.2021.03.010

Hernansanz-Agustín, P., & Enríquez, J. A. (2021b). Generation of Reactive Oxygen Species by Mitochondria. *Antioxidants*, *10*(3), 415. https://doi.org/10.3390/antiox10030415

Hernansanz-Agustín, P., Izquierdo-Álvarez, A., Sánchez-Gómez, F. J., Ramos, E., Villa-Piña, T., Lamas, S., Bogdanova, A., & Martínez-Ruiz, A. (2014). Acute hypoxia produces a superoxide burst in cells. *Free Radical Biology and Medicine*, *71*, 146–156. https://doi.org/10.1016/j.freeradbiomed.2014.03.011

Hernansanz-Agustín, P., Martí-Mateos, Y., Calvo, E., Vázquez, J., & Enríquez, J. A. (2023). Na+ /H+ antiporter activity by respiratory complex I controls mitochondrial Δψ and is impaired in LHON disease. *Biorxiv*. https://doi.org/10.1101/2023.05.30.542932

Hernansanz-Agustín, P., Ramos, E., Navarro, E., Parada, E., Sánchez-López, N., Peláez-Aguado, L., Cabrera-García, J. D., Tello, D., Buendia, I., Marina, A., Egea, J., López, M. G., Bogdanova, A., & Martínez-Ruiz, A. (2017). Mitochondrial complex I deactivation is related to superoxide production in acute hypoxia. *Redox Biology*, *12*, 1040–1051. https://doi.org/10.1016/j.redox.2017.04.025

Herrero Martín, J. C., Salegi Ansa, B., Álvarez-Rivera, G., Domínguez-Zorita, S., Rodríguez-Pombo, P., Pérez, B., Calvo, E., Paradela, A., Miguez, D. G., Cifuentes, A., Cuezva, J. M., & Formentini, L. (2024). An ETFDH-driven metabolon supports OXPHOS efficiency in skeletal muscle by regulating coenzyme Q homeostasis. *Nature Metabolism*. https://doi.org/10.1038/s42255-023-00956-y

Hodge, T., & Colombini, M. (1997). Regulation of Metabolite Flux through Voltage-Gating of VDAC Channels. *Journal of Membrane Biology*, *157*(3), 271–279. https://doi.org/10.1007/s002329900235

Horibata, Y., Ando, H., Zhang, P., Vergnes, L., Aoyama, C., Itoh, M., Reue, K., & Sugimoto, H. (2016). StarD7 Protein Deficiency Adversely Affects the Phosphatidylcholine Composition, Respiratory Activity, and Cristae Structure of Mitochondria. *Journal of Biological Chemistry*, *291*(48), 24880–24891. https://doi.org/10.1074/jbc.M116.736793

Horvath, S. E., Rampelt, H., Oeljeklaus, S., Warscheid, B., van der Laan, M., & Pfanner, N. (2015). Role of membrane contact sites in protein import into mitochondria. *Protein Science*, *24*(3), 277–297. https://doi.org/10.1002/pro.2625

Iommarini, L., Porcelli, A. M., Gasparre, G., & Kurelac, I. (2017). Non-Canonical Mechanisms Regulating Hypoxia-Inducible Factor 1 Alpha in Cancer. *Frontiers in Oncology*, *7*. https://doi.org/10.3389/fonc.2017.00286

Ishii, N., & Terao, T. (2018). Trace lithium and mental health. *Journal of Neural Transmission*, *125*(2), 223–227. https://doi.org/10.1007/s00702-017-1824-6

Jadiya, P., Cohen, H. M., Kolmetzky, D. W., Kadam, A. A., Tomar, D., & Elrod, J. W. (2023). Neuronal loss of NCLX-dependent mitochondrial calcium efflux mediates age-associated cognitive decline. *IScience*, *26*(3), 106296. https://doi.org/10.1016/j.isci.2023.106296

Jadiya, P., Kolmetzky, D. W., Tomar, D., Di Meco, A., Lombardi, A. A., Lambert, J. P., Luongo, T. S., Ludtmann, M. H., Praticò, D., & Elrod, J. W. (2019). Impaired mitochondrial calcium efflux contributes to disease progression in models of Alzheimer's disease. *Nature Communications*, *10*(1), 3885. https://doi.org/10.1038/s41467-019-11813-6

Jadiya, P., Kolmetzky, D. W., Tomar, D., Thomas, M., Cohen, H. M., Khaledi, S., Garbincius, J. F., Hildebrand, A. N., & Elrod, J. W. (2023). *Genetic ablation of neuronal mitochondrial calcium uptake halts Alzheimer's disease progression*. Neuroscience. http://biorxiv.org/lookup/doi/10.1101/2023.10.11.561889

Jakobsson, E., Argüello-Miranda, O., Chiu, S.-W., Fazal, Z., Kruczek, J., Nunez-Corrales, S., Pandit, S., & Pritchet, L. (2017). Towards a Unified Understanding of Lithium Action in Basic Biology and its Significance for Applied Biology. *The Journal of Membrane Biology*, *250*(6), 587–604. https://doi.org/10.1007/s00232-017-9998-2

Javanainen, M., Melcrová, A., Magarkar, A., Jurkiewicz, P., Hof, M., Jungwirth, P., & Martinez-Seara, H. (2017). Two cations, two mechanisms: interactions of sodium and calcium with zwitterionic lipid membranes. *Chemical Communications*, *53*(39), 5380–5383. https://doi.org/10.1039/C7CC02208E

Jiang, D., Zhao, L., & Clapham, D. E. (2009). Genome-Wide RNAi Screen Identifies Letm1 as a Mitochondrial Ca^{2+} /H^{+} Antiporter. *Science*, *326*(5949), 144–147. https://doi.org/10.1126/science.1175145

Jiménez-Gómez, B., Ortega-Sáenz, P., Gao, L., González-Rodríguez, P., García-Flores, P., Chandel, N., & López-Barneo, J. (2023). Transgenic NADH dehydrogenase restores oxygen regulation of breathing in mitochondrial complex I-deficient mice. *Nature Communications*, *14*(1), 1172. https://doi.org/10.1038/s41467-023-36894-2

Jung, D. W., Chávez, E., & Brierley, G. P. (1977). Energy-dependent exchange of K+ in heart mitochondria K+ influx. *Archives of Biochemistry and Biophysics*, *183*(2), 452–459. https://doi.org/10.1016/0003-9861(77)90380-0

Kaelin, W. G., & Ratcliffe, P. J. (2008). Oxygen Sensing by Metazoans: The Central Role of the HIF Hydroxylase Pathway. *Molecular Cell*, *30*(4), 393–402. https://doi.org/10.1016/j.molcel.2008.04.009

Kamerkar, S. C., Kraus, F., Sharpe, A. J., Pucadyil, T. J., & Ryan, M. T. (2018). Dynamin-related protein 1 has membrane constricting and severing abilities sufficient for mitochondrial and peroxisomal fission. *Nature Communications*, *9*(1), 5239. https://doi.org/10.1038/s41467-018-07543-w

Kaplan, J. H. (2002). Biochemistry of Na,K-ATPase. *Annual Review of Biochemistry*, *71*(1), 511–535. https://doi.org/10.1146/annurev.biochem.71.102201.141218

Katoshevski, T., Bar, L., Tikochinsky, E., Harel, S., Ben-Kasus Nissim, T., Bogeski, I., Hershfinkel, M., Attali, B., & Sekler, I. (2022). CKII Control of Axonal Plasticity Is Mediated by Mitochondrial Ca2+ via Mitochondrial NCLX. *Cells*, *11*(24), 3990. https://doi.org/10.3390/cells11243990

Kessing, L. V., Gerds, T. A., Knudsen, N. N., Jørgensen, L. F., Kristiansen, S. M., Voutchkova, D., Ernstsen, V., Schullehner, J., Hansen, B., Andersen, P. K., & Ersbøll, A. K. (2017). Association of Lithium in Drinking Water With the Incidence of Dementia. *JAMA Psychiatry*, *74*(10), 1005. https://doi.org/10.1001/jamapsychiatry.2017.2362

Kessing, L. V., Søndergård, L., Forman, J. L., & Andersen, P. K. (2008). Lithium Treatment and Risk of Dementia. *Archives of General Psychiatry*, *65*(11), 1331. https://doi.org/10.1001/archpsyc.65.11.1331

Kim, J., Tchernyshyov, I., Semenza, G. L., & Dang, C. V. (2006). HIF-1-mediated expression of pyruvate dehydrogenase kinase: A metabolic switch required for cellular adaptation to hypoxia. *Cell Metabolism*, *3*(3), 177–185. https://doi.org/10.1016/j.cmet.2006.02.002

Ko, Y. H., Hong, S., & Pedersen, P. L. (1999). Chemical Mechanism of ATP Synthase. *Journal of Biological Chemistry*, *274*(41), 28853–28856. https://doi.org/10.1074/jbc.274.41.28853

Kofman, O., & Belmaker, R. H. (1993). Biochemical, behavioral, and clinical studies of the role of inositol in lithium treatment and depression. *Biological Psychiatry*, *34*(12), 839–852. https://doi.org/10.1016/0006-3223(93)90052-F

Kostic, M., Ludtmann, M. H. R., Bading, H., Hershfinkel, M., Steer, E., Chu, C. T., Abramov, A. Y., & Sekler, I. (2015). PKA Phosphorylation of NCLX Reverses Mitochondrial Calcium Overload and Depolarization, Promoting Survival of PINK1-Deficient Dopaminergic Neurons. *Cell Reports*, *13*(2), 376–386. https://doi.org/10.1016/j.celrep.2015.08.079

Krall, A. R. (1967). Potassium and sodium-like effects of lithium on brain mitochondrial phosphorylation. *Life Sciences*, *6*(12), 1339–1344. https://doi.org/10.1016/0024-3205(67)90030-6

Lall, R., Mohammed, R., & Ojha, U. (2019). What are the links between hypoxia and Alzheimer's disease? *Neuropsychiatric Disease and Treatment*, *Volume 15*, 1343–1354. https://doi.org/10.2147/NDT.S203103

Lapuente-Brun, E., Moreno-Loshuertos, R., Acín-Pérez, R., Latorre-Pellicer, A., Colás, C., Balsa, E., Perales-Clemente, E., Quirós, P. M., Calvo, E., Rodríguez-Hernández, M. A., Navas, P., Cruz, R., Carracedo, Á., López-Otín, C., Pérez-Martos, A., Fernández-Silva, P., Fernández-Vizarra, E., & Enríquez, J. A. (2013). Supercomplex Assembly Determines Electron Flux in the Mitochondrial Electron Transport Chain. *Science*, *340*(6140), 1567–1570. https://doi.org/10.1126/science.1230381

Laskowski, M., Augustynek, B., Kulawiak, B., Koprowski, P., Bednarczyk, P., Jarmuszkiewicz, W., & Szewczyk, A. (2016). What do we not know about mitochondrial potassium channels? *Biochimica et Biophysica Acta (BBA) - Bioenergetics*, *1857*(8), 1247–1257. https://doi.org/10.1016/j.bbabio.2016.03.007

Letts, J. A., Fiedorczuk, K., Degliesposti, G., Skehel, M., & Sazanov, L. A. (2019). Structures of Respiratory Supercomplex I+III2 Reveal Functional and Conformational Crosstalk. *Molecular Cell*, *75*(6), 1131-1146.e6. https://doi.org/10.1016/j.molcel.2019.07.022

Leyhe, T., Eschweiler, G. W., Stransky, E., Gasser, T., Annas, P., Basun, H., & Laske, C. (2009). Increase of BDNF Serum Concentration in Lithium Treated Patients with Early Alzheimer's Disease. *Journal of Alzheimer's Disease*, *16*(3), 649–656. https://doi.org/10.3233/JAD-2009-1004

Li, W., Yu, J., Liu, Y., Huang, X., Abumaria, N., Zhu, Y., Huang, X., Xiong, W., Ren, C., Liu, X.-G., Chui, D., & Liu, G. (2014). Elevation of brain magnesium prevents synaptic loss and reverses cognitive deficits in Alzheimer's disease mouse model. *Molecular Brain*, *7*(1), 65. https://doi.org/10.1186/s13041-014-0065-y

Li, X.-X., Tsoi, B., Li, Y.-F., Kurihara, H., & He, R.-R. (2015). Cardiolipin and Its Different Properties in Mitophagy and Apoptosis. *Journal of Histochemistry & Cytochemistry*, *63*(5), 301–311. https://doi.org/10.1369/0022155415574818

Liesa, M., & Shirihai, O. S. (2013). Mitochondrial Dynamics in the Regulation of Nutrient Utilization and Energy Expenditure. *Cell Metabolism*, *17*(4), 491–506. https://doi.org/10.1016/j.cmet.2013.03.002

López Cascales, J. J., & Garcia de la Torre, J. (1997). Effect of lithium and sodium ions on a charged membrane of dipalmitoylphosphatidylserine: A study by molecular dynamics simulation. *Biochimica et Biophysica Acta (BBA) - Biomembranes*, *1330*(2), 145–156. https://doi.org/10.1016/S0005-2736(97)00156-9

López-Barneo, J., & Ortega-Sáenz, P. (2022). Mitochondrial acute oxygen sensing and signaling. *Critical Reviews in Biochemistry and Molecular Biology*, *57*(2), 205–225. https://doi.org/10.1080/10409238.2021.2004575

López-Corcuera, B., Giménez, C., & Aragón, C. (1988). Change of synaptic membrane lipid composition and fluidity by chronic administration of lithium. *Biochimica et Biophysica Acta (BBA) - Biomembranes*, *939*(3), 467–475. https://doi.org/10.1016/0005-2736(88)90093-4

Luongo, T. S., Lambert, J. P., Gross, P., Nwokedi, M., Lombardi, A. A., Shanmughapriya, S., Carpenter, A. C., Kolmetzky, D., Gao, E., van Berlo, J. H., Tsai, E. J., Molkentin, J. D., Chen, X., Madesh, M., Houser, S. R., & Elrod, J. W. (2017). The mitochondrial Na+/Ca2+ exchanger is essential for Ca2+ homeostasis and viability. *Nature*, *545*(7652), 93–97. https://doi.org/10.1038/nature22082

Luongo, T. S., Lambert, J. P., Yuan, A., Zhang, X., Gross, P., Song, J., Shanmughapriya, S., Gao, E., Jain, M., Houser, S. R., Koch, W. J., Cheung, J. Y., Madesh, M., & Elrod, J. W. (2015). The Mitochondrial Calcium Uniporter Matches Energetic Supply with Cardiac Workload during Stress and Modulates Permeability Transition. *Cell Reports*, *12*(1), 23–34. https://doi.org/10.1016/j.celrep.2015.06.017

Ma, X., Li, X., Wang, W., Zhang, M., Yang, B., & Miao, Z. (2022). Phosphatidylserine, inflammation, and central nervous system diseases. *Frontiers in Aging Neuroscience*, *14*. https://doi.org/10.3389/fnagi.2022.975176

Mahli, G. S., Bell, E., Outhred, T., & Berk, M. (2020). Lithium therapy and its interactions. *Australian Prescriber*, *43*(3), 91–93. https://doi.org/10.18773/austprescr.2020.024

Mannella, C. A., Lederer, W. J., & Jafri, M. S. (2013). The connection between inner membrane topology and mitochondrial function. *Journal of Molecular and Cellular Cardiology*, *62*, 51–57. https://doi.org/10.1016/j.yjmcc.2013.05.001

Mansfield, K. D., Guzy, R. D., Pan, Y., Young, R. M., Cash, T. P., Schumacker, P. T., & Simon, M. C. (2005). Mitochondrial dysfunction resulting from loss of cytochrome c impairs cellular oxygen sensing and hypoxic HIF-α activation. *Cell Metabolism*, *1*(6), 393–399. https://doi.org/10.1016/j.cmet.2005.05.003

Maranzana, E., Barbero, G., Falasca, A. I., Lenaz, G., & Genova, M. L. (2013). Mitochondrial Respiratory Supercomplex Association Limits Production of Reactive Oxygen Species from Complex I. *Antioxidants & Redox Signaling*, *19*(13), 1469–1480. https://doi.org/10.1089/ars.2012.4845

Martin, M., Rehani, K., Jope, R. S., & Michalek, S. M. (2005). Toll-like receptor–mediated cytokine production is differentially regulated by glycogen synthase kinase 3. *Nature Immunology*, *6*(8), 777–784. https://doi.org/10.1038/ni1221

Mastrototaro, L., Smorodchenko, A., Aschenbach, J. R., Kolisek, M., & Sponder, G. (2016). Solute carrier 41A3 encodes for a mitochondrial Mg2+ efflux system. *Scientific Reports*, *6*(1), 27999. https://doi.org/10.1038/srep27999

Maurer, I. C., Schippel, P., & Volz, H.-P. (2009). Lithium-induced enhancement of mitochondrial oxidative phosphorylation in human brain tissue. *Bipolar Disorders*, *11*(5), 515–522. https://doi.org/10.1111/j.1399-5618.2009.00729.x

McKnight, R. F., Adida, M., Budge, K., Stockton, S., Goodwin, G. M., & Geddes, J. R. (2012). Lithium toxicity profile: a systematic review and meta-analysis. *The Lancet*, *379*(9817), 721–728. https://doi.org/10.1016/S0140-6736(11)61516-X

McKnight, R. F., de La Motte de Broöns de Vauvert, S. J. G. N., Chesney, E., Amit, B. H., Geddes, J., & Cipriani, A. (2019). Lithium for acute mania. *Cochrane Database of Systematic Reviews*, *2019*(6). https://doi.org/10.1002/14651858.CD004048.pub4

Mejia, E. M., & Hatch, G. M. (2016). Mitochondrial phospholipids: role in mitochondrial function. *Journal of Bioenergetics and Biomembranes*, *48*(2), 99–112. https://doi.org/10.1007/s10863-015-9601-4

Mendels, J., & Frazer, A. (1973). Intracellular lithium concentration and clinical response: Towards a membrane theory of depression. *Journal of Psychiatric Research*, *10*(1), 9–18. https://doi.org/10.1016/0022-3956(73)90005-8

Miliara, X., Garnett, J. A., Tatsuta, T., Abid Ali, F., Baldie, H., Pérez-Dorado, I., Simpson, P., Yague, E., Langer, T., & Matthews, S. (2015). Structural insight into the TRIAP1/PRELI-like domain family of mitochondrial phospholipid transfer complexes. *EMBO Reports*, *16*(7), 824–835. https://doi.org/10.15252/embr.201540229

Mills, E. L., Kelly, B., Logan, A., Costa, A. S. H., Varma, M., Bryant, C. E., Tourlomousis, P., Däbritz, J. H. M., Gottlieb, E., Latorre, I., Corr, S. C., McManus, G., Ryan, D., Jacobs, H. T., Szibor, M., Xavier, R. J., Braun, T., Frezza, C., Murphy, M. P., & O'Neill, L. A. (2016). Succinate Dehydrogenase Supports Metabolic Repurposing of Mitochondria to Drive Inflammatory Macrophages. *Cell*, *167*(2), 457-470.e13. https://doi.org/10.1016/j.cell.2016.08.064

Mira, R. G., Quintanilla, R. A., & Cerpa, W. (2023). Mild Traumatic Brain Injury Induces Mitochondrial Calcium Overload and Triggers the Upregulation of NCLX in the Hippocampus. *Antioxidants*, *12*(2), 403. https://doi.org/10.3390/antiox12020403

Mishra, P., & Chan, D. C. (2016). Metabolic regulation of mitochondrial dynamics. *Journal of Cell Biology*, *212*(4), 379–387. https://doi.org/10.1083/jcb.201511036

Mohammadianinejad, S. E., Majdinasab, N., Sajedi, S. A., Abdollahi, F., Moqaddam, M. M., & Sadr, F. (2014). The Effect of Lithium in Post-Stroke Motor Recovery. *Clinical Neuropharmacology*, *37*(3), 73–78. https://doi.org/10.1097/WNF.0000000000000028

Moore, L. G. (2017). Measuring high-altitude adaptation. *Journal of Applied Physiology*, *123*(5), 1371–1385. https://doi.org/10.1152/japplphysiol.00321.2017

Murphy, E., & Eisner, D. A. (2009). Regulation of Intracellular and Mitochondrial Sodium in Health and Disease. *Circulation Research*, *104*(3), 292–303. https://doi.org/10.1161/CIRCRESAHA.108.189050

Muz, B., de la Puente, P., Azab, F., & Azab, A. K. (2015). The role of hypoxia in cancer progression, angiogenesis, metastasis, and resistance to therapy. *Hypoxia*, 83. https://doi.org/10.2147/HP.S93413

Nicholls, D. G. (1974). The Influence of Respiration and ATP Hydrolysis on the Proton-Electrochemical Gradient across the Inner Membrane of Rat-Liver Mitochondria as Determined by Ion Distribution. *European Journal of Biochemistry*, *50*(1), 305–315. https://doi.org/10.1111/j.1432-1033.1974.tb03899.x

Nicholls, D. G. (2008). Forty years of Mitchell's proton circuit: From little grey books to little grey cells. *Biochimica et Biophysica Acta (BBA) - Bioenergetics*, *1777*(7–8), 550–556. https://doi.org/10.1016/j.bbabio.2008.03.014

Nita, I. I., Hershfinkel, M., Lewis, E. C., & Sekler, I. (2015). A crosstalk between Na+ channels, Na+/K+ pump and mitochondrial Na+ transporters controls glucose-dependent cytosolic and mitochondrial Na+ signals. *Cell Calcium*, *57*(2), 69–75. https://doi.org/10.1016/j.ceca.2014.12.007

Noack, C. H., & Trautner, E. M. (1951). The lithium treatment of maniacal psychosis. *Medical Journal of Australia*, *2*(7), 219–222. https://doi.org/10.5694/j.1326-5377.1951.tb68249.x

Nolen, W. A., Licht, R. W., Young, A. H., Malhi, G. S., Tohen, M., Vieta, E., Kupka, R. W., Zarate, C., Nielsen, R. E., Baldessarini, R. J., & Severus, E. (2019). What is the optimal serum level for lithium in the maintenance treatment of bipolar disorder? A systematic review and recommendations from the ISBD/IGSLI Task Force on treatment with lithium. *Bipolar Disorders*, *21*(5), 394–409. https://doi.org/10.1111/bdi.12805

Nunes, P. V., Forlenza, O. V., & Gattaz, W. F. (2007). Lithium and risk for Alzheimer's disease in elderly patients with bipolar disorder. *British Journal of Psychiatry*, *190*(4), 359–360. https://doi.org/10.1192/bjp.bp.106.029868

Nytko, K. J., Maeda, N., Schläfli, P., Spielmann, P., Wenger, R. H., & Stiehl, D. P. (2011). Vitamin C is dispensable for oxygen sensing in vivo. *Blood*, *117*(20), 5485–5493. https://doi.org/10.1182/blood-2010-09-307637

Paggio, A., Checchetto, V., Campo, A., Menabò, R., Di Marco, G., Di Lisa, F., Szabo, I., Rizzuto, R., & De Stefani, D. (2019). Identification of an ATP-sensitive potassium channel in mitochondria. *Nature*, *572*(7771), 609–613. https://doi.org/10.1038/s41586-019-1498-3

Pak, V. V., Ezeriņa, D., Lyublinskaya, O. G., Pedre, B., Tyurin-Kuzmin, P. A., Mishina, N. M., Thauvin, M., Young, D., Wahni, K., Martínez Gache, S. A., Demidovich, A. D., Ermakova, Y. G., Maslova, Y. D., Shokhina, A. G., Eroglu, E., Bilan, D. S., Bogeski, I., Michel, T., Vriz, S., … Belousov, V. V. (2020). Ultrasensitive Genetically Encoded Indicator for Hydrogen Peroxide Identifies Roles for the Oxidant in Cell Migration and Mitochondrial Function. *Cell Metabolism*, *31*(3), 642-653.e6. https://doi.org/10.1016/j.cmet.2020.02.003

Palty, R., Silverman, W. F., Hershfinkel, M., Caporale, T., Sensi, S. L., Parnis, J., Nolte, C., Fishman, D., Shoshan-Barmatz, V., Herrmann, S., Khananshvili, D., & Sekler, I. (2010). NCLX is an essential component of mitochondrial Na+/Ca2+ exchange. *Proceedings of the National Academy of Sciences*, *107*(1), 436–441. https://doi.org/10.1073/pnas.0908099107

Pan, X., Liu, J., Nguyen, T., Liu, C., Sun, J., Teng, Y., Fergusson, M. M., Rovira, I. I., Allen, M., Springer, D. A., Aponte, A. M., Gucek, M., Balaban, R. S., Murphy, E., & Finkel, T. (2013). The physiological role of mitochondrial calcium revealed by mice lacking the mitochondrial calcium uniporter. *Nature Cell Biology*, *15*(12), 1464–1472. https://doi.org/10.1038/ncb2868

Panov, A., & Scarpa, A. (1996). Mg2+ Control of Respiration in Isolated Rat Liver Mitochondria. *Biochemistry*, *35*(39), 12849–12856. https://doi.org/10.1021/bi960139f

Pathak, T., Gueguinou, M., Walter, V., Delierneux, C., Johnson, M. T., Zhang, X., Xin, P., Yoast, R. E., Emrich, S. M., Yochum, G. S., Sekler, I., Koltun, W. A., Gill, D. L., Hempel, N., & Trebak, M. (2020). Dichotomous role of the human mitochondrial Na+/Ca2+/Li+ exchanger NCLX in colorectal cancer growth and metastasis. *ELife*, *9*. https://doi.org/10.7554/eLife.59686

Paumard, P., Vaillier, J., Coulary, B., Schaeffer, J., Soubannier, V., Mueller, D. M., Brèthes, D., di Rago, J.-P., & Velours, J. (2002). The ATP synthase is involved in generating mitochondrial cristae morphology. *The EMBO Journal*, *21*(3), 221–230. https://doi.org/10.1093/emboj/21.3.221

Pettegrew, J. W., Short, J. W., Woessner, R. D., Strychor, S., McKeag, D. W., Armstrong, J., Minshew, N. J., & Rush, A. J. (1987). The effect of lithium on the membrane molecular dynamics of normal human erythrocytes. *Biological Psychiatry*, *22*(7), 857–871. https://doi.org/10.1016/0006-3223(87)90084-9

Pfeiffer, K., Gohil, V., Stuart, R. A., Hunte, C., Brandt, U., Greenberg, M. L., & Schägger, H. (2003). Cardiolipin Stabilizes Respiratory Chain Supercomplexes. *Journal of Biological Chemistry*, *278*(52), 52873–52880. https://doi.org/10.1074/jbc.M308366200

Pickett, E. E., & O'Dell, B. L. (1992). Evidence for dietary essentiality of lithium in the rat. *Biological Trace Element Research*, *34*(3), 299–319. https://doi.org/10.1007/BF02783685

Pilchova, I., Klacanova, K., Tatarkova, Z., Kaplan, P., & Racay, P. (2017). The Involvement of Mg2+ in Regulation of Cellular and Mitochondrial Functions. *Oxidative Medicine and Cellular Longevity*, *2017*, 1–8. https://doi.org/10.1155/2017/6797460

Piruat, J. I., Pintado, C. O., Ortega-Sáenz, P., Roche, M., & López-Barneo, J. (2004). The Mitochondrial *SDHD* Gene Is Required for Early Embryogenesis, and Its Partial Deficiency Results in Persistent Carotid Body Glomus Cell Activation with Full Responsiveness to Hypoxia. *Molecular and Cellular Biology*, *24*(24), 10933–10940. https://doi.org/10.1128/MCB.24.24.10933-10940.2004

Poljsak, B., Šuput, D., & Milisav, I. (2013). Achieving the Balance between ROS and Antioxidants: When to Use the Synthetic Antioxidants. *Oxidative Medicine and Cellular Longevity*, *2013*, 1–11. https://doi.org/10.1155/2013/956792

Pomorski, T. G., & Menon, A. K. (2016). Lipid somersaults: Uncovering the mechanisms of protein-mediated lipid flipping. *Progress in Lipid Research*, *64*, 69–84. https://doi.org/10.1016/j.plipres.2016.08.003

Priesnitz, C., & Becker, T. (2018). Pathways to balance mitochondrial translation and protein import. *Genes & Development*, *32*(19–20), 1285–1296. https://doi.org/10.1101/gad.316547.118

Purroy, R., Britti, E., Delaspre, F., Tamarit, J., & Ros, J. (2018). Mitochondrial pore opening and loss of Ca2+ exchanger NCLX levels occur after frataxin depletion. *Biochimica et Biophysica Acta (BBA) - Molecular Basis of Disease*, *1864*(2), 618–631. https://doi.org/10.1016/j.bbadis.2017.12.005

Quinlan, C. L., Perevoshchikova, I. V., Hey-Mogensen, M., Orr, A. L., & Brand, M. D. (2013). Sites of reactive oxygen species generation by mitochondria oxidizing different substrates. *Redox Biology*, *1*(1), 304–312. https://doi.org/10.1016/j.redox.2013.04.005

Quintana-Cabrera, R., Quirin, C., Glytsou, C., Corrado, M., Urbani, A., Pellattiero, A., Calvo, E., Vázquez, J., Enríquez, J. A., Gerle, C., Soriano, M. E., Bernardi, P., & Scorrano, L. (2018). The cristae modulator Optic atrophy 1 requires mitochondrial ATP synthase oligomers to safeguard mitochondrial function. *Nature Communications*, *9*(1), 3399. https://doi.org/10.1038/s41467-018-05655-x

Quintana-Cabrera, R., & Scorrano, L. (2023). Determinants and outcomes of mitochondrial dynamics. *Molecular Cell*, *83*(6), 857–876. https://doi.org/10.1016/j.molcel.2023.02.012

Rabl, R., Soubannier, V., Scholz, R., Vogel, F., Mendl, N., Vasiljev-Neumeyer, A., Körner, C., Jagasia, R., Keil, T., Baumeister, W., Cyrklaff, M., Neupert, W., & Reichert, A. S. (2009). Formation of cristae and crista junctions in mitochondria depends on antagonism between Fcj1 and Su *e* / *g*. *Journal of Cell Biology*, *185*(6), 1047–1063. https://doi.org/10.1083/jcb.200811099

Rampelt, H., Bohnert, M., Zerbes, R. M., Horvath, S. E., Warscheid, B., Pfanner, N., & van der Laan, M. (2017). Mic10, a Core Subunit of the Mitochondrial Contact Site and Cristae Organizing System, Interacts with the Dimeric F 1 F o -ATP Synthase. *Journal of Molecular Biology*, *429*(8), 1162–1170. https://doi.org/10.1016/j.jmb.2017.03.006

Rizzuto, R., De Stefani, D., Raffaello, A., & Mammucari, C. (2012). Mitochondria as sensors and regulators of calcium signalling. *Nature Reviews Molecular Cell Biology*, *13*(9), 566–578. https://doi.org/10.1038/nrm3412

Rizzuto, R., Marchi, S., Bonora, M., Aguiari, P., Bononi, A., De Stefani, D., Giorgi, C., Leo, S., Rimessi, A., Siviero, R., Zecchini, E., & Pinton, P. (2009). Ca2+ transfer from the ER to mitochondria: When, how and why. *Biochimica et Biophysica Acta (BBA) - Bioenergetics*, *1787*(11), 1342–1351. https://doi.org/10.1016/j.bbabio.2009.03.015

Rizzuto, R., Pinton, P., Carrington, W., Fay, F. S., Fogarty, K. E., Lifshitz, L. M., Tuft, R. A., & Pozzan, T. (1998). Close Contacts with the Endoplasmic Reticulum as Determinants of Mitochondrial Ca $^{2+}$ Responses. *Science*, *280*(5370), 1763–1766. https://doi.org/10.1126/science.280.5370.1763

Robb, E. L., Hall, A. R., Prime, T. A., Eaton, S., Szibor, M., Viscomi, C., James, A. M., & Murphy, M. P. (2018). Control of mitochondrial superoxide production by reverse electron transport at complex I. *Journal of Biological Chemistry*, *293*(25), 9869–9879. https://doi.org/10.1074/jbc.RA118.003647

Roberts, P. G., & Hirst, J. (2012). The Deactive Form of Respiratory Complex I from Mammalian Mitochondria Is a Na+/H+ Antiporter. *Journal of Biological Chemistry*, *287*(41), 34743–34751. https://doi.org/10.1074/jbc.M112.384560

Rodríguez-Zavala, J. S., & Moreno-Sánchez, R. (1998). Modulation of Oxidative Phosphorylation by Mg2+ in Rat Heart Mitochondria. *Journal of Biological Chemistry*, *273*(14), 7850–7855. https://doi.org/10.1074/jbc.273.14.7850

Rouser, G., Fkeischer, S., & Yamamoto, A. (1970). Two dimensional then layer chromatographic separation of polar lipids and determination of phospholipids by phosphorus analysis of spots. *Lipids*, *5*(5), 494–496. https://doi.org/10.1007/BF02531316

Roux, M., & Bloom, M. (1990). Calcium, magnesium, lithium, sodium, and potassium distributions in the headgroup region of binary membranes of phosphatidylcholine and phosphatidylserine as seen by deuterium NMR. *Biochemistry*, *29*(30), 7077–7089. https://doi.org/10.1021/bi00482a019

Roy, S., Dey, K., Hershfinkel, M., Ohana, E., & Sekler, I. (2017). Identification of residues that control Li + versus Na + dependent Ca 2+ exchange at the transport site of the mitochondrial NCLX. *Biochimica et Biophysica Acta (BBA) - Molecular Cell Research*, *1864*(6), 997–1008. https://doi.org/10.1016/j.bbamcr.2017.01.011

Rozenfeld, M., Azoulay, I. S., Ben Kasus Nissim, T., Stavsky, A., Melamed, M., Stutzmann, G., Hershfinkel, M., Kofman, O., & Sekler, I. (2022). Essential role of the mitochondrial Na+/Ca2+ exchanger NCLX in mediating PDE2-dependent neuronal survival and learning. *Cell Reports*, *41*(10), 111772. https://doi.org/10.1016/j.celrep.2022.111772

Rybakowski, J. K. (2022). Antiviral, immunomodulatory, and neuroprotective effect of lithium. *Journal of Integrative Neuroscience*, *21*(2), 068. https://doi.org/10.31083/j.jin2102068

Rysted, J. E., Lin, Z., Walters, G. C., Rauckhorst, A. J., Noterman, M., Liu, G., Taylor, E. B., Strack, S., & Usachev, Y. M. (2021). Distinct properties of Ca2+ efflux from brain, heart and liver mitochondria: The effects of Na+, Li+ and the mitochondrial Na+/Ca2+ exchange inhibitor CGP37157. *Cell Calcium*, *96*, 102382. https://doi.org/10.1016/j.ceca.2021.102382

Salabei, J. K., Gibb, A. A., & Hill, B. G. (2014). Comprehensive measurement of respiratory activity in permeabilized cells using extracellular flux analysis. *Nature Protocols*, *9*(2), 421–438. https://doi.org/10.1038/nprot.2014.018

Scaini, G., Andrews, T., Lima, C. N. C., Benevenuto, D., Streck, E. L., & Quevedo, J. (2021). Mitochondrial dysfunction as a critical event in the pathophysiology of bipolar disorder. *Mitochondrion*, *57*, 23–36. https://doi.org/10.1016/j.mito.2020.12.002

Schlame, M., Brody, S., & Hostetler, K. Y. (1993). Mitochondrial cardiolipin in diverse eukaryotes. *European Journal of Biochemistry*, *212*(3), 727–733. https://doi.org/10.1111/j.1432-1033.1993.tb17711.x

Schlame, M., & Haldar, D. (1993). Cardiolipin is synthesized on the matrix side of the inner membrane in rat liver mitochondria. *The Journal of Biological Chemistry*, *268*(1), 74–79.

Schou, M., Juel-Nielsen, N., Stromgren, E., & Voldby, H. (1954). The treatment of manic psychoses by the administration of lithium salts. *Journal of Neurology, Neurosurgery & Psychiatry*, *17*(4), 250–260. https://doi.org/10.1136/jnnp.17.4.250

Scialò, F., Sriram, A., Fernández-Ayala, D., Gubina, N., Lõhmus, M., Nelson, G., Logan, A., Cooper, H. M., Navas, P., Enríquez, J. A., Murphy, M. P., & Sanz, A. (2016). Mitochondrial ROS Produced via Reverse Electron Transport Extend Animal Lifespan. *Cell Metabolism*, *23*(4), 725–734. https://doi.org/10.1016/j.cmet.2016.03.009

Scola, G., Kim, H. K., Young, L. T., Salvador, M., & Andreazza, A. C. (2014). Lithium reduces the effects of rotenone-induced complex I dysfunction on DNA methylation and hydroxymethylation in rat cortical primary neurons. *Psychopharmacology*, *231*(21), 4189–4198. https://doi.org/10.1007/s00213-014-3565-7

Semenza, G. L. (2007a). Hypoxia-Inducible Factor 1 (HIF-1) Pathway. *Science's STKE*, *2007*(407). https://doi.org/10.1126/stke.4072007cm8

Semenza, G. L. (2007b). Life with Oxygen. *Science*, *318*(5847), 62–64. https://doi.org/10.1126/science.1147949

Semenza, G. L. (2013). HIF-1 mediates metabolic responses to intratumoral hypoxia and oncogenic mutations. *Journal of Clinical Investigation*, *123*(9), 3664–3671. https://doi.org/10.1172/JCI67230

Semenza, G. L., & Wang, G. L. (1992). A Nuclear Factor Induced by Hypoxia via De Novo Protein Synthesis Binds to the Human Erythropoietin Gene Enhancer at a Site Required for Transcriptional Activation. *Molecular and Cellular Biology*, *12*(12), 5447–5454. https://doi.org/10.1128/mcb.12.12.5447-5454.1992

Shalbuyeva, N., Brustovetsky, T., & Brustovetsky, N. (2007). Lithium Desensitizes Brain Mitochondria to Calcium, Antagonizes Permeability Transition, and Diminishes Cytochrome c Release. *Journal of Biological Chemistry*, *282*(25), 18057–18068. https://doi.org/10.1074/jbc.M702134200

Shindo, Y., Fujii, T., Komatsu, H., Citterio, D., Hotta, K., Suzuki, K., & Oka, K. (2011). Newly Developed Mg2+–Selective Fluorescent Probe Enables Visualization of Mg2+ Dynamics in Mitochondria. *PLoS ONE*, *6*(8), e23684. https://doi.org/10.1371/journal.pone.0023684

Shindo, Y., Fujimoto, A., Hotta, K., Suzuki, K., & Oka, K. (2010). Glutamate-induced calcium increase mediates magnesium release from mitochondria in rat hippocampal neurons. *Journal of Neuroscience Research*, *88*(14), 3125–3132. https://doi.org/10.1002/jnr.22467

Shorter, E. (2009). The history of lithium therapy. *Bipolar Disorders*, *11*(s2), 4–9. https://doi.org/10.1111/j.1399-5618.2009.00706.x

Snitow, M. E., Bhansali, R. S., & Klein, P. S. (2021). Lithium and Therapeutic Targeting of GSK-3. *Cells*, *10*(2), 255. https://doi.org/10.3390/cells10020255

Song, Z., Ghochani, M., McCaffery, J. M., Frey, T. G., & Chan, D. C. (2009). Mitofusins and OPA1 Mediate Sequential Steps in Mitochondrial Membrane Fusion. *Molecular Biology of the Cell*, *20*(15), 3525–3532. https://doi.org/10.1091/mbc.e09-03-0252

Spuch, C., López-García, M., Rivera-Baltanás, T., Cabrera-Alvargonzález, J. J., Gadh, S., Rodrigues-Amorim, D., Álvarez-Estévez, T., Mora, A., Iglesias-Martínez-Almeida, M., Freiría-Martínez, L., Pérez-Rodríguez, M., Pérez-González, A., López-Domínguez, A., Longueira-Suarez, M. R., Sousa-Domínguez, A., Araújo-Ameijeiras, A., Mosquera-Rodríguez, D., Crespo, M., Vila-Fernández, D., … Olivares, J. M. (2022). Efficacy and Safety of Lithium Treatment in SARS-CoV-2 Infected Patients. *Frontiers in Pharmacology*, *13*. https://doi.org/10.3389/fphar.2022.850583

Stavsky, A., Stoler, O., Kostic, M., Katoshevsky, T., Assali, E. A., Savic, I., Amitai, Y., Prokisch, H., Leiz, S., Daumer-Haas, C., Fleidervish, I., Perocchi, F., Gitler, D., & Sekler, I. (2021). Aberrant activity of mitochondrial NCLX is linked to impaired synaptic transmission and is associated with mental retardation. *Communications Biology*, *4*(1), 666. https://doi.org/10.1038/s42003-021-02114-0

Stepanova, A., Valls, A., & Galkin, A. (2015). Effect of monovalent cations on the kinetics of hypoxic conformational change of mitochondrial complex I. *Biochimica et Biophysica Acta (BBA) - Bioenergetics*, *1847*(10), 1085–1092. https://doi.org/10.1016/j.bbabio.2015.05.012

Stoler, O., Stavsky, A., Khrapunsky, Y., Melamed, I., Stutzmann, G., Gitler, D., Sekler, I., & Fleidervish, I. (2022). Frequency- and spike-timing-dependent mitochondrial Ca2+ signaling regulates the metabolic rate and synaptic efficacy in cortical neurons. *ELife*, *11*. https://doi.org/10.7554/eLife.74606

Strauss, M., Hofhaus, G., Schröder, R. R., & Kühlbrandt, W. (2008). Dimer ribbons of ATP synthase shape the inner mitochondrial membrane. *The EMBO Journal*, *27*(7), 1154–1160. https://doi.org/10.1038/emboj.2008.35

Sun, X., Wang, J.-F., Tseng, M., & Young, L. T. (2006). Downregulation in components of the mitochondrial electron transport chain in the postmortem frontal cortex of subjects with bipolar disorder. *Journal of Psychiatry & Neuroscience : JPN*, *31*(3), 189–196.

Sun, Y. R., Herrmann, N., Scott, C. J. M., Black, S. E., Swartz, R. H., Hopyan, J., & Lanctôt, K. L. (2019). Lithium Carbonate in a Poststroke Population. *Journal of Clinical Psychopharmacology*, *39*(1), 67–71. https://doi.org/10.1097/JCP.0000000000000981

Surai, P. F., Fisinin, V. I., & Karadas, F. (2016). Antioxidant systems in chick embryo development. Part 1. Vitamin E, carotenoids and selenium. *Animal Nutrition*, *2*(1), 1–11. https://doi.org/10.1016/j.aninu.2016.01.001

Taylor, W. A., & Hatch, G. M. (2009). Identification of the Human Mitochondrial Linoleoyl-coenzyme A Monolysocardiolipin Acyltransferase (MLCL AT-1). *Journal of Biological Chemistry*, *284*(44), 30360–30371. https://doi.org/10.1074/jbc.M109.048322

Technikova-Dobrova, Z., Sardanelli, A. M., Speranza, F., Scacco, S., Signorile, A., Lorusso, V., & Papa, S. (2001). Cyclic Adenosine Monophosphate-Dependent Phosphorylation of Mammalian Mitochondrial Proteins: Enzyme and Substrate Characterization and Functional Role. *Biochemistry*, *40*(46), 13941–13947. https://doi.org/10.1021/bi011066p

Tomar, D., Thomas, M., Garbincius, J. F., Kolmetzky, D. W., Salik, O., Jadiya, P., Joseph, S. K., Carpenter, A. C., Hajnóczky, G., & Elrod, J. W. (2023). MICU1 regulates mitochondrial cristae structure and function independently of the mitochondrial Ca $^{2+}$ uniporter channel. *Science Signaling*, *16*(782). https://doi.org/10.1126/scisignal.abi8948

Treiser, S. L., Cascio, C. S., O'Donohue, T. L., Thoa, N. B., Jacobowitz, D. M., & Kellar, K. J. (1981). Lithium Increases Serotonin Release and Decreases Serotonin Receptors in the Hippocampus. *Science*, *213*(4515), 1529–1531. https://doi.org/10.1126/science.6269180

Tsujimoto, Y., & Shimizu, S. (2000). VDAC regulation by the Bcl-2 family of proteins. *Cell Death & Differentiation*, *7*(12), 1174–1181. https://doi.org/10.1038/sj.cdd.4400780

Tufi, R., Gleeson, T. P., von Stockum, S., Hewitt, V. L., Lee, J. J., Terriente-Felix, A., Sanchez-Martinez, A., Ziviani, E., & Whitworth, A. J. (2019). Comprehensive Genetic Characterization of Mitochondrial Ca2+ Uniporter Components Reveals Their Different Physiological Requirements In Vivo. *Cell Reports*, *27*(5), 1541-1550.e5. https://doi.org/10.1016/j.celrep.2019.04.033

Uwai, Y., Arima, R., Takatsu, C., Furuta, R., Kawasaki, T., & Nabekura, T. (2014). Sodium-phosphate cotransporter mediates reabsorption of lithium in rat kidney. *Pharmacological Research*, *87*, 94–98. https://doi.org/10.1016/j.phrs.2014.06.012

Valente, A. J., Maddalena, L. A., Robb, E. L., Moradi, F., & Stuart, J. A. (2017). A simple ImageJ macro tool for analyzing mitochondrial network morphology in mammalian cell culture. *Acta Histochemica*, *119*(3), 315–326. https://doi.org/10.1016/j.acthis.2017.03.001

van der Laan, M., Horvath, S. E., & Pfanner, N. (2016). Mitochondrial contact site and cristae organizing system. *Current Opinion in Cell Biology*, *41*, 33–42. https://doi.org/10.1016/j.ceb.2016.03.013

Vance, J. E. (1990). Phospholipid synthesis in a membrane fraction associated with mitochondria. *The Journal of Biological Chemistry*, *265*(13), 7248–7256.

Wasserman, M. J., Corson, T. W., Sibony, D., Cooke, R. G., Parikh, S. V, Pennefather, P. S., Li, P. P., & Warsh, J. J. (2004). Chronic Lithium Treatment Attenuates Intracellular Calcium Mobilization. *Neuropsychopharmacology*, *29*(4), 759–769. https://doi.org/10.1038/sj.npp.1300400

Weir, E. K., López-Barneo, J., Buckler, K. J., & Archer, S. L. (2005). Acute Oxygen-Sensing Mechanisms. *New England Journal of Medicine*, *353*(19), 2042–2055. https://doi.org/10.1056/NEJMra050002

Wolf, D. M., Segawa, M., Kondadi, A. K., Anand, R., Bailey, S. T., Reichert, A. S., van der Bliek, A. M., Shackelford, D. B., Liesa, M., & Shirihai, O. S. (2019). Individual cristae within the same mitochondrion display different membrane potentials and are functionally independent. *The EMBO Journal*, *38*(22). https://doi.org/10.15252/embj.2018101056

Xiong, Y., Ruan, Y.-T., Zhao, J., Yang, Y.-W., Chen, L.-P., Mai, Y.-R., Yu, Q., Cao, Z.-Y., Liu, F.-F., Liao, W., & Liu, J. (2022). Magnesium-L-threonate exhibited a neuroprotective effect against oxidative stress damage in HT22 cells and Alzheimer's disease mouse model. *World Journal of Psychiatry*, *12*(3), 410–424. https://doi.org/10.5498/wjp.v12.i3.410

Xu, Y., Malhotra, A., Ren, M., & Schlame, M. (2006). The Enzymatic Function of Tafazzin. *Journal of Biological Chemistry*, *281*(51), 39217–39224. https://doi.org/10.1074/jbc.M606100200

Yamanaka, R., Tabata, S., Shindo, Y., Hotta, K., Suzuki, K., Soga, T., & Oka, K. (2016). Mitochondrial Mg2+ homeostasis decides cellular energy metabolism and vulnerability to stress. *Scientific Reports*, *6*(1), 30027. https://doi.org/10.1038/srep30027

Zaken, V., Kohen, R., & Ornoy, A. (2000). The development of antioxidant defense mechanism in young rat embryos in vivo and in vitro. *Early Pregnancy*, *4*(2), 110–123.

Zanni, G., Michno, W., Di Martino, E., Tjärnlund-Wolf, A., Pettersson, J., Mason, C. E., Hellspong, G., Blomgren, K., & Hanrieder, J. (2017). Lithium Accumulates in Neurogenic Brain Regions as Revealed by High Resolution Ion Imaging. *Scientific Reports*, *7*(1), 40726. https://doi.org/10.1038/srep40726

Zborowski, J., Dygas, A., & Wojtczak, L. (1983). Phosphatidylserine decarboxylase is located on the external side of the inner mitochondrial membrane. *FEBS Letters*, *157*(1), 179–182. https://doi.org/10.1016/0014-5793(83)81141-7

Zhang, H. (2017). Thin-Film Hydration Followed by Extrusion Method for Liposome Preparation. *Methods in Molecular Biology (Clifton, N.J.)*, *1522*, 17–22. https://doi.org/10.1007/978-1-4939-6591-5_2

Zhang, M., Mileykovskaya, E., & Dowhan, W. (2002). Gluing the Respiratory Chain Together. *Journal of Biological Chemistry*, *277*(46), 43553–43556. https://doi.org/10.1074/jbc.C200551200

Zheng, Y., Gibb, A. A., Xu, H., Liu, S., & Hill, B. G. (2023). The metabolic state of the heart regulates mitochondrial supercomplex abundance in mice. *Redox Biology*, *63*, 102740. https://doi.org/10.1016/j.redox.2023.102740

ANNEXE

Directly related with the content of this Thesis, I have participated in the following article publications:

- Hernansanz-Agustín P, **Choya-Foces C**, Carregal-Romero S, Ramos E, Oliva T, Villa-Piña T, Moreno L, Izquierdo-Álvarez A, Cabrera-García JD, Cortés A, Lechuga-Vieco AV, Jadiya P, Navarro E, Parada E, Palomino-Antolín A, Tello D, Acín-Pérez R, Rodríguez-Aguilera JC, Navas P, Cogolludo Á, López-Montero I, Martínez-del-Pozo Á, Egea J, López MG, Elrod JW, Ruíz-Cabello J, Bogdanova A, Enríquez JA, & Martínez-Ruiz A. (2020). Na^+ controls hypoxic signalling by the mitochondrial respiratory chain. *Nature*, *586*(7828), 287–291.

- **Choya-Foces C**, (...), Hernansanz-Agustín P, & Martínez-Ruiz A. The mitochondrial Na^+/Ca^{2+} exchanger (NCLX) is implied in the activation of hypoxia-inducible factors. *In preparation*

Also, I have participated in one book chapter:

- Hernansanz-Agustín P, **Choya-Foces C**, & Martínez-Ruiz A. (2021). Measurement of Superoxide Production in Acute Hypoxia by Fixed-Cell Microscopy. *Methods in molecular biology* (pp. 43–50)*. Humana-Press (Springer Nature) New York.* ISBN: 978-1-0716-0895-1. https://doi.org/10.1007/978-1-0716-0896-8_3

Besides, during the research period of my thesis, I have participated in the following publications:

- Másedas G, Les F, **Choya-Foces C**, Hugo M, & López V. (2020). The Metabolite Urolithin-A Ameliorates Oxidative Stress in Neuro-2a Cells, Becoming a Potential Neuroprotective Agent. *Antioxidants (Basel, Switzerland), 9*(2), 177.

- González R, Rodríguez-Hernández MA, Negrete M, Ranguelova K, Rossin A, **Choya-Foces C**, Cruz-Ojeda P, Miranda-Vizuete A, Martínez-Ruiz A, Rius-Pérez S, Sastre J, Bárcena JA, Hueber AO, Padilla CA, & Muntané J. (2020). Downregulation of thioredoxin-1-dependent CD95 S-nitrosation by Sorafenib reduces liver cancer. *Redox biology*, *34*, 101528.

- Sevilla-Montero J, Munar-Rubert O, Pino-Fadón J, Aguilar-Latorre C, Villegas-Esguevillas M, Climent B, Agrò M, **Choya-Foces C**, Martínez-Ruiz A, Balsa E, Muñoz-Calleja C, Gómez-Punter RM, Vázquez-Espinosa E, Cogolludo A, & Calzada MJ. (2022). Cigarette smoke induces pulmonary arterial dysfunction through an imbalance in the redox status of the soluble guanylyl cyclase. *Free radical biology & medicine*, *193*(Pt 1), 9–22.

- Marañón P, Rey E, Isaza SC, Wu H, Rada P, **Choya-Foces C**, Martínez-Ruiz A, Martín MÁ, Ramos S, García-Monzón C, Cubero FJ, Valverde ÁM, & González-Rodríguez Á. (2024). Inhibition of ALK3-mediated signalling pathway protects against acetaminophen-induced liver injury. *Redox Biology*, 103088. https://doi.org/10.1016/j.redox.2024.103088

- Garbincius JF, Salik O, Cohen HM, **Choya-Foces C**, Mangold AS, Makhoul AD, Schmidt AE, Khalil DY, Doolittle JJ, Wilkinson AS, Murray EK, Lazaropoulos MP, Hildebrand AN, Tomar D, & Elrod JW. (2023). TMEM65 regulates NCLX-dependent mitochondrial calcium efflux. *Biorxiv*. *Under review at Nature Meatabolism*

- Gibb AA, LaPenna K, Gaspar RB, **Choya-Foces C**, Doiron J, Li Z, Xia H, Sharp T, Lazaropoulos MP, Conwell, M, Goodchild TT, Lefer DJ, Elrod JW. Defining the cardiac molecular signatures of HFpEF Utilizing Systems Biology Approaches. *In preparation*